



ScuDo

Scuola di Dottorato ~ Doctoral School  
WHAT YOU ARE, TAKES YOU FAR



Doctoral Dissertation  
Doctoral Program in Mechanical Engineering (33<sup>rd</sup> Cycle)

# Modelling the Physical Human- Exoskeleton Interface

**Divyaksh Subhash Chander**

\* \* \* \* \*

## **Supervisor**

Prof. Maria Pia Cavatorta

## **Doctoral Examination Committee:**

Prof. Michael Skipper Andersen, Referee, Aalborg University, Aalborg, Denmark

Prof. Simona Crea, Referee, Scuola Superiore Sant'Anna, Pisa, Italy

Dr. Lidia Ghibaudo, Referee, Stellantis, Turin, Italy

Dr. Jesús Ortiz, Referee, Istituto Italiano di Tecnologia, Genoa, Italy

Prof. Charles Pontonnier, Referee, École Normale Supérieure de Rennes, Rennes, France

Politecnico di Torino  
September \*\*, 2021



This thesis is licensed under a Creative Commons License, Attribution - Noncommercial - NoDerivative Works 4.0 International: see [www.creativecommons.org](http://www.creativecommons.org). The text may be reproduced for non-commercial purposes, provided that credit is given to the original author.

I hereby declare that, the contents and organisation of this dissertation constitute my own original work and does not compromise in any way the rights of third parties, including those relating to the security of personal data.



.....  
Divyaksh Subhash Chander  
Turin, July 27, 2021



# Summary

Development of exoskeletons has seen a boom in the last few years, and they are seeing increasing adoption in industrial and medical/rehabilitative fields. The design and assessment of exoskeletons have benefitted through virtual multibody models. The use of musculoskeletal models to evaluate the combined human-exoskeleton system allows estimating the effect of the exoskeleton on the user. However, models to investigate the physical human-exoskeleton interface are lacking. The use of contact models to investigate the interface properties is almost non-existent, even though they are used extensively in other applications in musculoskeletal models, e.g., ground reaction force prediction. The human-exoskeleton interface is generally simulated through reaction forces associated with kinematic joints that are used to constrain the exoskeleton to the user. The reaction forces can only provide limited information about the interface forces. However, the interface forces are of interest as they affect the overall comfort of the user and are being investigated to establish thresholds for discomfort.

Thus, the aim of this dissertation is to use a contact model, validated extensively in ground reaction force prediction, to simulate the forces at the human-exoskeleton interface. The contact model estimates the contact forces through contact elements that are configured to estimate the normal and frictional forces. The contact model is characterized by a coefficient of static friction and a maximum force-generating capacity of the contact elements (or the strength of the elements). The contact forces are estimated as the solution of an optimization problem that aims to minimize the activation of the contact elements and the muscles of the human model. The contact model could provide additional information about the interface forces that could be used to optimize the interface design. This thesis describes the application of the contact model in the context of the human-exoskeleton interface. Furthermore, the results of the contact model are compared to those from the conventional model of simulating the human-exoskeleton interface forces through the kinematic joints.

The thesis was developed over three studies that progressed in complexity from the simulation of a single interface as a planar surface, then as a curved surface, and finally the simulation of multiple curved interfaces. In the first study, the existing contact model was applied as it is to simulate the interface of a lower limb exoskeleton, the Chairless Chair. The exoskeleton has a simple interface that offered similar conditions to the existing use case of the contact model. In this

study, the exoskeleton was trialled by a subject simulating three different postures and body weight distribution between the user and the exoskeleton was used as a reference for the interface forces from the contact and conventional models. Both the contact and conventional model were able to capture the change in the body weight distribution with the change in posture. However, the conventional model showed an unreasonable reduction in the knee extension moment in more challenging postures, where a greater knee extension moment was expected. Further, parameters of the contact model, such as the coefficient of friction and the angle of contact, were investigated. The support from the exoskeleton dropped sharply for friction coefficients lower than 0.4 at the interface. The contact model also showed the dependence of the effectiveness of the exoskeleton on the angle of contact such that a more horizontal angle of contact required a lower friction coefficient for the exoskeleton model to support the user.

The second study aimed to simulate the seat of the Chairless Chair as a generalized curved surface since the angle of contact influenced the model results. This was done by simulating the surface of the seat through multiple planar surfaces distributed over the seat, each with its unique orientation. The discretization resulted in unrealistic solutions that required the optimization of the strength of the contact elements. The strength of the contact elements was optimized by considering only the virtual centre of pressure and predicted body weight distribution. The results of the contact model were compared with the results obtained from a pressure mat placed at the interface and the body weight distribution in three different use cases of the exoskeleton. The centre of pressure and the body weight distribution from the optimized contact model showed good agreement with the empirical measures.

The necessity to optimize the contact model in the second study motivated the third study where the contact model was implemented on another exoskeleton. The second exoskeleton is an active exoskeleton for the lower limb and consists of three interfaces that provided a 360° contact with the thigh, shank, and foot. Mocap data from eight trials were used as an input in the model. The contact model at multiple interfaces exploited the misalignments in the human and exoskeleton joints to unload the physiological muscles. A method is presented to ensure kinetic alignment between the human and exoskeleton, which prevents the contact elements from unloading the physiological muscles. The results of the contact and conventional model were compared to a reference model where the exoskeleton assistance was applied directly to the human model. The biomechanical outputs, such as the moments or the compression force at the knee and ankle joints, showed good agreement between the contact and reference

model. In general, the contact model showed more consistent results than the conventional model and provided more information about the interface forces than the conventional model, which was limited to only eight reaction forces.

In conclusion, the contact model was applied to two different exoskeletons that could be representative of the interface conditions of several exoskeletons. The thesis provides methods to successfully apply the contact model in different interface conditions. However, the contact model is limited as it simulates contact between rigid bodies and cannot account for compliance at the human-exoskeleton interface. Open issues concerning the validity of the contact forces and the ability to account for the undesired interface forces due to the misalignments between the human and exoskeleton in the contact model still remain. These topics could be of interest for future studies.





# Acknowledgment

The development of a doctoral thesis is a long and complex process, and it definitely requires the support of several people. First and foremost, I would like to acknowledge my supervisor, Prof. Maria Pia Cavatorta. Her support and guidance have been invaluable, and I especially appreciate her for instilling in me good work ethics and research practise. I also thank her for going beyond her role as a supervisor; for being a friend and advising me on matters that didn't always concern my doctoral research.

Next, I would like to acknowledge my collaborators. I would like to thank researchers from the ergonomics groups at Stellantis (formerly known as Fiat Chrysler Automobiles, FCA) and CRF (Fiat Research Centre) in Turin, Italy. I would like to thank them for supporting the development of the first two studies. Their feedback was immensely useful, as were the visits to their assembly lines and seeing first-hand trials of industrial exoskeletons on the production line. For the last study in this thesis, I would like to thank Mr. Max Böhme and Prof. Johannes Zentner from HTWK (University of Applied Sciences) Leipzig, Germany, and Prof. Michael Skipper Andersen and Prof. John Rasmussen from Aalborg University, Denmark. The exoskeleton used in the third study is being developed at HTWK Leipzig. I would like to thank the colleagues at HTWK Leipzig for believing in me and allowing me to continue my research using their exoskeleton. I wish them and their team all the best for success in their goals. I am deeply grateful to the colleagues at Aalborg University for welcoming and hosting me at the Biomechanics Research Group as a visiting PhD candidate. Their feedback on musculoskeletal modelling has significantly contributed to shaping the third study in this thesis.

Last but not the least, I would like to thank my family and friends for encouraging me and pushing me forward when I doubted myself.



# Contents

1. Introduction.....	1
1.1 Exoskeletons in brief.....	1
1.2 Virtual modelling of human-exoskeleton system .....	4
1.2.1 Exoskeleton concept.....	4
1.2.2 Exoskeleton model .....	5
Kinematic investigation.....	5
Kinetic investigation .....	6
1.3 Human-exoskeleton interface modelling .....	7
1.4 Aim of the thesis .....	9
1.5 Structure of the thesis.....	10
2. Modelling Methods.....	13
2.1 Musculoskeletal modelling .....	13
2.1.1 Human model .....	14
2.1.2 Kinematics.....	15
2.1.3 Kinetics .....	17
2.1.4 Ground reaction force prediction .....	18
2.2 Exoskeleton model.....	20
3. Simulating Planar Surface .....	23
3.1 Introduction.....	23
3.2 Materials and Methods.....	24
3.2.1 Exoskeleton .....	24
3.2.2 Use Case.....	25
3.2.3 Musculoskeletal modelling .....	27
Human-Exoskeleton model .....	27
Human-Exoskeleton Interface models .....	28
3.2.4 Analyses .....	30
3.3 Results.....	30
3.3.1 Comparison of the two interface models .....	30
3.3.2 Parametric studies .....	33

3.4	Discussion .....	35
3.4.1	Outputs of the two interface models .....	35
3.4.2	Parametric studies .....	37
3.4.3	Limitations .....	38
3.5	Conclusion .....	39
4.	Simulating Curved Surface .....	41
4.1	Introduction .....	41
4.2	Materials and Methods .....	42
4.2.1	Experiments .....	42
4.2.2	Musculoskeletal modelling .....	43
	Human-Exoskeleton Interface forces .....	44
4.2.3	Analyses .....	46
4.3	Results .....	46
4.3.1	Interface outputs .....	46
4.3.2	Biomechanical outputs .....	47
4.4	Discussion .....	48
4.4.1	Contact forces through optimization .....	48
4.4.2	Interface outputs and optimal strength .....	50
4.4.3	Biomechanical outputs .....	50
4.4.4	Application to other exoskeletons .....	51
4.4.5	Limitations .....	53
4.5	Conclusion .....	53
5.	Simulating Multiple Interfaces .....	55
5.1	Introduction .....	55
5.2	Materials and methods .....	57
5.2.1	Exoskeleton .....	57
5.2.2	Experiments .....	58
5.2.3	Musculoskeletal modelling .....	60
	Human-Exoskeleton model .....	61
5.2.4	Interface models .....	62
	Contact model .....	62
	Conventional model .....	64
	Reference models .....	65

5.2.5 Analyses .....	66
5.3 Results.....	66
5.3.1 Biomechanical outputs .....	66
5.3.2 Interface outputs.....	68
5.4 Discussion .....	70
5.4.1 Contact model .....	70
5.4.2 Comparison of different models: Biomechanical outputs.....	71
5.4.3 Comparison of different models: Interface outputs .....	72
5.4.4 Limitations .....	73
5.5 Conclusions.....	74
6. Discussion.....	77
6.1 Biomechanical outputs.....	77
6.2 Interface outputs.....	79
6.3 Comparison of modelling methods.....	80
6.4 Limitations .....	81
7. Conclusion .....	83
7.1 Summary of the thesis.....	83
7.2 Contributions of the thesis .....	85
8. Future Work.....	87
9. References.....	89



# List of Tables

Table 1: Comparison of the two interface models: contact model (Model 1) and reaction force-based model (Model 2).....	32
Table 2: Percentage of body weight supported by the exoskeleton and the joint moments at the hip, knee, and ankle joints for different values of the coefficient of friction ( $\mu$ ) at the human-exoskeleton interface. The coefficients of friction at the human-ground and exoskeleton-ground interfaces are 0.5 each. Negative “-” sign indicates an opposite moment. ....	34
Table 3: Mass of the exoskeleton parts and marker distribution .....	58
Table 4: Adjusted lengths of the exoskeleton to consider the anthropometry of the subject.....	59
Table 5: Interface models studied .....	65





# List of Figures

Figure 1: Number of exoskeleton publications per year (2000 – 2019) listed in Scopus. Search-phrase “Exoskeleton” and limited to “Engineering” subject area. Extracted on 16 December 2020. ....	1
Figure 2: The three test conditions: a.) Working at elbow height, b.) Reaching with arms raised, and c.) Lateral reaching (to the right). Note: The red sphere is the centre of mass of the mannequin. ....	27
Figure 3: Percentage of body weight supported by the exoskeleton by the contact model (Model 1), the reaction force-based model (Model 2), and empirical values in the three test conditions. ....	31
Figure 4: Knee extension moments by the contact model (Model 1) and the reaction force-based model (Model 2). In the case of lateral reaching, the trend line passes through the mean of the right and the left knee extension moment. ....	33
Figure 5: Parametric study of the coefficients of friction at the human-exoskeleton (Mu_SubExo) interface and ground (Mu_Ground). ....	34
Figure 6: Parametric study of the coefficient of friction at the human-exoskeleton interface (Mu_SubExo) and the angle of the exoskeleton seat (Angle_SubExo). ....	35
Figure 7: Virtual models of the low, comfort and high seat. Muscles of the left leg are hidden. ....	44
Figure 8: Empirical pressure maps for the left leg showing different areas of contact for the three sitting heights: low, comfort and high. The empirical area of contact was used as an input in the model. ....	45
Figure 9: Exoskeleton support and the centre of pressure for different strengths and strength gradients of the contact elements. ....	47
Figure 10: Joint moment and muscle activation for different strengths and strength gradients of the contact muscles. ....	48
Figure 11: A simple sketch of the model. a.) A moment $M$ about the knee is required to maintain the subject in static equilibrium. b.) and c.) depict two hypothetical solutions that result in an equal moment, $M_{exo}$ , about the knee due to the support from the exoskeleton ( $r_1 \times F_1 = r_2 \times F_2$ ) ....	49
Figure 12: Exoskeleton to support stair negotiation under development at HTWK Leipzig. The figure shows the exoskeleton for the right leg consisting of seven general parts. ....	57
Figure 13: Trial of a stair ascent with the supporting exoskeleton on both legs. The experiment was conducted at the biomechanical lab of the University of Leipzig. ....	60
Figure 14: Adding dummy segments in the human-exoskeleton model. On the left is the typical human-exoskeleton model with the kinetic constraints between	

the human and the exoskeleton. On the right, dummy segments are added to align the exoskeleton joints with the human joints.....64

Figure 15: Reference frames on the exoskeleton used for defining the kinematic joints. The number in the grey circle indicates the number of constraints added at that interface. ....65

Figure 16: Biomechanical outputs from the Ideal Assistance (IA) reference case and the 4 interface models (please refer to Table 5 for the interface models). The confidence bands indicate a 95% confidence interval about the IA.....68

Figure 17: Interface forces from the four different models. Solid lines represent the mean of the eight trials and the shaded region represents +/- 1 std. deviation. Please refer to Figure 15 for the coordinate system and to Table 5 for the interface models. ....69

# Chapter 1

## Introduction

This chapter briefly introduces exoskeletons and then describes in detail the state of the art in virtual modelling of exoskeletons. Virtual modelling is relevant in the design and analysis of exoskeletons and this thesis aims to contribute to the virtual modelling of the human-exoskeleton interaction.

### 1.1 Exoskeletons in brief

Exoskeletons are wearable mechanical devices that improve the physical capabilities of the user. They are typically designed for a target user group and optimized for specific tasks. Exoskeletons have seen a lot of interest in the last decade. Figure 1 shows the yearly publications listed in Scopus with the search phrase “Exoskeleton” and limited to “Engineering” subject area.

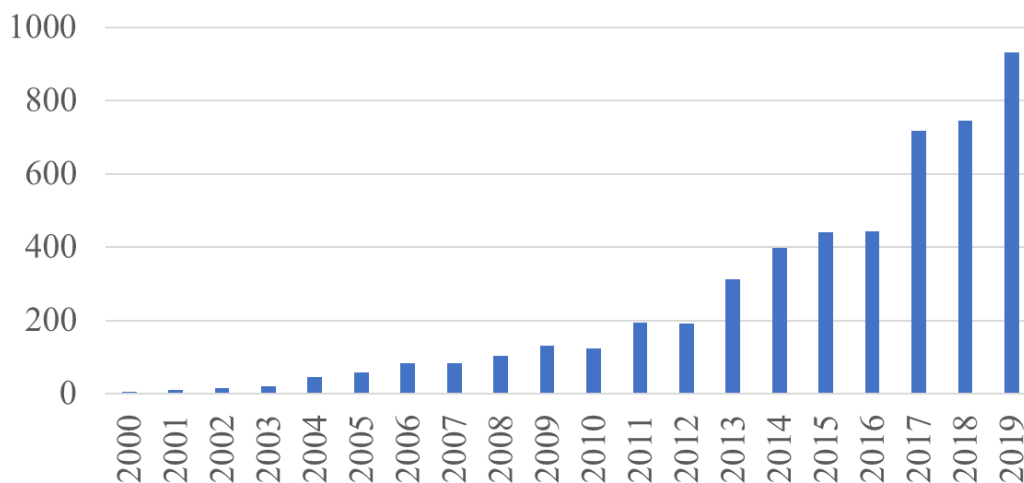


Figure 1: Number of exoskeleton publications per year (2000 – 2019) listed in Scopus. Search-phrase “Exoskeleton” and limited to “Engineering” subject area. Extracted on 16 December 2020.

Exoskeletons can be categorized in several ways. Based on their field of application, exoskeletons can be classified into military, medical, and industrial exoskeletons. The introduction of exoskeletons in industrial applications has been

more recent than military and medical applications. Exoskeletons could also be classified according to the target body parts such as a lower limb, upper limb, trunk or some combination, for example, a full-body exoskeleton. Exoskeletons could also be classified based on the assistance into passive, active, or quasi-passive exoskeletons. Passive exoskeletons typically use elastic elements to provide assistance. Instead, active exoskeletons use powered actuators to deliver the assistance. The actuators could be electric, pneumatic, or hydraulic amongst others and are typically accompanied by a battery and a controller of the actuator. Lastly, quasi-passive exoskeletons provide assistive force/torque through passive elements that are modulated by additional elements such as variable-dampers, clutches, etc. The modulating elements may be active elements.

A description of the different types of exoskeletons is beyond the scope of the thesis. The reader is referred to the following review articles that provide an interesting overview of the recent state of the art of exoskeletons (de Looze et al. 2016; Manna and Dubey 2018; Chen et al. 2019; Fox et al. 2019; Pamungkas et al. 2019; Shi et al. 2019).

The primary aim of exoskeletons is to augment the physical capacity of the user. Thus, the user of the exoskeleton plays a central role in the design and analysis of exoskeletons. It is important to understand how the exoskeleton affects the user and the aim should be to make an overall assessment of the human-exoskeleton system. There could be several aspects that must be investigated, starting with the intended benefit of the exoskeleton to the user, which is the primary aim of the exoskeleton. But also, other unwanted effects of the exoskeleton such as the added load at the human-exoskeleton interface, where the exoskeleton is attached to the user, should be investigated. The exoskeleton supports itself at the interface while assisting the user. Consequently, there would be a transfer of load to another part of the body, potentially leading to discomfort and rejection of the device by the user (Bosch et al. 2016; de Looze et al. 2016). While the target joint gets the assistance, another joint of the user could work a little harder (Weston et al. 2018). Another aspect that should be investigated is the influence of the exoskeleton on the natural motion of the user. The use of an exoskeleton could decrease the range of motion of the assisted joint (Baltrusch et al. 2018; Kim et al. 2018). Misalignment between the joints of the human and the exoskeleton can lead to an alteration of the natural movement of the user and impede the transfer of assistance from the exoskeleton to the user (Naf et al. 2018).

There are different ways to assess the effects of the exoskeleton. Experimental studies are often used to report the effects of the exoskeleton by comparing the with and without exoskeleton cases. The with-exoskeleton cases could be further comprised of different levels of assistance including no assistance or transparency mode. The transparency mode of the exoskeleton could be useful to segregate the negative effects of the exoskeleton (such as added weight, reduced range of motion, etc.) from the positive effects of the exoskeleton due to the assistance. The studies generally report objective measures such as measures of performance and time, muscle activity through electromyography (EMG), contact pressure, or

heart rate. They could also report subjective measures such as perceived exertion, discomfort, or usability. Spada et al. 2017 tested a passive exoskeleton for the upper limbs and reported the duration of a static posture maintenance task, the duration and the number of repetitions of a repeated material handling task, performance in terms of the number of successful attempts of a precision task, and subjective assessment of the exoskeleton. Baltrusch et al., 2018 reported the effects of a passive trunk exoskeleton on 12 functional performance tests and reported objective measures such as performance time, holding time, maximum weight lifted, distance walked amongst others. Additionally, subjective measures such as perceived task difficulty, discomfort, and user impression were reported. Huysamen et al. 2018a reported the muscle activity, perceived musculoskeletal effort, local perceived pressure and subjective usability of a passive exoskeleton for the upper limbs in static holding tasks, while Huysamen et al. 2018b reported the same measures along with the measured pressure at the human-exoskeleton interface of an active trunk exoskeleton in dynamic lifting tasks. Alabdulkarim & Nussbaum, 2019 compared different passive exoskeletons in a simulated overhead drilling task using maximum acceptable frequency and number of errors as performance measures, muscular effort using EMG, and perceived discomfort. Amandels et al., 2019 measured muscle activity using EMG and discomfort from a passive trunk exoskeleton.

Some experimental studies also use biomechanical models to estimate changes in muscle activities or joint moment requirements. Koopman et al., 2019 used a biomechanical model to report the net L5/S1 moment along with EMG based muscle activities for a passive trunk exoskeleton. Weston et al., 2018 used an EMG-assisted model to estimate the muscle forces and spinal loads for a passive exoskeleton for the upper limbs. While Picchiotti et al., 2019 used the same EMG-assisted spine model to compare two postural-assist passive exoskeletons. Gordon et al., 2018 used a musculoskeletal model to quantify the metabolic power consumption for an active pelvis exoskeleton.

While the previously mentioned studies evaluated commercially available exoskeletons using virtual models, the use of virtual models is far more extensive in the design and development of exoskeletons and as such is described in the next section. Naturally, experimental testing is an important aspect in the evaluation of the exoskeleton but, as a minimum, it would require a physical prototype. Virtual modelling can support the development stages before the construction of a prototype. Virtual modelling of the human-exoskeleton system, however, is only one of the several key stages during the design process. For instance, the involvement of target users of the exoskeleton throughout the development phase could be relevant in the user-centred design process. The user feedback could provide the context of the use of the exoskeleton along with constraints and requirements (Power et al. 2019; Ármannsdóttir et al. 2020). It is beyond the scope of this thesis to describe all the aspects of the exoskeleton design process and the focus will be on how virtual modelling can contribute to the design and evaluation of exoskeletons.

## **1.2 Virtual modelling of human-exoskeleton system**

Virtual modelling of the human-exoskeleton system can help to understand the functional aspects of the exoskeleton. Multibody modelling allows designing and simulating both the kinematics and kinetics of the exoskeleton. Moreover, it also allows for investigating the combined human-exoskeleton system. It could be useful to investigate the kinematic compatibility as well as the kinetic interaction between the human and exoskeleton. Several multibody tools are available currently. These could be general-purpose programs such as Adams© (MSC Software, USA) or MATLAB® (MathWorks, USA) and its toolboxes. There are also specialist musculoskeletal models that allow the possibility of detailed biomechanical investigations such as AnyBody Modeling Systems™ (AnyBody Technology A/S, Denmark), OpenSim (SimTK, USA), SIMM (MusculoGraphics Inc., USA) or CusToM (Muller et al. 2019), amongst others. Many studies advocate the use of musculoskeletal models to design, develop or analyse exoskeletons (Agarwal et al. 2010, 2016; Bai and Rasmussen 2011; de Kruif et al. 2017; Harant et al. 2017; Zhou et al. 2017; Hansen et al. 2018; Khamar et al. 2019; Tröster et al. 2020). These models allow investigating the effect of an exoskeleton on the biomechanical load of the human model using model outputs such as muscle force or activity, joint reaction forces, joint moment requirements, as well as the forces at the human-exoskeleton interfaces. Virtual models could be used to support the design process at different stages, starting from the definition of the exoskeleton concept to the evaluation of more realistic models of the exoskeleton.

### **1.2.1 Exoskeleton concept**

Musculoskeletal models could indeed be very useful right from the beginning of exoskeleton design. Firstly, models could help to understand if a specific task results in excessive loading and if the intervention of external assistance through an exoskeleton is needed. The biomechanical effort in a task could be compared to the effort in reference activities such as normal gait, which is a natural activity that we routinely perform for extended periods. Tröster et al. 2020 compared the biomechanical load of nursing staff during the handling of patients in a surgical department to reference loads in gait and a box lifting task. The comparison was used to quantify the excessive loading in the handling of patients.

Once the requirement of an exoskeleton to assist a specific task has been established, the design process of an exoskeleton would usually begin with defining a concept. Questions such as which joint should be assisted and how much assistance should be provided must be answered. Musculoskeletal models can help answer these questions purely virtually, without even considering the mechanical design of the exoskeleton. Shourijeh et al., 2017 looked at the estimated metabolic energy consumption using musculoskeletal models in a simulated box-lifting task. The kinematics of the model was predicted using an assumed vertical movement of the box. The study then modelled idealized

assistive torques proportional to the joint angles directly at the hip, knee, and ankle joints of the human model. In a parametric study, the authors varied the stiffness constant of the assistive torque for each joint individually and found that assistance at the hip joint led to the least metabolic energy consumption. Agarwal et al., 2010 also considered ideal assistive torques applied directly to the elbow joint in an arm curl motion with a load applied at the hand. They compared constant and variable ideal torques before modelling an exoskeleton mock-up and investigating the kinematic compatibility.

The key advantage of exoskeletons is that they are wearable, and they should permit the user to walk freely. Once a concept is identified, it could be relevant to go back to the natural biomechanical activities, such as gait, and apply the identified assistive torque in a simple gait simulation to investigate if there are unwanted consequences of the assistance concept during gait. Subsequently, an actuator concept could be designed from the ideal assistive torque defined previously. Design choices such as a rotational or linear actuator could be investigated using musculoskeletal models. Based on an actuator concept and the assistive torque identified previously, the actuator specifications could be determined such as motor power (Bai and Rasmussen 2011), or the stiffness constant of an elastic element in passive assistance. Technological and economic considerations of different concepts, such as active or passive assistance, should also be explored before selecting the actuator concept.

### **1.2.2 Exoskeleton model**

Finally, a digital mock-up of the exoskeleton can be built, defining the mechanical structure of the exoskeleton. This digital mock-up could be used to investigate the practical issues of exoskeletons that could be divided into kinematic and kinetic investigations.

### **Kinematic investigation**

Kinematic compatibility between the user and exoskeleton is an important issue. Exoskeletons can reduce the range of motion (Baltrusch et al. 2018; Kim et al. 2018). Kinematic compatibility can be divided into two separate issues. A kinematic mismatch occurs when the exoskeleton does not have all the degrees of freedom (DOFs) of the human and this is very much a design decision (Stegall et al. 2013; Olivier et al. 2015). The other issue is joint misalignment (Schiele and van der Helm 2009; Zanotto et al. 2015). Replicating the kinematic structure of the human model is generally the target of exoskeleton design. It not only allows a natural movement of the user but also allows for effective transmission of the assistive torque from the exoskeleton to the user (Naf et al. 2018; Mallat et al. 2019). In fact, all 26 industrial exoskeletons in the review article of de Looze et al., 2016 were anthropomorphic, that is, they had the exoskeleton joint axes aligned with the human joints. Nonetheless, human anatomical joints, such as the knee or shoulder, are complex joints with moving axes. These joints are often

simplified to ideal fixed axes joints in exoskeleton design. Thus, at least a minimal misalignment will be present and often some mechanism to compensate for the misalignment could be considered in the design of the exoskeleton.

Kinematic compatibility can be studied using multibody models by integrating a human model and a computer-aided design (CAD) model of the exoskeleton. Ferrati et al., 2013 used a musculoskeletal model to simulate its interaction with a real exoskeleton. They created a virtual model of the exoskeleton and improved its kinematic compatibility with the user by adding another degree of freedom (DOF) in the exoskeleton model. Agarwal et al., 2016 considered morphological measures in the virtual prototyping of a hand exoskeleton. Hansen et al., 2018 investigated if a hand exoskeleton model altered the finger kinematics using a musculoskeletal model. Agarwal et al., 2010 looked at the kinematic incompatibility between the joint of a simple exoskeleton model and the elbow joint of a musculoskeletal model.

## **Kinetic investigation**

Kinetic interactions are also the subject of some studies optimizing the mechanical structure of the exoskeleton. Tröster et al. 2020 optimized the attachment point of an upper limb exoskeleton model to the human using a musculoskeletal model by studying the estimated glenohumeral joint reaction force in a dynamic task. Panero et al., 2020 studied different locations of the exoskeleton assistance joint of a trunk exoskeleton in a dynamic lifting task using a multibody human model. They defined maps of favourable and unfavourable locations of the exoskeleton joint considering the torque at the human trunk and estimated interface forces for both stoop and squat lifting strategies. Cho et al., 2012 investigated two different configurations of attachments between the user and exoskeleton using a musculoskeletal model and considering the human joint torques in the two configurations.

Finally, with a detailed CAD model of the exoskeleton, the assistance from the exoskeleton model could be optimized considering biomechanical outputs. A detailed CAD model can allow a more realistic estimate of the mass and inertia properties of the exoskeleton, and these could be fed into the analyses. The exoskeleton assistance tends to be a key research question and there are indeed several studies that optimize the exoskeleton assistance or make parametric studies with different assistance (Zhou et al. 2012, 2015, 2017; Agarwal et al. 2016; Guan et al. 2016; Harant et al. 2017; Jensen et al. 2018; Tröster et al. 2018, 2020). Further, a detailed CAD model could also allow a study of the attachment points of the assistive element. Often, passive exoskeletons are designed to allow some adjustment of the path of the elastic element, thereby changing the moment arm and the assistance provided. For such exoskeletons, not only the stiffness constant but also the attachment point of the elastic element can be optimized (Guan et al. 2016; Jensen et al. 2018). The use of musculoskeletal models can be especially relevant in rehabilitative exoskeletons where subject-specific injury



level could be considered in the optimization of the exoskeleton assistance (Agarwal et al. 2016; Zhou et al. 2017; Jensen et al. 2018).

With a detailed CAD model of the exoskeleton, some studies have also considered the simulated human-exoskeleton interaction forces or pressure using multibody models (Cho et al. 2012; Harant et al. 2017; Jung et al. 2017; Zhou et al. 2017; Panero et al. 2020; Tröster et al. 2020). Cho et al., 2012 used a conditional contact model to simulate the effect of adding straps in a human-exoskeleton model using musculoskeletal modelling. The contact forces at the strap were generated by contact elements that were distributed along the strap surface. The contact elements generated unknown forces that were estimated, along with the muscle forces, as the solution of an optimization problem. Jung et al. 2017 also used a similar contact model approach to simulate the interaction forces between the human and exoskeleton and their model could provide interaction forces although the study did not report any results of the estimated interface forces. Instead, Harant et al., 2017; Panero et al., 2020; Zhou et al., 2017 modelled the human-exoskeleton interface forces through the reaction forces associated with the kinematic constraints that were added for attaching the exoskeleton to the human model. Tröster et al. 2020 also looked at the estimated pressure forces at the interface, although the study does not mention the kinetic model of the human-exoskeleton interface forces.

### **1.3 Human-exoskeleton interface modelling**

The human-exoskeleton interface forces are an important consideration in the use of exoskeletons. Some industrial exoskeletons lead to an increased localised discomfort at the human-exoskeleton interface (Bosch et al. 2016; Huysamen et al. 2018b). This could hinder the user comfort and acceptance as the exoskeletons must be used over extended periods in the industrial context (Bosch et al. 2016; de Looze et al. 2016). In the case of rehabilitative exoskeletons for spinal cord injury patients, the interface forces or pressures can be even more critical. The patients may have sensory limitations and extended use of exoskeletons can lead to pressure-related injuries. This has motivated the development of systems for real-time monitoring of interface forces (Rathore et al. 2016) and pressure (Tamezduque et al. 2015). Some other works have also looked into measuring the human-exoskeleton interface pressure or forces (De Rossi et al. 2010; Georgarakis et al. 2018). Indeed, the design of the human-exoskeleton interface is being recognized as relevant to ensure comfort during exoskeleton use (Levesque et al. 2017; Sposito et al. 2019). Moreover, there is active specialized research in the identification of discomfort thresholds for soft human-exoskeleton interface forces (Yandell et al. 2020) and pressures (Kermavnar et al. 2020a, b). There is an increasing interest in understanding the human-exoskeleton interface and it will continue to grow as specialized instruments to quantify the interface forces or pressure will become commonly available.

On the modelling side, not enough progress is being made towards using contact models in human-exoskeleton interaction. As mentioned previously, only

two studies used a contact model to simulate the human-exoskeleton interface forces (Cho et al. 2012; Jung et al. 2017). Recently, Mouzo et al., 2020 reported a multibody model-based method to estimate the contact forces of a lower leg exoskeleton (orthoses). However, the method must be calibrated one time with at least one force/torque sensor, thereby requiring a prototype. Furthermore, there are also models that consider the viscoelastic nature of the interface dynamics. However, the development of accurate models requires experimental work with a prototype exoskeleton. Schiele 2008 modelled the interaction forces due to the misaligned joint axes between the user and the exoskeleton using viscoelastic models of the coupled human-exoskeleton interface. A key challenge in using this approach is to obtain reliable estimates of the model parameters such as the stiffness constant of the coupled system. Alternatively, the interface power could be estimated as the dot product of the actuating force and the relative velocity between the human and the exosuit at the interface (Yandell et al. 2017). This could be used to investigate the energy absorbed and returned due to the viscoelastic nature of the interface during the entire assistive cycle of the exosuit. The findings of Yandell et al. 2017 were used by Gordon et al. 2018 to modulate the assistive force profile in the inverse dynamics analysis. This brings us to another issue, that is, the integration of the viscoelastic models in the classical inverse dynamics analysis that requires a priori the kinematic data, particularly, the relative motion between the human and exoskeleton due to the elastic deformation, which itself depends on the interface force. More sophisticated modelling methods, such as force-dependent kinematics (FDK) (Andersen et al. 2017), could be used to predict the elastic deformation and the relative human-exoskeleton motion in the inverse dynamics analysis using a quasi-static strategy. FDK has been predominantly used to study non-conforming joints (Marra et al. 2015; Halonen et al. 2017; Andersen et al. 2017), however, Rasmussen et al. 2014 applied the FDK modelling approach to demonstrate the change in H-point location in a cushioned seat in response to the pedal forces in the case of emergency braking.

Generally, the kinetic interaction between the human and exoskeleton is simulated through the reaction forces/moments typically associated with the kinematic constraints that are used to co-simulate the kinematics of the human and exoskeleton model (Ferrati et al. 2013; Agarwal et al. 2016; Guan et al. 2016; Harant et al. 2017; Zhou et al. 2017; Gordon et al. 2018; Jensen et al. 2018; Panero et al. 2020). In a few studies, the kinetic interactions are simulated using force-generating elements, which simulate the interaction force through the solution of the same optimization algorithm that determines the muscle forces in the model (Fournier et al. 2018; Tröster et al. 2018). The concept of using force-generating elements to simulate the interface forces is similar to the contact elements used in the contact models (Cho et al. 2012; Jung et al. 2017). Functionally, the force-generating element is identical, however, the configuration of the elements is different. Fournier et al. 2018; Tröster et al. 2018 simulate interface forces at a point and not as contact at the interface. Furthermore, despite

the evidence of different kinetic interaction models, no study has yet investigated the effect of the choice of the interaction model on the model outputs.

## **1.4 Aim of the thesis**

A research gap was identified in the current modelling practises of the human-exoskeleton interface. The kinetic interactions between the human and exoskeleton are generally simulated as point forces at the interfaces. This is an accepted method in multibody dynamics and has been the default approach for biomechanical investigations. However, this approach limits the possibility to investigate different interface shapes. Thus, the aim of this thesis is to develop methods for using contact models in the human-exoskeleton analysis. This thesis will focus on contact between rigid bodies, which allows the model to be more generic and readily applicable, especially during the virtual design phase, as compared to viscoelastic models of the interface. Although contact models have been used in the past (Cho et al. 2012; Jung et al. 2017), this thesis aims to make a more detailed investigation into the modelling methods and focuses on the methods rather than the physiological function of the exoskeleton. Moreover, the contact model has been used and validated extensively in ground reaction force prediction (Fluit et al. 2014; Karatsidis et al. 2017; Skals et al. 2017). This thesis aims to disseminate the details of the modelling methods for applying the contact model on two vastly different exoskeletons that will illustrate some of the practical issues in modelling the human-exoskeleton interaction for different types of interfaces. The primary aim of using musculoskeletal models is to make a biomechanical assessment of the exoskeleton in different stages of the design and evaluation process. In this regard, the thesis will consider the use of kinematic constraints and the associated reaction forces as the standard approach and compare the biomechanical evaluations from the contact model with the conventional model using kinematic constraints. As such, no work exists that compares the different methods to model the interface forces and this thesis will attempt to fill this gap. If the biomechanical assessment from the two models is similar, the contact model could provide an added layer of information that could potentially be used to consider different interface shapes.

Exoskeleton research is evolving rapidly and that has drastically changed the state of the art during the development of this thesis over the last three years. While the thesis was motivated by the lack of realistic interface modelling methods, the need for realistic models has been further accentuated in parallel by the current research on the human-exoskeleton interface. As mentioned in section 1.3, there is active research in quantifying the interface forces and pressure. Specialized instruments are being developed for this purpose and investigations are being made to define discomfort thresholds. As new empirical quantitative data for human-exoskeleton interface forces and pressure becomes available, contact models could add another dimension in the design of exoskeletons, especially their interfaces.

To summarize, the goals of this thesis are:

- Develop and disseminate methods for applying a contact model to simulate the forces at the human-exoskeleton interface of two different types of exoskeletons. The first exoskeleton consists of a single interface of a generalized shape but provides support from a single side. The second exoskeleton consists of multiple interfaces wrapping completely around the limb and providing support from all sides.
- Compare the biomechanical and interface outputs from the contact model with those from the conventional model of simulating interface forces using reaction forces associated with kinematic constraints for both the exoskeletons.

## 1.5 Structure of the thesis

Simulating contact at the human-exoskeleton interface brings several considerations that must be addressed. First and foremost is the intricate shape of the interfaces. Exoskeleton interfaces are often characterized by the presence of moulded surfaces to fit the shape of the user or cuffs that wrap around the limbs of the user. Another layer of complexity is added by the presence of multiple interfaces that are used to transfer the load from one part of the body to another. Thirdly, the exoskeleton assistance could create additional challenges.

This thesis works its way from a simple case of a contact model applied in a human-exoskeleton interface to a more complex case. The contact model is applied to two different exoskeletons. The first exoskeleton consists of a single human-exoskeleton interface that could be simplified and allows an investigation of the different parameters of the contact model. At first, contact is simulated as contact between planar surfaces. Then, the contact is simulated as contact between curved surfaces. Finally, the contact model is implemented in the second exoskeleton that consists of multiple curved interfaces.

The current chapter provides the aim and motivation of the thesis along with the current state of the art in modelling the human-exoskeleton interface. The rest of the thesis has the following structure:

- Chapter 2 introduces musculoskeletal modelling and describes the modelling methods in general. It describes a general workflow for biomechanical analysis using inverse dynamics analysis. It also describes an existing contact model that has been used to predict ground reaction forces and serves as a reference for the more specific human-exoskeleton contact modelling that is described in the subsequent chapters.
- Chapter 3 simulates the human-exoskeleton interface as a planar surface. It describes the first study where the existing contact model, which has been extensively validated in the prediction of ground reaction forces, was implemented directly at the interface of a lower limb exoskeleton. The exoskeleton consists of a single interface that provides support from a single side of the limb. This interface was

approximated as a planar surface in the first study. This chapter serves as an initial investigation into the application of the contact model to simulate human-exoskeleton interface forces. It compares the results with the conventional model and investigates the parameters of the contact model.

- Chapter 4 simulates the human-exoskeleton interface as a generalized curved surface. It uses the same exoskeleton as from chapter 3 and builds on the findings from chapter 3 to develop methods to apply the contact model to simulate contact forces between curved surfaces. The curved surface is simulated by representing the surface by multiple planar surfaces and implementing the planar contact model from Chapter 3 at each of these planar surfaces. However, this approach leads to unrealistic results and Chapter 4 describes methods to identify and rectify the unrealistic contact forces.
- Chapter 5 simulates the contact on a different exoskeleton. This exoskeleton represents a more generic example of modelling an exoskeleton than the first exoskeleton from chapters 3 and 4. Contrary to the first exoskeleton, the second exoskeleton consists of multiple interfaces that wrap around the limb. The contact forces are simulated by the same approach of representing the curved interfaces by multiple planar surfaces. However, the use of the contact model could lead to unrealistic results, especially when using real data. Practical issues such as human-exoskeleton joint misalignments using actual data collected in a lab could affect the virtual analysis of exoskeletons. Chapter 5 presents a method to simulate contact forces that could also allow the evaluation of existing exoskeletons using real data. Indeed, when compared to chapter 4, the differences in the two exoskeletons result in a different method to rectify the unrealistic results.
- Chapter 6 discusses the overall work. It compares the findings from the three studies. Furthermore, it compares the contact and conventional model in terms of modelling methods, besides the outputs from the models. The chapter also expands on the limitations faced during the development of the thesis.
- Chapter 7 summarizes and concludes this thesis.
- Chapter 8 indicates possible future work.

Chapters 3, 4, and 5 form the principal contribution of this thesis and each of these chapters follows the standard structure of scientific writing: Introduction, methods, results, discussion, and conclusion. The work in chapters 3 and 4 was developed with support from Fiat Chrysler Automobiles (FCA) and its research and development subsidiary, Centro Ricerche Fiat (CRF), in Turin, Italy. FCA conducted several studies investigating different industrial exoskeletons for their assembly lines (Spada et al. 2018, 2019a, b). The Ergonomics groups in FCA and CRF kindly provided access to the exoskeleton, their laboratories and data from their experiments, while the scientific investigation into the modelling of the

human-exoskeleton interface was the contribution of the author of this thesis. The work in chapter 5 was developed as a result of a three-way research cooperation between the Politecnico di Torino (Turin, Italy), the Leipzig University of Applied Sciences (HTWK Leipzig) (Leipzig, Germany), and Aalborg University (Aalborg, Denmark). The exoskeleton used in chapter 5 was being developed by a multi-disciplinary team at the Faculty of Engineering at HTWK Leipzig and a research cooperation was set up with the research groups of Profs. Jens Jäkel and Johannes Zentner. The colleagues from Leipzig organized the trials with the exoskeleton in Leipzig and provided the data required for developing the musculoskeletal models such as the CAD model of the exoskeleton and the mocap data from the lab. However, the human-exoskeleton model and the interface model were developed primarily by the author with valuable inputs from the biomechanical experts at Prof. John Rasmussen's research group in Aalborg University, where the PhD candidate spent a five-month visiting period from February to June 2020. The work described in chapter 5 was predominantly developed in 2020 and was, unfortunately, affected by the various restrictions imposed to contain the pandemic caused by Covid-19. Not only was the data collection in Leipzig delayed and limited, but also the author could not be physically present in Leipzig during the data collection.

# Chapter 2

## Modelling Methods

In this chapter, the basics of musculoskeletal modelling and the workflow for biomechanical analysis are introduced. The purpose of this chapter is to provide details that would be common to the rest of the chapters.

### 2.1 Musculoskeletal modelling

Musculoskeletal modelling is essentially based on multibody dynamics with a focus to model the musculoskeletal structure of living beings. It aims to study the mechanics of the musculoskeletal structure, also known as the biomechanical analysis of the movement of the musculoskeletal system. The skeletal system consists of bones and joints that are generally modelled as rigid bodies (also called segments) connected by idealized joints that constrain the movement in specific degrees of freedom (DOF). Muscles are modelled as force-generating elements that connect two or more segments through their origin and insertion points.

In this thesis, a commercially available software, AnyBody Modeling Systems™ (AMS) (AnyBody Technology A/S, Denmark) was used for musculoskeletal modelling. While the musculoskeletal analyses were conducted with a specific tool, the contribution of the thesis is not limited to the tool itself. The methods used during the development of this thesis are well documented in the literature and could be applied by other researchers, irrespective of the tool. The working and functionality of AMS have been described in the literature and the reader is referred to Damsgaard et al., 2006 for the full and detailed mathematical treatment along with Rasmussen, 2019 for a more detailed and updated description of AMS than can be provided in this thesis. AMS solves the kinematics first and then uses inverse dynamics analysis to solve the kinetics of the musculoskeletal structure. The developers of the software also maintain an open repository of models that can be readily used in AMS. This model repository is known as the AnyBody Managed Model Repository™ (AMMR) (AnyBody

Technology A/S, Denmark) (Lund et al. 2020). Most importantly, the AMMR consists of a detailed human model, which has been built using the work of several researchers.

### **2.1.1 Human model**

As mentioned earlier, the human model is built up of bones that are modelled as rigid segments and muscles that are modelled as force-generating elements. A model can only be as accurate as the input in the model. A key challenge in making the models realistic is to obtain realistic data. Not only is it important to know the dimension and mass of the segments (including the mass of the soft tissue surrounding the bone), but also the size of the muscles and their attachments to the bones. Such data are, naturally, quite difficult to obtain and often cadaver studies are needed to define a detailed model. The human model in the AMMR assembles the effort of different research groups that have provided detailed datasets of different body models. For instance, the leg model is based on the Twente Lower Extremity Model (TLEM) that was originally based on the work described in Horsman et al. 2007. It has subsequently been updated to the second version, TLEM 2, based on a more recent dataset (Carbone et al. 2015). The leg model consists of the pelvis, femur, patella, tibia, talus, and foot. The hip joint is defined as a spherical joint, while the knee, patellofemoral, talocrural and subtalar joints are defined as hinge joints with a fixed rotation centre and axis. The pelvis connects to the trunk at the L5S1 joint, which is modelled as a spherical joint. The model contains 55 muscle actuators described by 166 muscle-tendon elements. The study also undertook the measurement of the volume of different muscles, which was used to estimate the physiological cross-section area (PCSA) of the muscles. The PCSA is used to define the strength of the muscle model. Further, muscle paths were measured, including via points and wrapping surfaces, which can be subjected to large forces and can be relevant in the analysis. The TLEM 2 model has been integrated into the AMMR since version 2.0.0 (Lund et al. 2017b). The shoulder-arm model is based on the work of the Dutch Shoulder Group (Veeger et al. 1991, 1997; Van der Helm et al. 1992). It consists of three DOFs at the sternoclavicular joint, three at the glenohumeral joint, and two at the elbow joint. A detailed description of the spine model is provided in de Zee et al. 2007.

Finally, the different body models are assembled to represent a roughly 50% European male. Depending on the application, the model can be scaled to different levels of precision. On the simple side, the model can be scaled using standard linear scaling laws that use the height and mass to scale the model. On the other end, advanced image-based morphing methods could be used for subject-specific models necessary in clinical practice (Marra et al. 2015). In this work, the length-mass-fat scaling law is used (Rasmussen et al. 2005) that scales model longitudinally considering the stature. The weight of the subject, along with the fat percentage, is used to scale cross-sectional dimensions of the model, i.e., the width and depth. The fat percentage, if not specified, is estimated from the



body mass index (BMI) using the regression equations from Frankenfield et al. 2001. The scaling law also scales the strength of the muscles using the regression equations, while subject-specific strength measurements could also be used for more precise strength scaling of the model (Castro et al. 2019).

Besides the strength of the muscle, the functional model of the muscle is also important. It determines how the strength of the muscle is affected by the working condition of the muscle such as its length or contraction velocity. The most advanced muscle model in AMS is the three-element muscle model that is based on a modified model of the Hill muscle model (Zajac 1989). It consists of the contractile muscle unit, serial elasticity of the tendon, and passive elasticity of the muscle. The strength of the muscle model depends on the working condition of the muscle through the force-length and force-velocity relations of the muscle. It also accounts for other properties such as the pennation angle of the muscle fibres. Alternatively, there is also a simple muscle model that only considers the contractile muscle element and models the strength of the muscle as a constant throughout the working conditions of the muscle.

### 2.1.2 Kinematics

Kinematics analysis aims to determine the position ( $\mathbf{q}$ ), velocity ( $\mathbf{v}$ ), and acceleration ( $\dot{\mathbf{v}}$ ) of the mechanical system during the entire period of the analysis to feed in the inverse dynamics analysis. The kinematics are solved using the full Cartesian formulation, where the configuration of each unconstrained rigid segment can be described using three translations and three rotations in the Cartesian coordinate system (Nikravesh 1988). To avoid singularity problems, the three rotations are, instead, described using four Euler parameters, with the four parameters related by an equation. Thus, the  $i^{\text{th}}$  segment is described by the coordinates  $\mathbf{q}_i = [\mathbf{r}_i^T \mathbf{p}_i^T]^T$ , where  $\mathbf{r}_i$  is the global position vector of the centre of mass and  $\mathbf{p}_i$  is the vector of the four Euler parameters. The velocity of the segments is defined as  $\mathbf{v}_i = [\dot{\mathbf{r}}_i^T \omega'_i{}^T]^T$ , where  $\omega'_i$  is the angular velocity of the segment measured in its body-fixed reference frame. Then, the coordinates of a system composed of  $n$  segments can be assembled and written as position vector  $\mathbf{q} = [\mathbf{q}_1^T \mathbf{q}_2^T \dots \mathbf{q}_n^T]^T$  and velocity vector  $\mathbf{v} = [\mathbf{v}_1^T \mathbf{v}_2^T \dots \mathbf{v}_n^T]^T$ . The solution to the kinematics requires that sufficient information is provided in the system in the form of kinematic constraints, which are usually of two types. The different segments in the system are usually linked to each other through joints, giving rise to holonomic constraints. Secondly, there are constraints, known as kinematical drivers, that are time-dependent and describe the motion. The first step of kinematics analysis is the position analysis where all the kinematic constraints are written in the form of

$$\Phi(\mathbf{q}, t) = 0 \quad (1)$$

The equation (1) is generally a non-linear system of equations and is solved by the Newton-Raphson method. Its solution allows determining the position of all the coordinates of the system. Subsequently, velocity analysis is performed by

taking the time derivative of the constraint equation (1), resulting in a linear set of equations in terms of velocities.

$$\Phi_{\hat{\mathbf{q}}}\mathbf{v} = -\Phi_t \quad (2)$$

where  $\Phi_{\hat{\mathbf{q}}}$  is the Jacobian matrix of the constraint equations with respect to a virtual set of positions,  $\hat{\mathbf{q}}$ , that corresponds to  $\mathbf{v}$ .  $\hat{\mathbf{q}}$  are not meaningful as finite values due to the rotational entries in  $\mathbf{v}$ , but they make sense as infinitesimal values in differentiation (Damsgaard et al. 2006).  $\Phi_t$  is the partial derivative of the constraint equations with respect to time. Finally, acceleration analysis is performed by taking the time derivative of the velocity equations, resulting in a linear set of equations in terms of accelerations.

$$\Phi_{\hat{\mathbf{q}}}\dot{\mathbf{v}} = \boldsymbol{\gamma}(\mathbf{q}, \mathbf{v}, t) \quad (3)$$

A key requirement for the solution of (1) is that sufficient information about the mechanical system is available, that is, the number of constraint equations is at least equal to the number of unknown coordinates describing the system. This is known as a kinematically determinate system. If sufficient information about the mechanical system, in terms of constraints from joints and drivers, is not available then the system is kinematically indeterminate and cannot be solved to a unique solution. On the other hand, if the mechanical system has more constraints than the coordinates in the system, then the system is kinematically over-determinate. This can happen in two ways: the same constraint is somehow added multiple times and leads to redundancy in the system, or conflicting constraints are added in the system. Only the latter is considered as kinematically over-determinate. Redundant constraints can be dealt with quite simply by ignoring them and returning the system to a kinematically determinate state. Conflicting constraints, instead, cannot be solved without violating some constraints.

Kinematically over-determinate systems are quite common in biomechanical analysis using musculoskeletal models. Musculoskeletal models are often driven using data collected with motion-capture (also known as mocap) systems. Two types of mocap systems, optical and inertial, are commonly used in biomechanical analysis. Optical systems consist of markers that are stuck on to the subject and their position is recorded using multiple cameras to reconstruct the 3D trajectories of the markers. Inertial systems consist of sensors that contain gyroscopes and accelerometers and are attached to the subject. It is beyond the scope of the thesis to compare the two systems and it focuses on the optical system as it was used in one of the experiments in this thesis. In the optical system, typically at least three markers are attached to every segment giving at least nine drivers to define the six independent DOFs of the segment. Optical systems are susceptible to noise and errors, like any measurement. A key source of noise in the measurement of human movement comes from the location of the markers (or sensors in the inertial systems) on the skin. There is relative motion between the skin and the bone during the movement due to the elastic nature of the skin. Muscles can bulge underneath the skin, or the skin can be stretched at extreme joint angles. The error or noise in the measurement due to the relative movement between the skin and bone are known as soft tissue artefacts (STA). Another source of error could be

the inaccuracy in the location of the markers in the model in comparison to the location of the actual markers on the subject. Further, the rigid segments are generally constrained by ideal joints in the model that may not be sufficient to capture the motion of actual joints in the human body. There could also be errors in the recording of the markers by the cameras and the subsequent reconstruction of the marker trajectories. Thus, a kinematically over-determinate state is achieved quite easily when working with real measurements.

A method to solve a kinematically over-determinate system by allowing the violation of some constraints was developed by Andersen et al., 2009. The method classifies the kinematic constraints as hard ( $\Phi(\mathbf{q}, t)$ ) or soft ( $\Psi(\mathbf{q}, t)$ ) constraints. Hard constraints must always be respected such as the joints between the segments, while soft constraints can be violated such as the drivers from the markers. The soft constraints are solved as well as possible through an optimization problem that minimizes the weighted least-square errors in the constraints at each time-step

$$\begin{aligned} \min_{\mathbf{q}} \quad & G(\Psi(\mathbf{q}, t)) \\ \text{s.t.} \quad & \Phi(\mathbf{q}, t) = 0 \end{aligned} \quad (4)$$

where  $G(\Psi(\mathbf{q}, t))$  is the scalar objective function of the soft constraints that can be violated

$$G(\Psi(\mathbf{q}, t)) = \frac{1}{2} \Psi(\mathbf{q}, t)^T \mathbf{W}(t) \Psi(\mathbf{q}, t) \quad (5)$$

where  $\mathbf{W}(t)$  is the time-dependent weight matrix. In addition, the method reported in Andersen et al., 2010 allows identifying the constant parameters of the model such as model marker locations, segment lengths, or joint axes from the experimental marker data using an optimization routine. It would be prudent of the modeller to make a distinction between markers placed on bony landmarks and markers placed elsewhere on the body when considering the optimization routines mentioned above. Markers on bony landmarks would show lower STA and can be located more accurately in the model to be considered as fixed markers in the optimization routines.

### 2.1.3 Kinetics

Once the kinematics are solved, the kinetics are solved through the inverse dynamics analysis by setting up the dynamic equilibrium equations. Newton-Euler equations are set up for each segment and use the kinematics data from the previous step along with the mass and inertia data of each segment to find the sum of all the forces and moments acting on each segment:

$$\begin{bmatrix} m_i \mathbf{I} & \mathbf{0} \\ \mathbf{0} & \mathbf{J}'_i \end{bmatrix} \dot{\mathbf{v}}_i + \begin{bmatrix} \mathbf{0} \\ \tilde{\omega}'_i \mathbf{J}'_i \omega'_i \end{bmatrix} = \mathbf{g}_i \quad (6)$$

where  $m_i$  and  $\mathbf{J}'_i$  are the mass and inertia tensor referring to the body-fixed reference frame.  $\mathbf{g}_i$  is the total force, containing the three forces and the three moments in the body-fixed reference frame. The forces are divided into internal forces caused by the muscles ( $\mathbf{g}_i^{(M)}$ ) and reaction forces at the joints ( $\mathbf{g}_i^{(R)}$ ) and external forces caused by known loads ( $\mathbf{g}_i^{(app)}$ ) such as gravity, ground reaction

force (GRF), and any other applied load to the model such as holding a box of a given weight or exoskeleton assistance. The dynamics equilibrium equation is set up as:

$$\mathbf{C}\mathbf{f} = \mathbf{d} \quad (7)$$

$\mathbf{C} = [\mathbf{C}^{(M)}\mathbf{C}^{(R)}]$  is the coefficient matrix of the unknown internal forces,  $\mathbf{f} = [\mathbf{f}^{(M)T}\mathbf{f}^{(R)T}]^T$ , where M and R refer to the muscle and joint reaction forces, respectively. On the right-hand side,  $\mathbf{d} = [\mathbf{d}_1^T \mathbf{d}_2^T \dots \mathbf{d}_n^T]^T$  is the vector of the known external and inertial forces, where

$$\mathbf{d}_i = \mathbf{g}_i^{(\text{app})} - \begin{bmatrix} m_i \mathbf{I} & 0 \\ 0 & \mathbf{J}'_i \end{bmatrix} \dot{\mathbf{v}}_i - \begin{bmatrix} 0 \\ \tilde{\omega}'_i \mathbf{J}'_i \omega'_i \end{bmatrix} \quad (8)$$

The dynamics equilibrium equation (7) would have infinitely many solutions as the number of unknown muscle forces far exceeds the DOFs in the model. Thus, an optimization problem is set up to recruit the muscles in a way to replicate the central nervous system. The optimization problem is defined on the assumption that the physiological phenomenon of recruiting muscles is based on doing a task in the most efficient way, i.e., by expending the minimum effort possible. The optimization problem, also known as the muscle recruitment problem, is then framed to minimize the effort required:

$$\min_{\mathbf{f}} H(\mathbf{f}^{(M)}) = \sum_{i=1}^{n^{(M)}} \left( \frac{f_i^{(M)}}{N_i^{(M)}} \right)^p \quad (9)$$

subject to:

$$\mathbf{C}\mathbf{f} = \mathbf{d} \quad (10)$$

and

$$f_i^{(M)} \geq 0 \quad \text{for } i = 1 \dots n^{(M)} \quad (11)$$

The equation (9) is a polynomial function of the normalized muscle forces and the power  $p = 3.0$  is used in this work. However, it is not the only function and there could be other functions of the effort required (Rasmussen et al. 2001). The effort required is measured by the ratio  $f_i^{(M)}/N_i^{(M)}$  where  $f_i^{(M)}$  is the force produced by the  $i^{\text{th}}$  muscle and  $N_i^{(M)}$  is its strength. This ratio is also known as muscle activity and is used as a measure of the activation of the muscle. Constraint (10) has been described above and constraint (11) restricts the muscles to unidirectional force generation as the muscles can only pull and not push.

#### 2.1.4 Ground reaction force prediction

As described in section 2.1.3, the known external forces are used to calculate the internal muscle and joint reaction forces (10). The ground reaction force (GRF) is a crucial component in the external forces. The ground provides support against the force of gravity that always acts on us. The term “ground” is metaphorical in the sense that the subject could be seated, or the model could consist of only the trunk and arms that must be “grounded” such that the model can support its own weight somehow. In the lab, force plates, synchronized with the mocap system, are typically used to measure the ground reaction forces.

However, sometimes force plates are not available and GRF needs to be estimated. A method to predict GRF has been described in Fluit et al., 2014; Skals et al., 2017. The model predicts the GRF through force-generating elements that are modelled like muscles. These force-generating elements are unidirectional and included in the muscle recruitment problem (section 2.1.3) along with the physiological muscles to estimate the GRF.

In the GRF prediction method, contact forces are simulated by creating a contact detection zone on the ground and creating 25 contact nodes under each foot of the model. At each contact node, five force-generating elements (also called contact elements henceforth) are configured to simulate contact forces, approximating a static Coulomb friction model. One contact element simulates the normal contact force. The remaining four contact elements are arranged in the shear directions to simulate the shear contact forces in the positive and negative directions as the contact elements are unidirectional force-generating elements. The contact elements in the shear directions are configured such that the generation of the shear force,  $F_s$ , is accompanied by the generation of a normal force,  $F_n$ , that is related to the shear force ( $F_s = \mu F_n$ ) by the coefficient of friction,  $\mu$ . Thus, the net normal force is the sum of the forces from the dedicated contact element in the normal direction and the normal components created by the contact elements arranged in the shear directions. The ground reaction forces and moments can then be obtained as the resultant of the forces from the contact elements at the 25 contact nodes. Further, force-generating elements are also added to the pelvis to generate small residual forces and moments to improve numerical stability. The magnitude of the residual forces indicates the imbalance in the system that could not be resolved through the dynamic equilibrium equation. Mathematically, with the GRF prediction method, the muscle recruitment problem, equation (9), can be modified to include the contact elements and the residual forces:

$$\min_{\mathbf{f}} H(\mathbf{f}^{(M)}) = \sum_{i=1}^{n^{(M)}} \left( \frac{f_i^{(M)}}{N_i^{(M)}} \right)^p + \sum_{i=1}^{5n^{(C)}} \left( \frac{f_i^{(C)}}{N_i^{(C)}} \right)^p + \sum_{i=1}^{n^{(S)}} \left( \frac{f_i^{(S)}}{N_i^{(S)}} \right)^p \quad (12)$$

subject to:

$$\begin{aligned} \mathbf{C}\mathbf{f} &= \mathbf{d} \\ f_i^{(M)} &\geq 0 \quad \text{for } i = 1 \dots n^{(M)} \\ f_i^{(C)} &\geq 0 \quad \text{for } i = 1 \dots 5n^{(C)} \\ f_i^{(S)} &\geq 0 \quad \text{for } i = 1 \dots n^{(S)} \end{aligned} \quad (13)$$

where  $\mathbf{C}$  is the coefficient matrix of the unknown internal forces  $\mathbf{f}$ ; both with additional terms for the unknown contact and residual forces besides the muscle and joint reaction forces.  $f_i^{(C)}$  is the force of the  $i^{\text{th}}$  contact element,  $n^{(C)}$  is the number of contact nodes,  $N_i^{(C)}$  is the strength of the  $i^{\text{th}}$  contact element,  $f_i^{(S)}$  is the  $i^{\text{th}}$  residual force,  $n^{(S)}$  is the number of residual forces, and  $N_i^{(S)}$  is the strength of the  $i^{\text{th}}$  residual force. The muscles, contact elements, and the residual forces are weighted equally in the muscle recruitment problem. However, the contact elements have higher strength (0.4 times body weight) compared to the

physiological muscles, ensuring a low activation cost of the contact elements. This would allow the solver to still minimize the muscle forces while estimating the contact forces. Instead, the residual forces and moments have a low strength of 10 N and 10 Nm to ensure a high activation cost of the residual forces. This would ensure that the residual forces are recruited as a last resort to balance the system.

The contact nodes simulate the contact forces only when they are inside the contact detection zone and have a velocity lower than a threshold velocity to distinguish between the static and dynamic phases of the movement. This is implemented by a nonlinear strength function of the contact elements such that the strength is zero when either the contact detection or velocity threshold is exceeded. Further, a smoothing function is defined between the zero and nominal strength of the contact elements to prevent discontinuities in the predicted GRF due to the transition from the inactive to fully active state. This allows a gradual increase of the strength of the contact elements in the transition phase. The reader is referred to Skals et al., 2017 for greater details on the nonlinear strength function and, in general, the GRF prediction method.

The GRF prediction method is well accepted now. It has shown good results in not only activities of daily living (Fluit et al. 2014) and sports (Skals et al. 2017), but also with inertial mocap systems (Karatsidis et al. 2017, 2019; Larsen et al. 2020), allowing the possibility to make measurements outside the laboratory. The GRF prediction model served as a validated contact model that could potentially be adapted to simulate contact forces at the human-exoskeleton interface as well.

## 2.2 Exoskeleton model

Modelling the contact forces at the human-exoskeleton interface would, firstly, require a model of the exoskeleton and its addition into the musculoskeletal analysis. The first step in this process is to add the exoskeleton segments in the mechanical system consisting of the human model to have a combined human-exoskeleton model. The definition of the exoskeleton segments requires the mass, inertia, and centre of mass of the segments. As described earlier in this chapter (section 2.1.2), the addition of each segment in the mechanical system would introduce unknown coordinates in the system. Thus, the next step would be to add the kinematic constraints in the form of joints and kinematic drivers and include them in equation (1). The joints could be between the exoskeleton segments as well as between the human and exoskeleton segments. The kinematic analysis can be completed if as many constraint equations are introduced as the unknown coordinates due to the exoskeleton segments. Moreover, the concept of over-determinate kinematics can be extended to include the exoskeleton as well, for instance, if the motion of an actual exoskeleton is recorded using markers in the optical mocap system. Recall that the description in section 2.1.2 is of a generic mechanical system. Finally, for the inverse dynamics analysis, equation (7) can be extended to include the unknown reaction forces in the exoskeleton joints and their corresponding coefficients on the left-hand side

and the known assistive force of the exoskeleton on the right-hand side. The unknown human-exoskeleton interface forces would also need to be considered in the inverse dynamics analysis and this would be discussed subsequently in the thesis.

Although not strictly necessary, a dedicated 3-dimensional (3D) computer-aided design (CAD) software can immensely benefit the integration of the exoskeleton model in musculoskeletal analysis. The CAD program could be used to make 3D models of the individual segments of the exoskeleton and estimate the mass, centre of mass, and inertia properties of the segment. Moreover, an assembly of the exoskeleton could be created by defining the joints between the exoskeleton segments. The human-exoskeleton interfaces are usually curved surfaces that are designed to match the shape of the corresponding human body part. The CAD software can be especially beneficial if it offers the necessary features to design the intricate shape of the interfaces. The complex interface shapes could be imported in the musculoskeletal analysis as a collection of points by distributing a mesh of reference points on the CAD surface and extracting their position in the body-fixed reference frame.

In this thesis, first, a CAD model of the entire exoskeleton was created or imported into SolidWorks™ (Dassault Systèmes S.A., France). Then, the AnyExp4SOLIDWORKS™ (AnyBody Technology A/S, Denmark) plugin was used for translating the CAD model of the exoskeleton into a script file that could be loaded into AMS and subsequently integrated with the human model. The translation generates the different segments with their corresponding mass, the centre of mass and inertia properties as estimated in SolidWorks. Further, reference features (such as points, planes, axes, etc.) created in the CAD model are also exported as reference nodes with their position and orientation relative to the body-fixed reference frame of the segment. These reference features can be useful for recreating the geometry by identifying the location of the joints or the points for recreating the shape of the interface. Moreover, the add-in allows translating an entire assembly of multiple components, preserving the joints between these components. In case modifications were needed, they could be done directly in AMS or in SolidWorks with a retranslation.





# Chapter 3

## Simulating Planar Surface

In this chapter, the initial investigation of the ground reaction force (GRF) prediction model as a contact model for human-exoskeleton interaction is described. The focus of this chapter is to simulate the human-exoskeleton interface as a planar surface. Part of the work described in this chapter has been previously published in Chander and Cavatorta 2019 and Spada et al. 2019a

### 3.1 Introduction

The aim of this thesis is to develop methods for applying contact models to simulate the human-exoskeleton interface as contact between rigid bodies. As described in the previous chapter (section 2.1.4), the literature already consists of a contact model that has been used to predict the ground reaction forces (GRF). The GRF prediction method uses contact elements that are included in the muscle recruitment problem, along with the physiological muscles, to simulate the contact forces. The method has been validated extensively in the literature. Naturally, the validation studies focussed on the prediction of GRF in different use cases and conditions. This validated model could be adapted for simulating the human-exoskeleton interface. However, the use of the GRF prediction model as a contact model for human-exoskeleton interface brings several considerations that must be addressed due to the use of the contact elements to simulate the contact forces. While the ground is aptly modelled as a planar surface, exoskeleton interfaces are anything but planar. Exoskeleton interfaces are often characterized by the presence of braces to fit the shape of the user or cuffs that wrap around the limbs of the user. Secondly, exoskeletons consist of multiple interfaces that are used to transfer the load from one part of the body to another. Thirdly, the kinetics of the human-exoskeleton system could create additional challenges. Both the kinematics and the assistance provided by the exoskeleton become points of differences between modelling the ground and human-exoskeleton interface.

Therefore, the application of the GRF prediction method as a contact model for human-exoskeleton interface requires that the complexities be broken down and studied incrementally, starting from the simplest model, and moving towards more complex models. The aim of this chapter is to make an initial investigation into the application of the GRF prediction model as a contact model for simulating the human-exoskeleton interface. Initial investigation means to implement the contact model with as few deviations from the GRF prediction model as possible and to understand if the results of the contact model are reasonable. To this objective, a simplified model of the human-exoskeleton interface is developed, and the results of the contact model are compared with the results of the conventional model, utilizing reaction forces associated with a kinematic joint. Furthermore, parameters that affect the results of the contact model are studied. The end goal of this chapter is to understand if the GRF prediction model has the potential to be used as a contact model for simulating the human-exoskeleton interface and, subsequently, to understand the parameters that could be relevant in making more realistic models.

This study was developed with support from Fiat Chrysler Automobiles (FCA) and its research subsidiary, Centro Ricerche Fiat (CRF). At that time, FCA was investigating several exoskeletons for their introduction into the assembly lines (Spada et al. 2018, 2019a, b). One exoskeleton that allowed the possibility to construct a simple model was the Chairless Chair. The Chairless Chair is an exoskeleton that allows the user to replace working with a bent trunk by working in a seated posture. The exoskeleton consists of two load-bearing interfaces or seats, one for each leg, on which the user sits while working. In the seated posture, the interfaces provide support only from the underside of the thighs. Thus, the seats could be reasonably approximated by a planar surface for this simple model even though they have a curved surface. Additionally, the motion of the exoskeleton and the lower limbs is negligible in the seated posture and can be approximated by a static condition. Thus, the overall condition of support offered by this exoskeleton allowed making a couple of assumptions to simplify the model without sacrificing the functionality of the exoskeleton.

## **3.2 Materials and Methods**

### **3.2.1 Exoskeleton**

The exoskeleton used in this study, the Chairless Chair, is a commercially available ergonomic sitting support developed by the Swiss company, Noonee. It is a passive exoskeleton for the lower limbs or as its developers prefer to call it, an “ergoskeleton”. At the time of writing this thesis, the second version of the device is available in the market. However, only the first version of the device was available at the time FCA made its investigations and was thus used for the study.

The Chairless Chair is a wearable device that is developed for use in an industrial setting and it aims to replace working with a bent trunk or a squatting/crouching posture by working in a seated posture. The mechanical

frame of the device consists of two “legs” that mimic the structure of the thigh and the shank with the knee joint between the two. The device is worn through braces and belts around the thighs, waist and over the shoulders. Additionally, there are flexible couplings that connect the feet of the user with the lower end of each frame. In the standing configuration, the frame of the device is loosely attached to the leg of the user through the strap at the thigh and the coupling at the feet. As the user walks, the frame follows the movement of the leg without touching the ground. The device allows fast switching between standing, walking, and sitting. When the user starts to sit, the device makes contact with the ground and starts to bend at its central revolute joint, in correspondence with the knee of the user. The device stops at a user-selected angle, allowing the user to “sit” on the exoskeleton, and supports up to 70% of the subject’s body weight. Thus, the device allows the flexibility to the user to work in a seated posture instead of working with a bent trunk.

The Chairless Chair can be adjusted to the anthropometry of different users. Both the lower and upper frames of the device consist of individual telescopic adjustment. Either telescopic adjuster can be set at one of the four pre-defined stops, allowing a discrete change in the length of the frame of the device. The device must be adjusted to the user’s anthropometry before wearing the device. Once the device is worn, the user can adjust the sitting height by pulling on a lever on the right frame that controls the sitting height of both frames simultaneously. The sitting height of the device is adjusted by changing the stopping angle of the revolute joint between the upper and lower frames as the user sits. In the literal sense, the sitting height, or the distance between the ground and the seat, would also depend on the lengths of the upper and lower frames of the Chairless Chair. But, in the context of this study, the sitting height would refer to the adjustment of the seat height only due to the change in the angle between the upper and lower frames. The sitting height of the device can be continuously adjusted between the lowest sitting height and the highest sitting height allowed by the device. Correspondingly, these end sitting heights will be referred to as the low and high seat configurations of the Chairless Chair. Additionally, a third sitting height, the comfort seat configuration, is defined as the sitting height selected by the user as the most comfortable for the task. A slightly padded but otherwise rigid seat is attached to the upper frame through a slotted joint that allows limited translation along the length of the upper frame and simultaneous rotation about a moving axis parallel to the revolute joint between the upper and lower frame. This joint helps to adapt the seat orientation to the user’s body at different sitting heights.

### **3.2.2 Use Case**

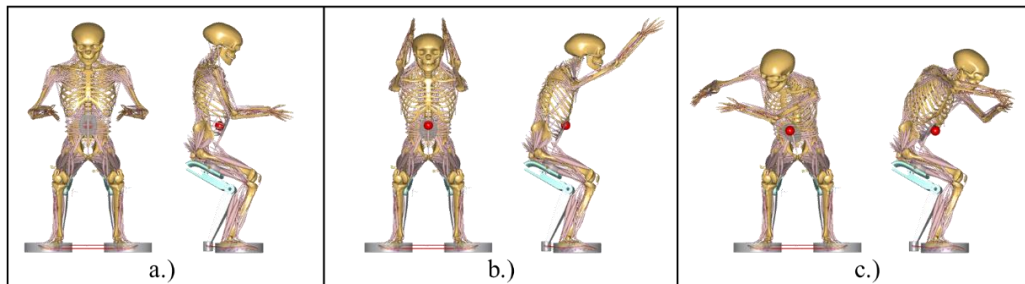
This initial investigation into the application of the GRF prediction method as a contact model was made with support from CRF, who shared the data from their investigations of the body weight distribution between the user and the Chairless Chair. In fact, the modelling study commenced after the data had already been

collected at CRF. The weight distribution was identified as a key performance metric for the interface model. The human-exoskeleton interface of the Chairless Chair allows the user to support a part of his/her weight through the device, resulting in an easily-measurable body weight distribution between the user's legs and the frame of the Chairless Chair. Due to the exploratory nature of this study, it was decided to proceed with the data provided by CRF instead of conducting further trials. This modelling study aimed at investigating the applicability of the contact model at the interface and not the statistical significance of the results.

As described in Spada et al. 2019, several experimental campaigns were conducted by Fiat Chrysler Automobiles (FCA) for their investigations into the introduction of the Chairless Chair in their assembly lines. The operators from the assembly lines volunteered for trials with the exoskeleton in both the laboratory and the factory. The purpose of these tests was for FCA to obtain subjective feedback on the usability of the exoskeleton in the assembly line. The Chairless Chair was also voluntarily tested by 14 technical employees of both genders in an internal study at CRF. They designed tests to verify if the body weight distribution between the user and the exoskeleton remained within a given range regardless of the stature of the user and the sitting height of the Chairless Chair whilst also collecting subjective feedback on the stability of the posture, equilibrium, and comfort. The weight distribution was noted at three sitting heights: the low, comfort, and high seats. Three measurements were taken at each sitting height in the recommended working posture with the hands at elbow height in front of the subject. Results from these tests showed no significant influence of either the anthropometry of the subject or the sitting height of the exoskeleton on the weight distribution. Instead, training and user confidence with the device appeared to be relevant for the effective use of the exoskeleton.

While the studies at CRF focused mainly on the manufacturer-recommended use cases, deviations from the recommended posture, such as reaching a distant point, could also be occasionally encountered during the execution of a task. Thus, the weight distribution of a single subject, trained in the use of the exoskeleton, was also measured in three different conditions to check if it varied substantially with a deviation from the recommended posture. The data collected by CRF for these three conditions were used for the investigation of the interface model. The subject (male, 163.0 cm, and 73.8 kg) simulated working at elbow height, reaching with arms raised and lateral reaching to the right (Figure 2). Both the upper and lower frame of the exoskeleton were set to their smallest lengths to adapt to the anthropometry of the user. The posture was documented through photographs from the front and side view and key joint angles such as knee flexion, trunk flexion, etc. were approximated from the photos. For this initial study on the modelling of the interface, a precise reproduction of the posture was not necessary and approximate postures should have sufficed at capturing at least the trend of the change in body weight distribution in the three different conditions. The weight distribution between the subject and the device was measured by CRF using a simple set-up consisting of a scale placed below the user's feet, while the exoskeleton frame was grounded through a rigid platform

that was raised to the same height as the scale. The body weight distribution allowed calculating at least the vertical component, which is the most significant, of the interface force. Force plates would have provided a greater insight but were neither necessary for the objectives of the study by CRF nor was their laboratory equipped with force plates.



**Figure 2: The three test conditions: a.) Working at elbow height, b.) Reaching with arms raised, and c.) Lateral reaching (to the right). Note: The red sphere is the centre of mass of the mannequin.**

### 3.2.3 Musculoskeletal modelling

Some key concepts of musculoskeletal modelling have been explained in Chapter 2. In this section, details specific to this study will be provided. The musculoskeletal model was built and analysed in version 7.0.1 of AnyBody Modeling Systems (AMS) using the human model available in version 1.6.6 of the AnyBody Managed Model Repository (AMMR) (Lund et al. 2017a). The muscle recruitment problem was solved using the polynomial criterion with power 3 (Rasmussen et al. 2001). The human model was scaled to the subject height (163.0 cm) and weight (73.8 kg) using the length-mass-fat scaling law (Rasmussen et al. 2005). The three-element muscle model, based on the modified Hill muscle model (Zajac 1989), was used after calibrating the model for the tendon lengths.

A CAD model of the Chairless Chair was created in SolidWorks 2012 software. The exoskeleton model was imported into AMS using version 1.1.0 of the AnyExp4SOLIDWORKS plugin for SolidWorks.

#### Human-Exoskeleton model

The human-exoskeleton model required the definition of the kinematic and kinetic interactions between the human and the exoskeleton model. The Chairless Chair is essentially a sitting support and assists in a practically static posture. The lower limbs remain relatively stationary during the use of the exoskeleton. In fact, as mentioned earlier, the Chairless Chair was chosen as the exoskeleton for this initial study as it allowed to simplify the modelling aspects and static simulations were made replicating the posture and position of the subject and the exoskeleton in the three test conditions.

The addition of the exoskeleton model in the mechanical system introduced unknown coordinates in the system. Kinematic constraints were added in the form of joints between the exoskeleton segments and kinematic drivers, that is, the joint

angles. The joint angles approximated from the photos were used to set the posture of the human model and the joint angles of the exoskeleton. Further, the model was superimposed on the photographs to refine the posture and reduce the errors due to the reproduction of postures from 2D images.

The kinetic interactions also needed to be set up for the inverse dynamics analysis. The body weight distribution between the user and the exoskeleton was a key output. Thus, a kinetic path was needed that could allow the exoskeleton to transfer the weight of the subject to the ground. In the model, the ground reaction force (GRF) was predicted using the method reported in Skals et al., 2017. Contact detection zones were created for the right and left foot and 25 contact nodes were created at the bottom of each foot. At each contact node, five contact elements, with strength 0.4 times the body weight, were created and configured to simulate normal and frictional forces as described in section 2.1.4. Weak residuals were also added at the pelvis. The GRF prediction method was also adopted for predicting the forces at the interface between the exoskeleton and the ground. However, only 11 contact nodes were created at the base of each “leg” of the Chairless Chair due to its small area of contact. The strength of the contact elements for the exoskeleton-ground contact was also 0.4 times the body weight. Even though the number of contact nodes at the exoskeleton “leg” was lower than the number of contact nodes at the foot, each exoskeleton “leg” could support up to 4.4 times the body weight, which should have been sufficient for these simulations. Separate contact detection zones were created at the ground for the right and left frames of the Chairless Chair. Further, the joints between the lower and upper frame, and the upper frame and seat were modelled to provide all the reaction forces and moments necessary to support the user. Finally, a kinetic connection between the subject and the exoskeleton was needed and it is described in the next sub-section.

## **Human-Exoskeleton Interface models**

The aim of this study is to investigate the applicability of the GRF prediction method as a contact model for simulating the human-exoskeleton interface force. Secondly, the results of the contact model are to be compared to the conventional approach of simulating the human-exoskeleton interface. Thus, two interface models were built:

The first model (model 1) or the contact model simulated the kinetic interactions at the human-exoskeleton interface using the GRF prediction method. In this initial investigation, the method was applied with as few deviations as possible. The seat of the exoskeleton was considered as the “ground” in the method and a contact detection zone was created on the seat. The contact detection zone was defined by a reference frame on the exoskeleton seat that lay on the central curve along the length of the seat. This reference frame was located at a distance of one-third of the length of the central curve from the front of the seat. This reference frame defined the normal and shear directions of the contact detection zone, which is defined as a planar surface in this way. The contact

detection zone was tangential to the seat surface at the central curve so that the normal to the planar surface was also the normal to the seat surface at the reference frame. The anterior-posterior axis was defined along the length of the seat. On the human side, 21 contact nodes were created on each thigh. The strength of the contact elements was 0.4 times the body weight. In the contact model, overall, there were six implementations of the GRF prediction method with three each (human-exoskeleton, human-ground, and exoskeleton-ground) for the right and left sides. The method introduced three coefficients of friction for the three interfaces, and they were set as 0.5 each, based on a parametric study to check the influence of the three coefficients on the body weight distribution.

The second model (model 2) simulated the kinetic interactions at the human-exoskeleton interface by using reaction forces associated with a rigid kinematic joint between the human and the exoskeleton. This model represented the conventional approach of simulating the human-exoskeleton interface. The reaction forces were added between the same reference frame that was used to define the contact detection zone on the exoskeleton and a reference frame on the thigh that corresponded with the location of the central contact node on the thigh. The reaction forces were added in all the six coordinates (forces in the three translational and moments in the three rotational) to define a “rigid” or “weld” joint between the human and the exoskeleton. Thus, the contact model at the human-exoskeleton interface was substituted by a conventional model based on the kinematic joint. The remaining two interfaces (human-ground and exoskeleton-ground) were maintained the same between the two interface models.

Besides the simulation of the interface forces as contact or point forces, the key difference between the two models can be explained by considering the formulation of the muscle recruitment problem. As described in section 2.1.4, with the GRF prediction method, the formulation is modified to include the contact elements and the weak residuals. Rewriting equations (12) and (13) below:

$$\min_{\mathbf{f}} H(\mathbf{f}^{(M)}) = \sum_{i=1}^{n^{(M)}} \left( \frac{f_i^{(M)}}{N_i^{(M)}} \right)^p + \sum_{i=1}^{5n^{(C)}} \left( \frac{f_i^{(C)}}{N_i^{(C)}} \right)^p + \sum_{i=1}^{n^{(S)}} \left( \frac{f_i^{(S)}}{N_i^{(S)}} \right)^p \quad (14)$$

subject to:

$$\begin{aligned} \mathbf{Cf} &= \mathbf{d} \\ f_i^{(M)} &\geq 0 \quad \text{for } i = 1 \dots n^{(M)} \\ f_i^{(C)} &\geq 0 \quad \text{for } i = 1 \dots 5n^{(C)} \\ f_i^{(S)} &\geq 0 \quad \text{for } i = 1 \dots n^{(S)} \end{aligned} \quad (15)$$

In model 1, the interface force is estimated as contact force via contact elements that are included in equation (14) in the function to be minimized. That is, the contact force is minimized, and its recruitment has a cost associated with the strength of the contact elements. Instead, in model 2, the interface force is estimated as reaction force that is included as constraints in the dynamic equilibrium equation (15). The reaction forces do not have any cost associated with them and infinitely large reaction forces could be generated if they allow minimizing equation (14). For both the models, the reaction forces at the

exoskeleton joints are also included in the dynamic equilibrium equation (15), whereas the contact elements for predicting the GRF for the subject and the exoskeleton are included in equation (14).

### **3.2.4 Analyses**

The experimental data provided the body weight distribution between the subject and the exoskeleton in the three test conditions. In the model, the body weight supported by the subject was defined as the net vertical force at human-ground interface. The body weight supported by the exoskeleton was calculated as the difference between the subject weight and the weight supported by the subject. Further, the biomechanical load in the three conditions was noted by measures of muscle activity and joint moments. Static simulations were developed for the three test conditions to compare the two interface models. The same postures were used for both the interface models. In addition to the model outputs previously mentioned, the predicted interface forces were also compared for the two interface models.

As part of the initial investigation, parameters of the contact model were also studied. As mentioned in the previous section, the influence of the three coefficients of friction (human-exoskeleton, human-ground, and exoskeleton-ground) on the results was studied. Each of the three coefficients was varied from 0.2 to 0.8 in steps of 0.025. This parametric study was performed only for the posture ‘working at elbow height’, typical during the actual use of the Chairless Chair. The other two postures should show a similar influence of the friction coefficients on the results as they have the same posture of the lower limbs. Additionally, a second parameter study was devised to study the angle of inclination of the seat along with the coefficient of friction at the human-exoskeleton interface. The Chairless Chair offered the possibility to adjust the sitting height. However, adjusting the sitting height also changed the inclination of the seat. The low-seat configuration offered a more horizontally aligned seat compared to the high seat. Indeed, subjective feedback from the trials in FCA mentioned an increased tendency to slip at the human-exoskeleton interface in the high-seat configuration. Thus, the high-seat configuration was simulated for the parametric study of the angle of contact of the seat and the coefficient of friction. The angle of contact was varied from the normal inclination of the high-seat configuration to a 28° more horizontal inclination in steps of 1°. The coefficient of friction at the human-exoskeleton interface was varied from 0.2 to 0.8 in steps of 0.025.

## **3.3 Results**

### **3.3.1 Comparison of the two interface models**

Figure 3 shows the empirical and the predicted body weight supported by the exoskeleton in the three test conditions. Both the models captured the trend of



decreasing body weight supported by the exoskeleton as the test condition changes from elbow height to lateral reaching. The average error in the percentage body weight distribution for the reaction force-based model (model 2) was 10% in the elbow height and the arms raised condition. Whereas the error was only 1.5% for the contact model (model 1) in the same postures. Instead, in the third posture, lateral reaching to the right, the reaction force model correctly predicted the body weight distribution, while the contact model overestimated the weight supported by the exoskeleton by 5%. Comparing the two interface models, the reaction force model estimated lower support by the exoskeleton with respect to the contact model in each of the three test conditions.

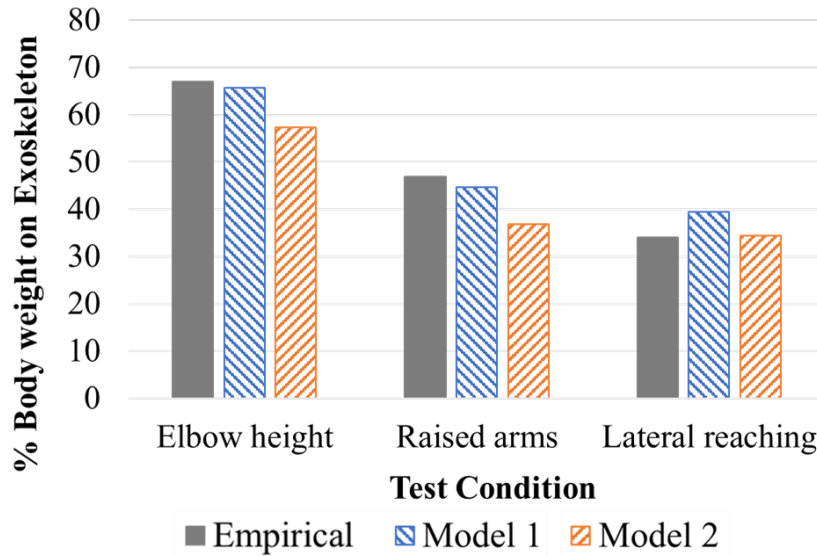



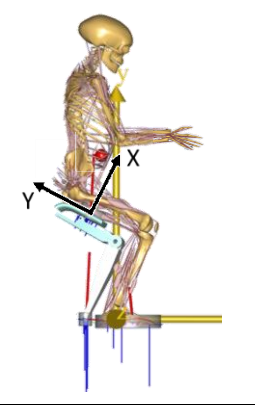
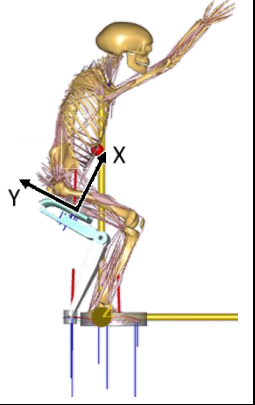
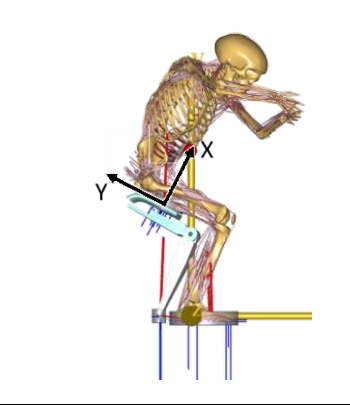
Figure 3: Percentage of body weight supported by the exoskeleton by the contact model (Model 1), the reaction force-based model (Model 2), and empirical values in the three test conditions.

Table 1 compares the interface forces, muscle activation, and joint moment requirements from the two interface models. The table reports the values for both right (R) and left (L) sides only for the asymmetric test condition, lateral reaching to the right. The other two symmetric conditions, working at elbow height and reaching with raised arms, had equal values on both sides. The predicted reaction forces at the human-exoskeleton interface are expressed as a percentage of body weight in the local reference frame that was used to define the interface models. The X-axis was defined as normal to the seat surface with positive upwards. The Y-axis was defined along the length of the seat with the positive direction pointing to the rear of the seat. The Z-axis was defined by the conventional Cartesian system.

While, generally, the two models show similar trends, a key finding in Table 1 is the different trends of the knee extension moment from the two models. In fact, the knee extension moment has been plotted separately in Figure 4. The figure shows the trend line passing through the three test conditions. The trend line passes through the mean of the right and left knee extension moments for the lateral reaching condition. As the test condition changes from elbow height to lateral reaching, the reaction force-based model shows a clear decrease in the knee

extension moment. Instead, the contact model shows a slight increase in the knee extension moment.

**Table 1: Comparison of the two interface models: contact model (Model 1) and reaction force-based model (Model 2)**

Test condition	Working at elbow height		Reaching with raised arms		Lateral reaching (to the right)				
 Local Reference System									
Model	Model 1	Model 2	Model 1	Model 2	Model 1	Model 2			
<b>Estimated reaction forces at the human-exoskeleton interface (percentage of body weight in the local reference system)</b>									
F <sub>x</sub>	30	25	20	15	R: 34	L: 2	R: 23	L: 7	
F <sub>y</sub>	14	17	10	13	R: 17	L: 1	R: 18	L: 4	
F <sub>z</sub>	0	8	0	5	R: 0	L: 0	R: 7	L: 4	
<b>Muscle Activation (percentage)</b>									
Trunk	23	23	40	40	100		100		
Upper Limbs	17	17	45	45	R: 99	L: 79	R: 99	L: 79	
Lower Limbs	4	4	12	12	R: 18	L: 14	R: 18	L: 14	
<b>Joint Moments (Nm)</b>									
Hip extension	20.4	20.4	38.1	38.1	R: 48.3	L: 37.4	R: 48.1	L: 37.6	
Knee extension	10.6	7.5	11.2	5.8	R: 7.6	L: 15.4	R: 3.0	L: 5.2	
Ankle plantar-flexion	9.0	7.1	16.6	13.8	R: 18.7	L: 29.9	R: 15.4	L: 17.4	

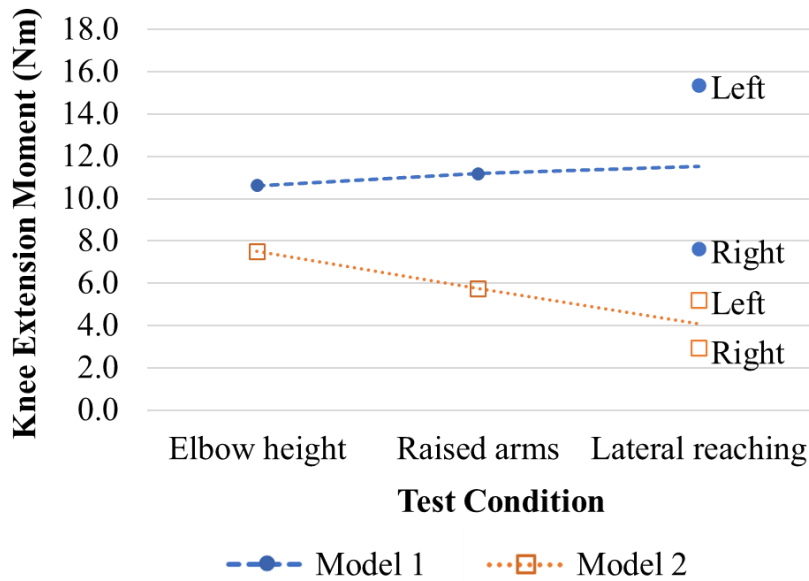


Figure 4: Knee extension moments by the contact model (Model 1) and the reaction force-based model (Model 2). In the case of lateral reaching, the trend line passes through the mean of the right and the left knee extension moment.

### 3.3.2 Parametric studies

The result of the first parametric study of the influence of the coefficients of friction at each of the three interfaces (human-exoskeleton, human-ground, and exoskeleton-ground) on the percentage of body weight supported by the exoskeleton is shown in Figure 5. The coefficients at the human-ground and exoskeleton-ground were treated as equal and denoted by the coefficient of friction at the ground. The plot shows a distinct division into two zones as the coefficient of friction at the human-exoskeleton interface is varied. For coefficients greater than 0.4, the exoskeleton supported 66% of the body weight of the subject. As the coefficient changes from 0.4 to 0.3, a sharp drop in the body weight supported by the exoskeleton is observed. The percentage of body weight supported by the exoskeleton remained largely unaffected by the changes in the coefficient of friction at the ground except for a small transition zone for coefficients lower than 0.3. Additionally, the condition of no support from the exoskeleton was investigated further by studying the key biomechanical outputs. Table 2 shows the percentage of body weight supported by the exoskeleton and the joint moments at the hip, knee, and ankle for different values of the coefficient of friction at the human-exoskeleton interface.

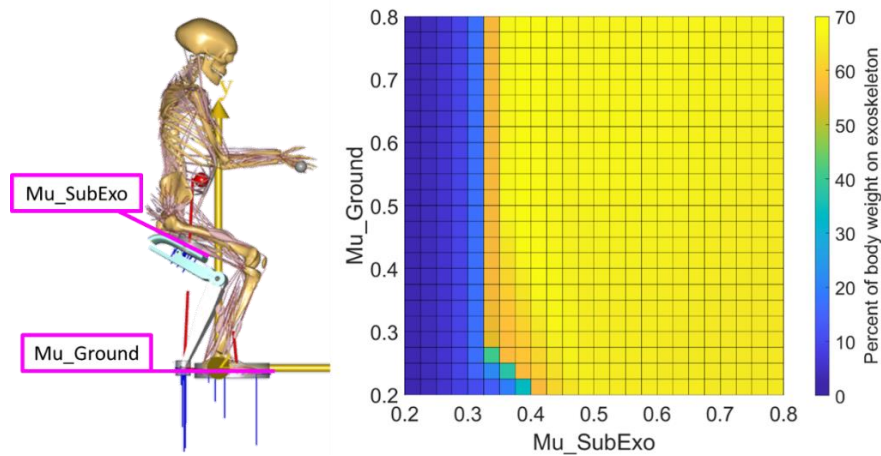


Figure 5: Parametric study of the coefficients of friction at the human-exoskeleton ( $\text{Mu\_SubExo}$ ) interface and ground ( $\text{Mu\_Ground}$ ).

Table 2: Percentage of body weight supported by the exoskeleton and the joint moments at the hip, knee, and ankle joints for different values of the coefficient of friction ( $\text{Mu}$ ) at the human-exoskeleton interface. The coefficients of friction at the human-ground and exoskeleton-ground interfaces are 0.5 each. Negative “-” sign indicates an opposite moment.

Mu at human-exoskeleton	0.6	0.5	0.4	0.3	0.2
% body weight on exoskeleton	66 %	66 %	66 %	17 %	3 %
Hip extension moment (Nm)	20.3	20.3	20.3	20.3	20.3
Knee extension moment (Nm)	10.3	10.6	13.9	53.5	55.4
Ankle plantarflexion moment (Nm)	9.0	9.0	11.1	-7.3	-11.9

The results of the second parametric study of the influence of the angle of the exoskeleton seat and the coefficient of friction at the human-exoskeleton interface are shown in Figure 6. The figure plots the percentage of body weight supported by the exoskeleton as the angle of inclination of the seat and the coefficient of friction are changed.  $0^\circ$  represents the normal inclination of the exoskeleton seat in the high-seat configuration. From this orientation, the angle was increased up to  $28^\circ$  in steps of  $1^\circ$  to achieve a more horizontal orientation of the contact. Again, the figure shows a distinct division into two zones based on the support provided by the exoskeleton, just like in Figure 5. An interaction between the angle of contact and the coefficient of friction can be observed, demonstrating the rather obvious: a more horizontal orientation of the seat required a lower coefficient of static friction for the exoskeleton to effectively support the body weight.

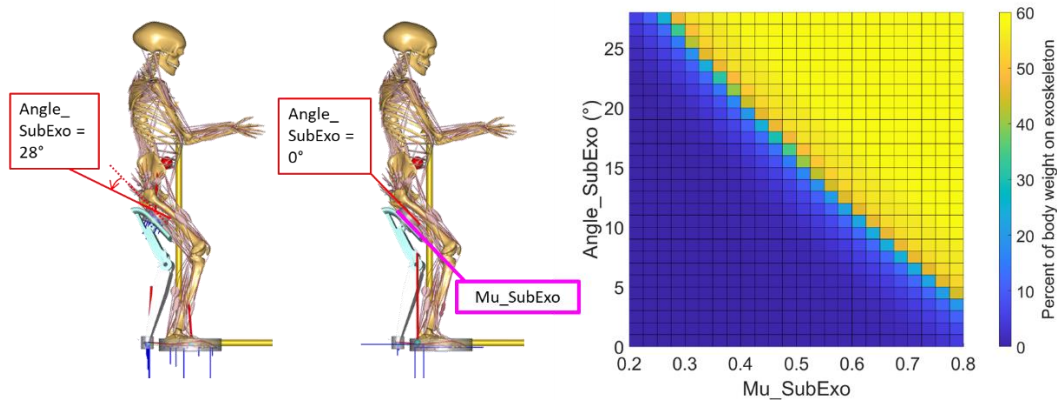


Figure 6: Parametric study of the coefficient of friction at the human-exoskeleton interface ( $\text{Mu\_SubExo}$ ) and the angle of the exoskeleton seat ( $\text{Angle\_SubExo}$ ).

### 3.4 Discussion

#### 3.4.1 Outputs of the two interface models

One aim of this study was to compare the two interface models: the GRF prediction-based contact model and the reaction force-based based conventional model. The comparison considers not only the forces at the interface but also how these forces affect the biomechanical outputs. As far as the body weight distribution is concerned, both the interface models allowed a reasonable body weight distribution given the uncertainty in the reproduction of the postures (Figure 3). The values from both models showed errors of less than 10% in the percentage body weight distribution. More importantly, both models could follow the trend. As the test conditions became more challenging with leaning and reaching, the subject received reduced support from the exoskeleton. This trend was also observed in the predicted body weight distribution from both the interface models with a consistent difference across the three conditions between the empirical and the predicted body weight distributions.

However, it is clear from Table 1 that there are some differences between the two interface models. First and foremost, a difference in the interface forces can be seen. The contact elements in the contact model were configured to simulate the normal and frictional forces and this was reflected in the interface forces of Model 1, where the frictional force along the length of the seat was limited to approximately half the normal force at the seat. It correctly reflected the choice of the coefficient of friction at the human-exoskeleton interface, 0.5. On the other hand, the reaction force-based model did not simulate frictional forces. Resolving the net interface force from Model 2 in the normal and shear components, no consistency could be observed between the ratio of the shear to normal force and the friction coefficient across the three test conditions. Secondly, the contact model showed almost no interface force at the left side in the case of lateral reaching to the right. This would not be very far from a realistic situation of a subject reaching a distant point asymmetrically. Depending on the amount of trunk bending, one of the four supports could become unloaded with the body

weight being distributed between the feet of the subject and the right frame of the exoskeleton.

With regards to the biomechanical outputs from the two interface models, a major discrepancy can be observed in the trends of the knee extension moment across the three test conditions (Figure 4). As the conditions became more challenging and forced the user to support a greater proportion of the body weight through his legs, the contact model showed a small increase in the knee extension moment requirement. On the other hand, and rather counter-intuitively, the reaction force-based model showed a reduction in the knee extension moment despite showing an increase in the body weight supported through the legs of the subject. However, there are limitations in the accuracy of the knee moment without accurate measurement of GRF through force plates. Nonetheless, it is unlikely that the Chairless Chair, which is essentially a sitting support, would be able to reduce the knee extension moment as it becomes less effective. In the reaction force model, the interface supplied the additional forces and, crucially, higher moments that unloaded the knee unrealistically as the test conditions became more critical. With the contact model, the exoskeleton was able to protect the knee from a substantial increase in the extension moment despite the increased body weight supported through the legs of the subject. The effect of the exoskeleton could also be observed in lateral reaching to the right. As the subject leaned to the right, a greater portion of the body weight was supported on the right side (65%) compared to the left side (35%). However, on the right side, the exoskeleton was able to offload a significant proportion of the body weight to the ground. Consequently, it resulted in a reduced knee extension moment on the right side compared to the left side, where almost all the body weight was supported by the left leg of the subject as evidenced by the almost non-existent interface forces on the left side.

At the ankle joint, the ankle plantarflexion moment showed a difference in the values from the two models, but showed similar trends, with both models predicting an increased ankle plantarflexion moment as the test conditions became more challenging. The remaining biomechanical outputs concern the joints of the body (hips, trunk, shoulders) present above the human-exoskeleton interface. Their load depended on the posture of the upper half of the body and was unaffected by the interface model. In fact, their values were virtually the same from both the models as the same postures were used for both the models.

To conclude this subsection on the comparison of the biomechanical outputs from the two interface models, it appeared from the knee extension moment that changing the interface model can change the results of the biomechanical analysis. Critically, the two interface models showed different trends of the key biomechanical outputs for the same inputs. These outputs are directly affected by the assistance from the exoskeleton. Different interface models simulate the interface forces differently and these external forces to the human model could generate different muscle forces. However, these results are based on the study of a single subject and a detailed investigation with multiple subjects would be needed to generalize the conclusions. Nonetheless, the human-exoskeleton

interface model must be given due attention, especially in purely virtual assessments of exoskeletons (Agarwal et al. 2016; Zhou et al. 2017; Jensen et al. 2018). The author is not aware of other past works comparing different interface models between the human and the exoskeleton.

### 3.4.2 Parametric studies

The contact model simulates normal and frictional forces, and this introduces parameters such as the coefficient of friction that can affect the results of the model. The contact model potentially allows the investigation of different interface materials and how their properties could affect the effectiveness of the exoskeleton. This could be considered as an advantage of the contact model over the reaction force model. As part of the initial investigation of the GRF prediction method as the human-exoskeleton interface model, it was of interest to study how the coefficient of friction could influence the results of the model.

The results of Figure 5 indicated the importance of the coefficient of friction at the human-exoskeleton interface compared to the coefficient at the ground. The exoskeleton seat presented an inclined surface to the user. The figure showed the existence of a threshold of the coefficient at the human-exoskeleton interface, below which the exoskeleton was unable to provide support to the user. The role of the frictional force is important on an inclined surface for the subject to not slip. This was subsequently confirmed in the second parametric study that looked at the angle of inclination of the seat and the coefficient of friction at the human-exoskeleton interface simultaneously (Figure 6). The threshold of the coefficient of friction for the subject to be supported by the exoskeleton changed as the inclination of the exoskeleton seat changed. It is important that the contact model was able to capture this interaction between the angle of contact and the coefficient of friction at the interface, especially for an exoskeleton like the Chairless Chair. The Chairless Chair is designed to be used at different sitting heights that change the inclination of the exoskeleton seat. The high-seat configuration presents a more vertically oriented seat compared to the low-seat configuration. Indeed, the increased tendency to slip in the high-seat configuration was noted not only by the subjects in the experimental testing undertaken by FCA but also in another study with the Chairless Chair (Luger et al. 2019; Spada et al. 2019a). The ability of the contact model to consider the angle of contact and the coefficient of friction could be relevant to select appropriate textiles for the seat fabric and the clothing of the user.

The loss of the support from the exoskeleton for low values of the coefficient of friction at the human-exoskeleton interface resulted in the subject supporting the body weight through his legs. Consequently, considering that the same posture was hypothetically maintained, differences in the knee extension moment and the ankle plantarflexion moment could be observed. The moment at the ankle changed its sign indicating a requirement of a dorsiflexion moment. This would indicate a situation where the manikin was no more in equilibrium and would fall backwards as the centre of mass of the manikin was behind its ankles. Instead, at

the knee joint, supporting all the body weight through the legs of the user resulted in a more than five-fold increase in the knee extension moment compared to the condition where the exoskeleton supported 66% of the body weight. The hip extension moment remained unaffected as it was above the human-exoskeleton interface and the same posture was maintained.

In summary, the frictional forces at the human-exoskeleton interface of the Chairless Chair are a relevant aspect of the model. A contact model that is capable to consider the changes in the interface forces due to the changes in the inclination of the seat can allow for making more realistic models. Additionally, the parametric studies confirmed that the choice of the coefficient of friction has a rather binary effect on the effectiveness of the exoskeleton in the model. There is a sharp transition between the effective and ineffective zones. This ensures that identifying a precise value of the coefficient of friction to input in the model is not critical. Reasonable approximations of the coefficient of friction will not influence the results significantly.

### **3.4.3 Limitations**

The Chairless Chair consists of a strap around the thigh to secure the location of the seat relative to the leg of the user, especially during walking. This strap constitutes the human-exoskeleton interface and would have contributed towards the interface forces. However, in the seated posture, the contribution of the strap would have been negligible compared to the support provided by the seat. For the sake of simplicity, the strap at the thigh was not modelled in the contact model. The unidirectional force actuators in the GRF prediction method did not simulate any force that would prevent the separation of the contacting surfaces. However, in the reaction force model, all the six coordinates had reaction forces providing support in both positive and negative directions. This difference in the constraints from the two models might have influenced the comparison between the contact and the reaction force model, especially in the lateral reaching posture with its asymmetry. The rest of the straps were not modelled as they essentially helped the subject to wear the exoskeleton and were not functional for the intended assistance of the device.

Secondly, there were limitations in the reproduction of the empirically observed postures from the photographs. This was especially true for the lateral reaching posture with its asymmetry. However, the three test conditions were substantially different, and it was possible to study the trends despite the approximations in the posture.

Thirdly, the location of the reference frame on the seat that defined the interface was approximated. The approximation was based to an extent on the feedback of the subject, who confirmed that he had no contact at the rear portion of the seat that curved away from the subject in the comfort-seat configuration. However, we had no objective measure of the centre of pressure. The seat of the Chairless Chair has a curved surface that offers a continuously changing angle of contact to the user. The curvature at the rear of the seat is greater than at the



central portion of the seat, and this is useful to allow a more horizontally oriented portion of the seat in the high-seat configuration. We assumed that the rear one-third of the length of the seat was not making contact and then chose the centre of the front two-thirds of the length of the seat as the reference frame. More importantly, the choice was consistent for both the interface models. Translating the reference frame along the length of the seat would have changed the orientation of the reference frame and, consequently, the angle of contact. The influence of the angle of contact was indeed studied through a parametric study for the contact model and it influenced the results of the contact model. Thus, changing the location of the reference frame could have influenced the trends observed across the three test conditions from the two models.

### **3.5 Conclusion**

The aim of this chapter was to make an initial investigation into the applicability of the GRF prediction method as a contact model to simulate the human-exoskeleton interface forces and compare the outputs with a conventional model. This study showed the potential of using a contact model to simulate the interface. While there was a slight difference in the predicted support from the exoskeleton in the two models, both the models showed similar trends to the empirically observed trend as the test conditions became more challenging. However, a difference in the trend of a key biomechanical output was seen. The knee extension moment, which is directly affected by the assistance of the exoskeleton, showed different trends as the test conditions became more challenging, with the contact model showing the more reasonable trend.

Further, the parameters of the contact model were studied. The influence of the coefficient of friction and the angle of contact on the results was studied. The angle of contact appeared to be a relevant parameter in the simulation of the support by the contact model. This indicated the limitation of modelling the contact as a planar contact when the interface of the exoskeleton is a curved surface. A more sophisticated approach is needed for simulating the curved surface and that is dealt with in the next chapter.



# Chapter 4

## Simulating Curved Surface

The focus of this chapter is to simulate the human-exoskeleton interface as a generalized curved surface. An approach is described to model the curved surface using the contact model. Part of the work described in this chapter has been previously published in Chander & Cavatorta, 2020.

### 4.1 Introduction

In the previous chapter, an initial investigation was made into the application of the ground reaction force (GRF) prediction method (Skals et al. 2017) as a contact model for simulating the interface forces at the human-exoskeleton interface of the Chairless Chair. As the first step, a simple model was constructed, adopting the method as it is for simulating the seat of the Chairless Chair as a planar surface. Overall, the contact model showed reasonable results and confirmed the potential of using a contact model to simulate the interface.

However, the simplification of the exoskeleton seat as a planar surface by the contact model also confirmed the associated limitations of using a planar surface to model a curved surface. The interface forces through the contact model depended on the angle of contact and only a small area of the curved surface could be approximated with the planar implementation of the contact model. Moreover, the identification of the location of support at the interface could be difficult. These limitations are relevant not only for the Chairless Chair that has a curved seat but also, in general, for most exoskeletons. Exoskeleton interfaces generally consist of braces or straps for transferring the assistance to the user. The ability to simulate curved surfaces through a contact model is of interest and a necessary step in the development of this thesis.

Thus, the aim of this chapter is to simulate the contact forces at a generalized curved human-exoskeleton interface. The work in this chapter builds on the findings of the previous chapter. In fact, the same exoskeleton, the Chairless Chair, is used in this study as well. The Chairless Chair allowed benefitting from

the work already conducted in the previous study and to focus on adding the next layer of complexity in modelling the human-exoskeleton interface. Thus, a comparison with the conventional model is not repeated. Instead, this study focuses on the modifications needed in the existing method to simulate the interface as a curved surface rather than a planar surface.

## **4.2 Materials and Methods**

The Chairless Chair has been described in detail in section 3.2.1. The focus of this study is on simulating the curved seat of the Chairless Chair. The seat of the Chairless Chair has a slightly concave shape along the breadth of the seat to accommodate the thigh of the user. Instead, the seat has a convex curvature along the length of the seat. The curvature in the central part of the seat is much reduced compared to the front and rear of the seat. At the front, the seat tapers off sharply in a narrow region. Compared to the front, the seat curves more gradually and over an extended portion at the rear. The curvature of the seat along its length serves to optimize the contact for different sitting heights. The sitting height of the Chairless Chair is adjusted by changing the angle between the upper and the lower frame of the device, which changes the inclination of the exoskeleton seat with respect to the ground. The curvature of the seat and the joint between the seat and the upper frame allow a limited compensation in the seat inclination, if necessary, to offset the inclination determined by the angle between the upper and lower frames at the chosen sitting height.

### **4.2.1 Experiments**

In contrast to the previous study, in this study, three different sitting heights were studied: low-seat, high-seat, and comfort-seat. The low-seat and high-seat were respectively the lowest and highest sitting heights allowed by the exoskeleton. Whereas the comfort-seat was the sitting height selected by the user as the most comfortable. A resting posture for the trunk and arms was maintained across the different sitting heights. As described earlier, in section 4.2, the different sitting heights allowed the use of different inclinations of the seat, thereby changing the contact conditions. It was expected that the area of contact and the centre of pressure at the human-exoskeleton interface would change with different sitting heights, especially when comparing the two limit conditions, the low-seat and high-seat. As mentioned in section 3.4.3, the subject from the previous chapter had confirmed that not all the surface of the seat was in contact during the use of the Chairless Chair. Thus, an objective measure of the area of contact was considered essential when comparing different sitting heights and, in the current study, a pressure mat (PX200:20.40.05, XSensor) was fixed on the right seat of the Chairless Chair. The pressure mat served to record the area of contact at the human-exoskeleton interface and to compare the empirically observed centre of pressure (CoP) with the virtual CoP. The pressure mat recorded the interface pressure at 60 Hz and the recorded data for the right leg

was mirrored about the sagittal plane to obtain the data for the left leg due to the symmetry of the posture. A total of 800 cells, with each cell having an area of  $0.51 \times 0.51 \text{ cm}^2$ , constituted the pressure mat. The cells were arranged in an array of  $40 \times 20$  with a sensing area of  $20.4 \times 10.2 \text{ cm}^2$ , which matched well with the area of the seat,  $20.5 \times 11.5 \text{ cm}^2$ .

This study was developed with support from Centro Ricerche Fiat (CRF). CRF kindly provided access to the exoskeleton and their facilities for conducting the experiments. As described in the previous study (section 3.2.2), training and user confidence with the device appeared to be relevant for the effective use of the Chairless Chair. The study was limited to a single subject as training other subjects was not feasible due to the constraints of time. A male subject (163.0 cm and 73.8 kg), trained in the use of the Chairless Chair, simulated a static resting posture in the three sitting heights (Figure 7). The upper and lower frames of the Chairless Chair were both adjusted to their smallest lengths to adjust the exoskeleton to the anthropometry of the user. The body weight distribution between the subject and the exoskeleton was recorded with a scale using the same setup as described in section 3.2.2. Unfortunately, the laboratory was not equipped with force plates. The pressure mat was fixed on the seat with the front edges of the sensing area and the seat aligned. Along the width, the sensing area was centred with the seat. Three trials were done for each sitting height. The pressure data were recorded for at least three seconds after the subject assumed the seated posture and provided a verbal confirmation of being ready and feeling stable. The pressure data were averaged over the three trials to obtain a single snapshot of the interface pressure for comparison with the static virtual simulations.

An attempt was made to record the posture of the subject using an inertial mocap system (Xsens Technologies, The Netherlands). However, it was not possible to correctly calibrate the system and obtain an accurate recording of the motion. This could have been due to the magnetic distortion from the exoskeleton, the pressure mat, and generally from the laboratory. Unfortunately, updated MVN software (Xsens Technologies, The Netherlands) providing magnetic immunity was not available during the data collection. Finally, the posture of the subject was recorded through photographs from the front and the side view.

#### **4.2.2 Musculoskeletal modelling**

The musculoskeletal model was built and analysed in version 7.1.2 of AnyBody Modeling Systems (AMS) using the human model available in version 2.1.1 of the AnyBody Managed Model Repository (AMMR) (Lund et al. 2018). The muscle recruitment problem in the inverse dynamics analysis was solved using the polynomial criterion with power 3 (Rasmussen et al. 2001). The human model was scaled to the subject height (163.0 cm) and weight (73.8 kg) using the length-mass-fat scaling law (Rasmussen et al. 2005).

The CAD model of the Chairless Chair was updated in SolidWorks 2017 software. As would be explained subsequently, multiple reference frames were

needed on the seat surface to simulate the curved surface. The reference frames on the seat surface were created in SolidWorks and oriented to have one axis normal to the seat surface and one axis parallel to the length of the seat. The exoskeleton model was imported into AMS using version 1.1.0 of the AnyExp4SOLIDWORKS plugin for SolidWorks. As the central revolute joint of the exoskeleton provided support by stopping at a user-selected angle, this revolute joint was modelled to provide all the reaction forces and moments necessary to support the user.

The human-exoskeleton model was built using the same methods as described in section 3.2.3. Static simulations were built replicating the postures and positions of the human and the exoskeleton from the empirical trials (Figure 7). Key joint angles were approximated from the photos. Further, the model was superimposed on the photographs to refine the posture. The GRF at the subject's feet and the base of the exoskeleton were predicted individually using the method reported in Skals et al. 2017. 25 contact nodes were created at either foot and 11 contact nodes were created at the base of either lower frame of the exoskeleton. The strength of the contact elements was 0.4 times the body weight. The net vertical predicted force at the feet was used as the body weight supported by the subject and the predicted body weight supported by the exoskeleton was calculated as the difference of the body weight supported by the subject from the subject's weight.

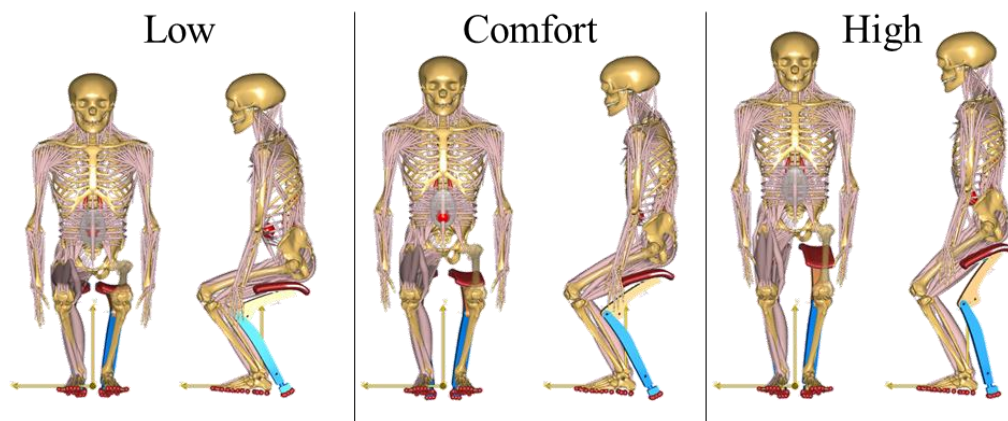
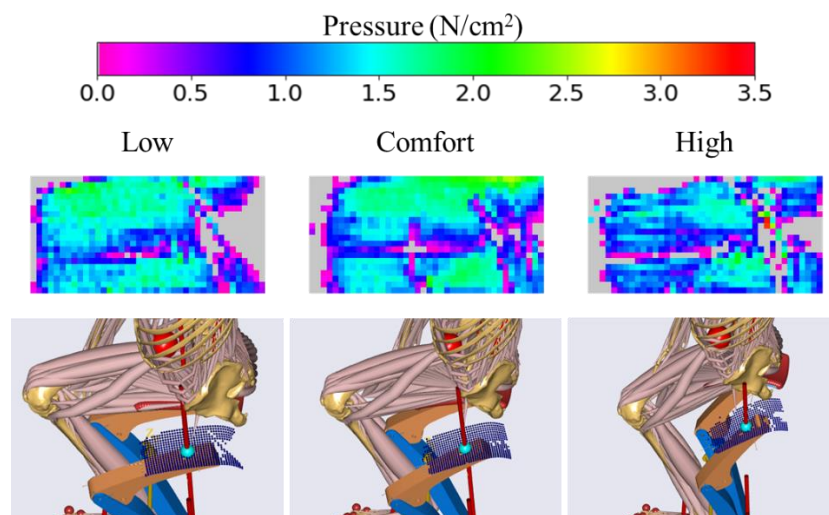


Figure 7: Virtual models of the low, comfort and high seat. Muscles of the left leg are hidden.

## Human-Exoskeleton Interface forces

The forces at the human-exoskeleton interface were simulated by modifying the approach of simulating the contact at the interface. In the previous study (section 3.2.3), the interface was simulated as a planar surface. Instead, in the current study, multiple implementations of the GRF prediction method were used to simulate the curved surface by simulating multiple planar surfaces. Multiple contact detection zones or virtual force plates (VFPs) were created and distributed on the seat surface. The approach of using multiple VFPs has been previously used to predict the GRF with the ground simulated as a planar surface (Jung et al. 2014).

Multiple VFPs on the seat not only allowed a more realistic representation of the seat surface, but they also allowed individual control of each of these VFPs for simulating a realistic area of contact. The simulation of a realistic area of contact was especially an important issue for the Chairless Chair as the different sitting heights led to different inclinations of the seat and consequently different areas of contact with the user. Thus, it was decided to use the experimentally observed area of contact from the pressure mat as an input in the model for the different sitting heights. So, the model also consisted of a grid of 40 rows x 20 columns for a total of 800 VFPs, each corresponding to the individual cell of the pressure mat. This facilitated the input of the empirically observed area of contact into the model through a one-to-one correspondence between the cells of the pressure mat and the VFPs in the model (Figure 8). The seat width exceeded the sensing area of the pressure mat by 1.3 cm. No VFPs were defined on the seat beyond the sensing area of the pressure mat. The reference frames for defining these VFPs were created in the CAD model to correctly locate and orient these reference frames. The 800 VFPs were distributed over 88% of the seat surface and each VFP was locally tangential to the seat surface. Corresponding to each VFP on the exoskeleton, a unique contact node was created on the human thigh. Five contact elements were created and configured to simulate the normal and frictional contact forces at each contact node. The contact force from the contact elements at each node was subsequently processed to locate the virtual centre of pressure (CoP) relative to the seat surface. Thus, in comparison with the previous study (section 3.2.3), instead of having a single VFP with multiple contact nodes, the current study had multiple VFPs, each with a single contact node.



**Figure 8: Empirical pressure maps for the left leg showing different areas of contact for the three sitting heights: low, comfort and high. The empirical area of contact was used as an input in the model.**

In Jung et al. 2014, the strength of the contact elements was selected after a parametric study. Similarly, a parametric study was performed to select the strength of the contact elements in this work as well. The results of the parametric study are presented and discussed in the subsequent sections. Briefly, the parametric study of the strength revealed a preference of the model to provide support at the rear of the seat. This preferential support at the rear of the seat was

manually offset through an additional parameter to control the distribution of the strength of the contact elements across the seat surface. A linear gradient in the distribution of the contact elements strength was added such that the contact elements at the rear of the seat had a reduced strength relative to those at the front of the seat. The VFPs were arranged in a grid of 40 x 20. The row of the VFP determined its relative position along the length of the seat. The strength of the contact element was determined by the equation:

$$S_{ij} = \begin{cases} 0.0 & \text{if } P_{ij} = 0 \\ S_0 * [c_1 + (i - 1) * (c_2 - c_1)/39] & \text{if } P_{ij} > 0 \end{cases} \quad (16)$$

where,

$S_{ij}$  is the strength of the contact element at the  $i^{\text{th}}$  row and  $j^{\text{th}}$  column.

$P_{ij}$  is the recorded pressure of the cell at the  $i^{\text{th}}$  row and  $j^{\text{th}}$  column.

$S_0$  is a constant factor for multiplying the strength.

$c_1$  and  $c_2$  are constants for controlling the linear gradient of the strength.

$i$  is the row number ranging from 1 – 40.

Thus, the strength at the first row ( $i = 1$ ) was  $S_0 * c_1$ , while the strength at the last row ( $i = 40$ ) was  $S_0 * c_2$ .

### 4.2.3 Analyses

Parametric studies were performed with different input values of  $S_0$ ,  $c_1$ , and  $c_2$ . The influence of these parameters on the interface and biomechanical outputs was studied. The interface outputs consisted of the virtual CoP and the body weight distribution between the user and the exoskeleton, which provided an indirect validation of the net vertical force at the human-exoskeleton interface. Biomechanical outputs of interest were the outputs about the knee and ankle as they were affected directly by the assistance from the exoskeleton. Joint moments at the knee and ankle and the activation of the vastus lateralis and gastrocnemius muscles were noted.

## 4.3 Results

### 4.3.1 Interface outputs

Figure 9 shows the virtual CoP and the percentage of body weight supported by the exoskeleton for different values of the strength and strength gradient (including no gradient) of the contact elements. It also shows the empirically observed values of the CoP and body weight distribution. The CoP was measured from the front edge of the seat in one dimension only, along the length of the seat, which is 20.5 cm long. The lateral location of the CoP did not change significantly with the strength of the contact elements and was consistent with the empirically observed values. The values of the strength and the gradient are indicated in the figure. The strength ( $S_0$ ) of the contact elements is indicated in the callouts while the gradients ( $c_1$  and  $c_2$ ) are indicated by different colours. The figure shows that



at high strength of contact elements (150 N), the virtual CoP is at the rear of the seat, while at low strength of the contact elements (5 N), the exoskeleton is unable to provide adequate support to the user. As the strength is increased from 5 N to about 9 N, the bodyweight supported by the exoskeleton increases without a substantial change in the CoP. Beyond 9 N, the CoP starts to shift rearwards. At strength 9 N and no gradient ( $c_1 = c_2 = 1.0$ ), the root mean square errors (RMSE) in the body weight supported by the exoskeleton and CoP across the three sitting heights are 1.94 % (1.4 % of the mean) and 1.04 cm (10.1 % of the mean).

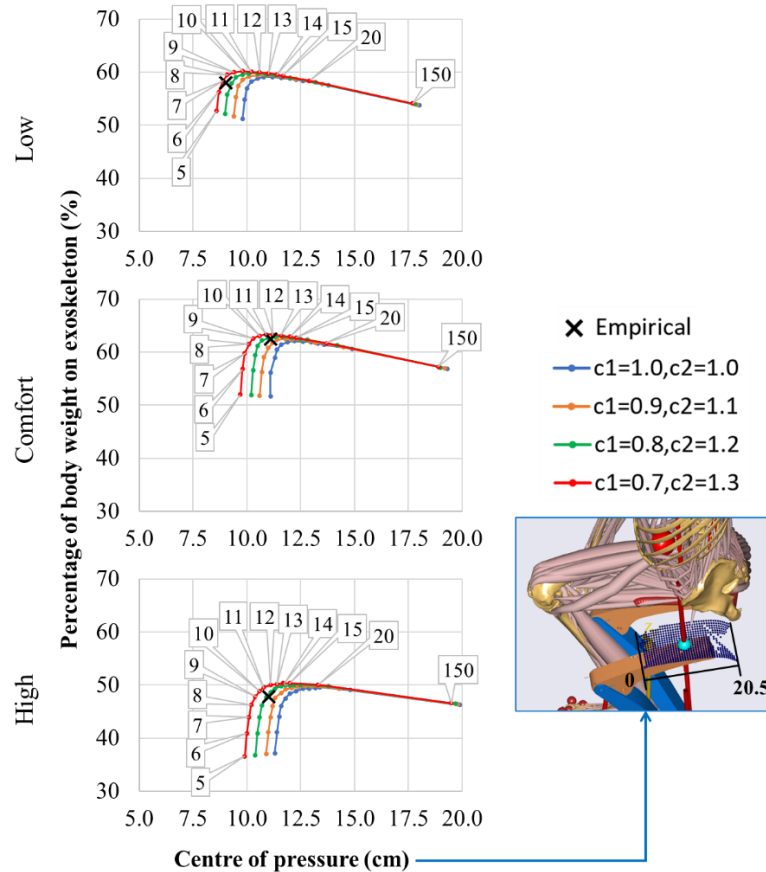


Figure 9: Exoskeleton support and the centre of pressure for different strengths and strength gradients of the contact elements.

### 4.3.2 Biomechanical outputs

Figure 10 plots the knee extension moment, ankle plantarflexion moment, and the muscle activation of the gastrocnemius and vastus lateralis muscles. The outputs are plotted for different values of the strength and strength gradient of the contact muscles. The figure shows the variation in the outputs with the strength of the contact muscles.

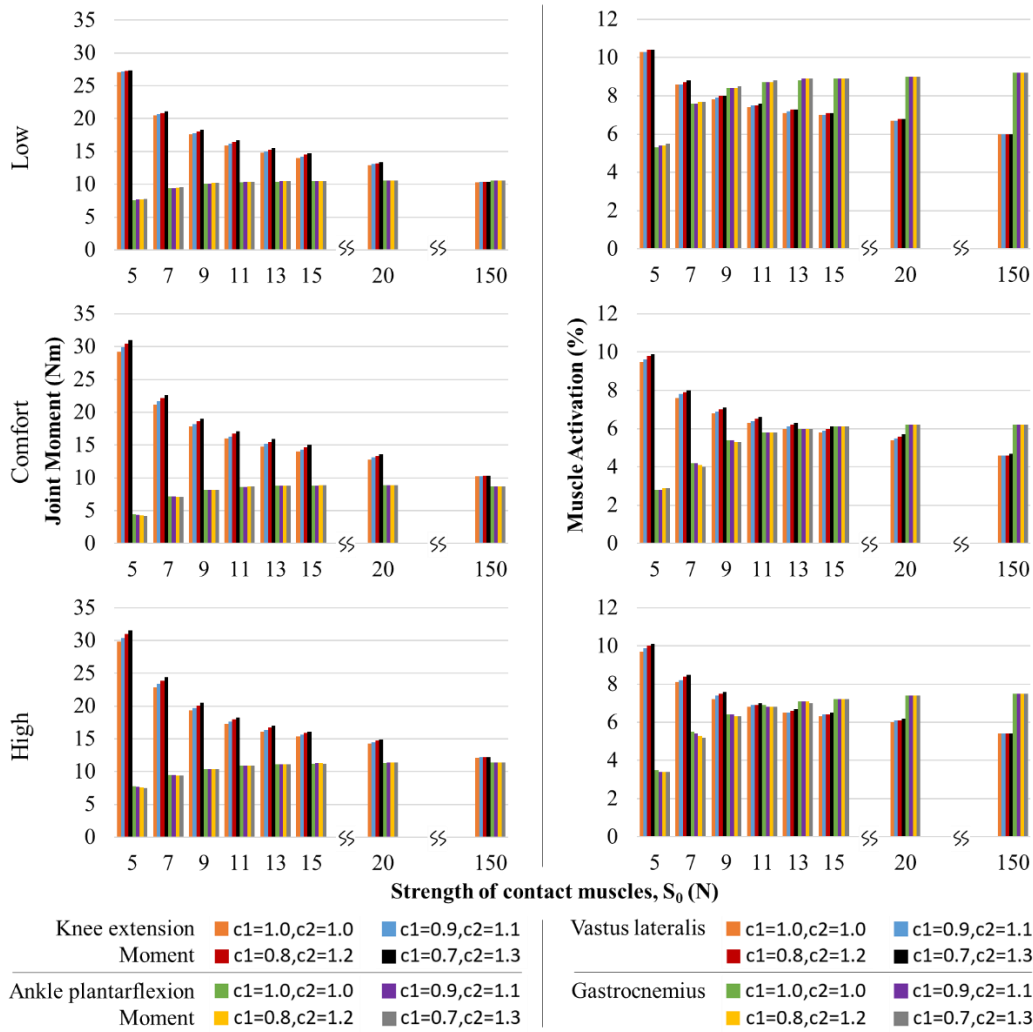


Figure 10: Joint moment and muscle activation for different strengths and strength gradients of the contact muscles.

## 4.4 Discussion

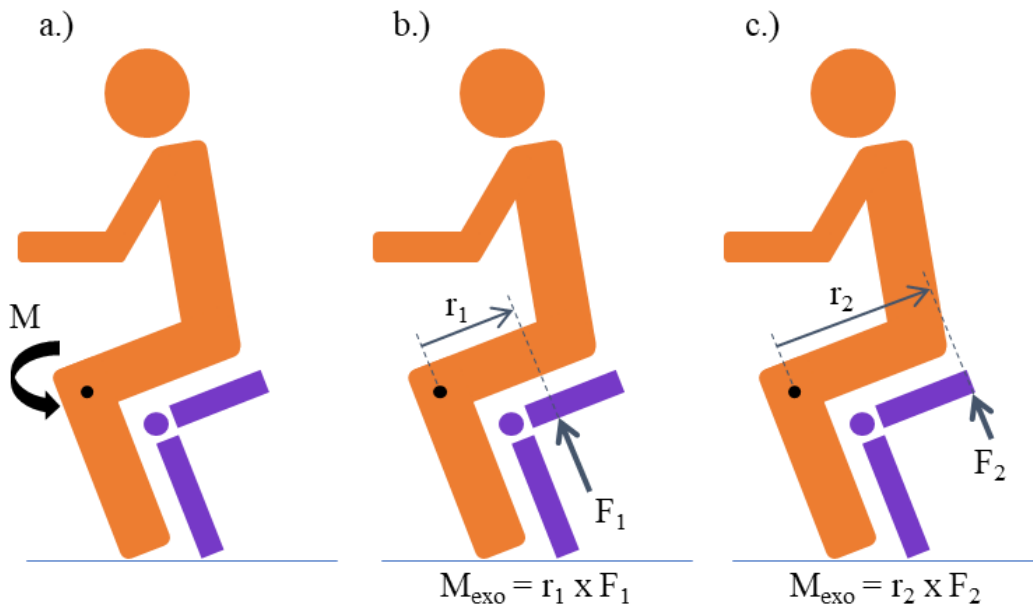
### 4.4.1 Contact forces through optimization

The solution of the contact forces through the muscle recruitment optimization problem can lead to unrealistic results as seen in Figure 9. However, this is not unexpected. The goal of the optimization problem is to minimize a polynomial function of the activation of the contact elements and muscles while respecting the overall equilibrium equations of the model and the non-negative force of the contact elements and muscles.

Consider a simple sketch of the model, shown in Figure 11. Figure 11 a.) depicts that the static posture of the subject requires a moment  $M$  about the knee to maintain the equilibrium. Suppose that Figure 11 b.) and c.) depict two alternate solutions that result in the same moment,  $M_{\text{exo}}$ , about the knee due to the support from the exoskeleton. Figure 11 c.) consists of a solution with a higher moment arm but a lower force compared to the solution in Figure 11 b.). If the model is to find a solution of the contact force through optimization using a single

contact node, c.) depicts a more optimal solution as it results in a lower contact force and lower activation of the contact elements. Extending this concept to the general case of the seat with multiple contact nodes, the optimal solution will, invariably, result in a solution that utilizes the contact nodes at the rear of the seat more than those at the front. By virtue of their distance from the knee, the contact elements at the rear of the seat can produce a greater moment about the knee for the same activation compared to the contact elements at the front of the seat, provided the strength of the contact elements does not change.

Furthermore, the contact elements are not being optimized in isolation. They are not constrained to generate a fixed moment about the knee by the exoskeleton. The optimization problem is defined to find a solution that will minimize the activation of both the contact elements and the muscles. This means that also the distribution between the moment generated by the exoskeleton (through the contact elements) and the moment generated by the user (through the muscles) can change. This can affect the biomechanical results and is discussed in section 4.4.3.



**Figure 11: A simple sketch of the model. a.) A moment  $M$  about the knee is required to maintain the subject in static equilibrium. b.) and c.) depict two hypothetical solutions that result in an equal moment,  $M_{\text{exo}}$ , about the knee due to the support from the exoskeleton ( $r_1 \times F_1 = r_2 \times F_2$ )**

In contrast with the previous study where the contact was limited in a small area, in the current study, the model must determine the activation of the contact elements that are distributed on the entire seat. As described above, the optimal solution will prefer the utilization of the contact elements at the rear of the seat. If the strength of contact elements is sufficiently high (in the order of a few kN), only a few contact elements would be activated at the rear of the seat to provide support from the exoskeleton. However, this solution is not a realistic representation of the use of the exoskeleton. The next section discusses how to select the strength of the contact elements to obtain a more realistic solution.

#### 4.4.2 Interface outputs and optimal strength

Figure 9 showed how the strength and the strength gradient of the contact elements affected the body weight distribution between the user and the exoskeleton and the virtual CoP. An important observation is the shape of the curves in the figure. The curves are formed by joining the plots of different strength values ( $S_0$ ) with the same strength gradient ( $c_1$  and  $c_2$ ). The curves have a similar shape for different gradients and sitting heights.

At high values of the strength of the contact elements, the virtual CoP was at the rear end of the seat. This follows the discussion in the previous section where it was explained why using the contact elements at the rear of the seat was the optimal solution for the model. As the strength values were decreased, the CoP shifted towards the centre of the seat without a substantial change in the support provided by the exoskeleton. Decreasing the strength of the contact elements increased their activation cost, resulting in a greater distribution of the interface force across the contact nodes. This trend continued until the vertex of the curve was reached. Decreasing the strength of the contact elements further did not change the CoP much. Instead, it led to a reduction in the support provided by the exoskeleton. That is, the strength was reduced to a level where the contact elements could not be optimally activated to generate sufficient interface forces to provide the necessary support to the user. Instead, it was more optimal to activate the muscles and increase the effort from the user.

Thus, the shape of the curves indicated the existence of an optimal strength of the contact elements that could be identified at the vertex of the curve. At low values of the strength, inadequate support was seen, whereas, at high values of strength, a rearward shifting of the CoP was seen. Further, the artificial gradient in the strength distribution also shifted the CoP towards the front of the seat as per its purpose. The gradient increased the strength of the contact muscles at the front of the seat relative to those at the rear. The higher the gradient, the higher was the offset to the front of the seat.

The observations about the existence of the optimal strength could be compared to the approach used in Jung et al. 2014 to select the maximum force of their 'smart force elements'. Jung et al. 2014 also performed a parametric study of the maximum force of the smart force elements and selected the lowest value at which the GRF converged. At lower values of the maximum force, they saw that the GRF was inadequate, similar to the observations described here. Increasing the maximum force of the force elements beyond the threshold for adequate GRF did not increase the GRF further.

#### 4.4.3 Biomechanical outputs

The human-exoskeleton interface is a critical aspect of the human-exoskeleton model. Ultimately, the interface model defines how the assistance from the exoskeleton is translated into external forces applied to the subject during the inverse dynamics analysis and can affect the biomechanical analysis.

As seen in Figure 10, the strength of the contact elements affected the biomechanical outputs. At low values of the strength, a sharp increase in knee extension moment and activation of vastus lateralis can be seen. As the strength of the contact elements was reduced, their activation cost increased to the point that the most optimal solution favoured an increased effort from the user instead of providing support from the exoskeleton. Instead, at high values of the strength of the contact elements, a rearward shifting of the CoP can be seen (Figure 9). This indicated that the activation cost of the contact elements was reduced to a level where the optimal solution could exploit the advantage of the contact nodes at the rear of the seat, as discussed in section 4.4.1. The advantage of using the contact nodes at the rear of the seat was also shared by the user as indicated by a decreasing knee extension moment and vastus lateralis activation as the strength of the contact elements was increased. Similarly, effects about the ankle joint due to the change in the strength of the contact elements can be seen.

A marginal effect of the strength gradient ( $c_1$  and  $c_2$ ) was also seen on the biomechanical outputs, as shown in Figure 10. A slight variation in the biomechanical outputs was observed as the gradient changed for the same value of the strength ( $S_0$ ) of the contact elements. The virtual CoP for the gradient  $c_1 = 0.8$  and  $c_2 = 1.2$  was the closest to the empirical CoP. In the zone of optimal strength, the offset in the virtual CoP, compared to the case with no gradient, was less than 1.0 cm. 1.0 cm is 2.7% of the length of the thigh of this specific model. Thus, the effect of the gradient itself on the biomechanical outputs was relatively small.

#### **4.4.4 Application to other exoskeletons**

This work has shown how to simulate the contact forces at a curved human-exoskeleton interface. Multiple VFPs were used to simulate the realistic shape of the interface. It was seen that the strength of the contact elements influenced the model results, and this work discussed a method to identify the optimal value of the strength of the contact elements. The approach was used to correctly simulate the interface of the Chairless Chair in three different sitting heights, which resulted in different inclinations of the seat and support received by the user. However, the approach was developed using the Chairless Chair and some considerations must be discussed when applying this modelling approach of simulating curved surfaces to other exoskeletons.

The empirical area of contact was used as an input in the model. The data from the pressure mat was used to identify the VFPs that were to be deactivated in the model for simulating the different sitting heights. However, this problem of identifying the area of contact is also specific to the Chairless Chair due to its construction. The Chairless Chair is designed to allow this variation in the inclination of the seat and consequently, the seat is designed to adjust for the different inclinations. It results in different areas of contact for the different sitting heights. In the case of other exoskeletons, often the human-exoskeleton interface is firmly secured using straps and is not designed to allow a change in contact during the use. In such cases, it could be assumed that the entire area of the

interface remains in contact. In addition to the area of contact, empirical data were also needed to identify the correct gradient in the strength of the contact elements. However, the effect of the gradient is relatively small compared to the identification of the correct strength value. Thus, the results without the gradient could be considered acceptable if no experimental data is available.

There could be more unknowns when applying this modelling approach to simulate a general human-exoskeleton interface of another exoskeleton. The Chairless Chair is essentially a sitting support and provides support only from one side of the limb. In this work, static simulations were developed that simulated the seated support under the thighs of the user. Several exoskeletons assist during a movement and could have braces that support the user from all around the limb. The behaviour of the contact model in such dynamic activities with contact nodes present all around the limb could lead to complications that might not have been observed with the Chairless Chair.

This work also highlighted an important aspect concerning the necessity to identify the optimal strength of the contact elements. The contact elements and the physiological muscles are included in the same optimization problem to determine the contact and muscle forces in the inverse dynamics analysis. The problem aims to minimize an objective function of the activation of the contact elements and the physiological muscles, and cannot distinguish between the two. As described earlier (section 4.4.3), if the strength of the contact elements is too low, the contact elements would have a high activation to generate the necessary interface forces. If their activation is comparable to the activation of the physiological muscles, it could be more optimal for the solver to recruit physiological muscles if it helps to reduce the activation of the contact elements and results in a more “optimal” solution of the muscle recruitment problem. Conversely, if the strength of the contact elements is much greater than the strength necessary for adequate support, the solver will exploit this additional capacity to unload the physiological muscles if possible. The modeller must understand this general limitation of introducing additional contact elements in the muscle recruitment problem and check for conditions allowing the interference between the recruitment of the contact elements and physiological muscles. Thus, the selection of the optimal strength of the contact elements is a critical issue and it should not be too high or too low, as was also mentioned in Fournier et al., 2018. In this work, a maximum activation of 1.5% was seen for the artificial contact elements at strength  $S_0 = 5.0$  N. It reduced for higher strengths of the contact elements. Further, the optimal strength of the contact elements might need to be adjusted for different users, or, for different assistance levels in the case of another exoskeleton. In this study, a subject with a significantly different body weight would require a different optimal strength of the contact elements such that the Chairless Chair is able to support around 60% of the body weight as in the low and comfort-seat configurations of the Chairless Chair. A similar adjustment was also suggested in Jung et al. 2014 for predicting the GRF of obese subjects.

The alternative approach to using contact elements is to simulate the interface forces through reaction forces associated with kinematic constraints as also done

in chapter 3. The reaction forces do not have a cost associated with them. If needed, an infinitely large reaction force can be generated in the inverse dynamics analysis. In this way, the use of reaction forces is similar to using contact elements with infinitely large strength. That is, the muscle recruitment optimization problem will exploit the reaction forces if the conditions allow for the reaction forces to reduce the activation of the physiological muscles.

#### **4.4.5 Limitations**

There were some limitations in the data collection. Unfortunately, the study was conducted with a single subject only as training other subjects would have been prohibitive due to the time required but essential based on the feedback we had from FCA and CRF. Secondly, the posture of the subject was approximated from the photos and there could be errors in the reproduction of the postures in the model. An attempt was made to record the posture using an inertial mocap system. However, the system could not be calibrated correctly, perhaps due to magnetic distortion. Based on the experience of the previous study, where the reproduction of the postures from photos could capture the trends across the three conditions, we decided to proceed with the photos. Thirdly, force plates were not available in the laboratory, and this affects the accuracy of the estimated biomechanical outputs. Lastly, the sensing area of the pressure mat was about 88% of the area of the seat. Crucially, the length of the sensing area matched the length of the seat and only the width of the sensing area was narrower than the width of the seat. Thus, narrow regions along the lateral edges of the seat, about 0.65 cm wide on each side, were excluded from the coverage of the pressure mat and, consequently, also in the model. The change in the sitting height changed the longitudinal coordinate of the CoP and was of interest for this study. The lateral coordinate of the CoP was not affected significantly by the change in the sitting height and remained mostly in the centre of the seat.

#### **4.5 Conclusion**

This chapter presented an approach to simulate the contact forces at a curved human-exoskeleton interface. The method to simulate the curved surface consisted of representing the surface by smaller planar surfaces. The approach allowed to add an extra layer of detail compared to simulating a planar surface (Chapter 3). In the planar contact model, the modeller would need to approximate the location of the support on the exoskeleton, which would determine the angle of contact with the user. Instead, the curved contact model could predict the change in exoskeleton support and CoP in different sitting heights. Although the model required the empirically observed area of contact as an input, this is also a specific requirement for the Chairless Chair, where the area of contact changes with the sitting height. The approach showed a significant influence of a model parameter, that is, the strength of the contact elements, on the results of the model and this work described how to select the optimal strength of the contact elements.

The modelling approach was developed using a particular exoskeleton and the implications for applying this approach on another exoskeleton have been discussed in detail. This approach could be too specific to the Chairless Chair or exoskeletons like the Chairless Chair. There are several considerations to be taken into account when modelling the interface of another exoskeleton. It would be desirable to have a generic contact model that could be applied to several exoskeletons and not just to a particular kind of exoskeleton. This idea defined the aim for the next chapter, that is, to apply the contact model to another, more generic, exoskeleton.



# Chapter 5

## Simulating Multiple Interfaces

The focus of this chapter is to use the approach developed in the previous chapter to simulate the contact forces at the interfaces of another exoskeleton consisting of multiple interfaces that wrap around the limb. Such an exoskeleton represents a more typical exoskeleton than the Chairless Chair that was used in the previous two chapters.

### 5.1 Introduction

In the previous chapter (chapter 4), an approach was developed to simulate the contact forces at a curved human-exoskeleton interface. This was an important step after the work described in chapter 3 where the interface was modelled as a planar surface. However, the approach for the curved surface demonstrated a heightened sensitivity of the model results to the strength of the contact elements and a method to identify the optimal strength of the contact elements was developed. While this method of simulating the contact forces at a curved surface and finding the optimal strength worked on the Chairless Chair, it must also be considered that the Chairless Chair is a very specific kind of exoskeleton. It is essentially a sitting support and acts as a surface on which the user sits. The assistance provided by the exoskeleton is rather static. Secondly, the Chairless Chair consists of a single interface that provides support only from one side of the thigh. The exoskeleton transfers the load to the ground and not to another part of the body. These points are often in contrast with other exoskeletons. Indeed, the Chairless Chair was selected as the exoskeleton to apply the contact model due to its simplicity and similarity with ground reaction force (GRF) prediction, with the idea being to progressively add complexities in the model (section 3.1).

Thus, the aim of this chapter is to simulate the contact forces at the interface for another exoskeleton that provides dynamic assistance through multiple load-bearing interfaces that wrap around the limb. Primarily, the aim is to add the next layer of complexity in the development of the contact model by simulating contact

forces for a more general exoskeleton. In addition to the simulation of the contact forces at the human-exoskeleton interface, this study also aims to present a comparison with the conventional model of simulating the interface using kinematic joints and the associated reaction forces. As the target exoskeleton for this study is substantially different from the Chairless Chair, the comparison with the kinematic joints must be made again.

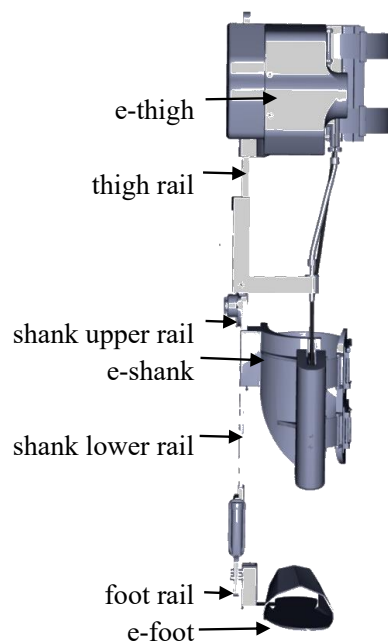
This chapter describes the work conducted to arrive at a generalized method for simulating the contact forces at the human-exoskeleton interface. The exoskeleton used in this study is an active exoskeleton for the lower limbs that has the function to assist the elderly in stair negotiation. At the time of writing this thesis, the exoskeleton was under development at the University of Applied Sciences (HTWK) in Leipzig, Germany. The exoskeleton met the requirements for the aim of this work as described earlier. It consists of interfaces that wrap around the limb at the thigh, shank and foot, and assist during a movement, that is, stair ascent and descent. A prototype of the exoskeleton was constructed by the researchers at HTWK Leipzig and used for trials in the biomechanical lab at the University of Leipzig. As the trials were conducted with a prototype exoskeleton, the reader is requested not to read the results presented in this study in the context of the “benefits” of the exoskeleton as the exoskeleton could likely be updated. In fact, this study will not present a comparison of the with and without exoskeleton cases as it is not necessary for the aim of this work.

The work described in this chapter was developed in 2020 through a research cooperation with HTWK Leipzig and Aalborg University. HTWK Leipzig provided the exoskeleton model and data from the trials for developing the musculoskeletal model. Instead, the human-exoskeleton interface models were developed by the author with valuable inputs from the Biomechanics Research Group at Aalborg University, where the author spent a five-month visiting period from February to June 2020. Unfortunately, the timeline of this work in 2020 meant that this work was affected by the unforeseeable pandemic due to Covid-19. The study was limited to experiments with a single subject only as approval for a more elaborate study with multiple subjects could not be obtained under the circumstances. Moreover, specialized instruments for measuring interface forces were not available at the laboratory in Leipzig. The continuously changing restrictions and guidelines to contain the spread of Covid-19 rendered arranging a sensor for the interface force or pressure or organizing the trials in another laboratory practically impossible in the timeframe for the delivery of this thesis. It is hoped that further trials could be organized soon to collect some empirical measures of the interface outputs with multiple subjects allowing for a thorough investigation of the interface models.

## 5.2 Materials and methods

### 5.2.1 Exoskeleton

The exoskeleton developed at HTWK Leipzig is a unilateral and rigid system consisting of seven parts per leg as shown in Figure 12. The segments and joints of the exoskeleton will be prefixed with “e-” (e.g.: e-thigh) to avoid confusion with human segments and joints. Three of the seven parts connect to the corresponding human segments and form the human-exoskeleton interface: e-thigh, e-shank, and e-foot. The remaining four parts are rails that serve to create two rotational joints between the three interfaces and accommodate users of different anthropometries. A rotational joint with one degree of freedom (DOF) connects the thigh rail and the shank upper rail to form the e-knee. The axis of the e-knee joint should be coaxial with the knee joint of the human leg. Likewise, there is a rotational joint with one DOF between the distal end of the shank lower rail and the foot rail. This rotational joint, called the e-ankle, should be coaxial with the human ankle joint ideally. The rails allow not only a continuous adjustment of the distance of the e-ankle from the ground and the distance between the e-ankle and e-shank but also the relative position of the e-shank and e-thigh interfaces from the e-knee. Further, the e-foot can also be adjusted laterally in the frontal plane. The masses of the different parts are given in Table 3.



**Figure 12: Exoskeleton to support stair negotiation under development at HTWK Leipzig. The figure shows the exoskeleton for the right leg consisting of seven general parts.**

All three interface components (e-thigh, e-shank, and e-foot) surround the human segments. The anterior side of e-thigh is a rigid structure, whereas two straps, linked through a shaped rigid element, surround the posterior side of the human thigh. The e-shank is made of two rigid parts. One part is a quarter rigid

element anterior to the human shank. Medially attached to that part is another rigid shaped element with two straps in between. Two more straps surround the posterior side of the human shank. One of the posterior straps is horizontal and the other one is diagonal from the horizontal band to the e-shank. The interface attachment component of the e-foot surrounds the foot. The sole of the human foot stands on the base of the e-foot. Furthermore, the e-foot consists of a compliant material to allow the foot to roll off. This design is intended to take into account the second DOF in the ankle joint so that lateral movements in the frontal plane are enabled to increase the user comfort. All the three interface attachment components are adjustable to consider individual anthropometry and enable the user to fasten the interface himself/herself to increase comfort.

The assistive force to support stair negotiation is implemented through a cable connecting the e-thigh and e-shank, anterior to the human knee joint. An active motor pulls the cable and creates a pulling force. The force vector is independent of the knee angle as the cable has a fixed distance from the patella of the knee. The pulling force results in an external moment through the rigid structure of the exoskeleton, to support knee extension. This external force is active only if the corresponding leg is in the stance phase of the movement.

## 5.2.2 Experiments

The exoskeleton was trialled in stair ascent in the biomechanical laboratory at the University of Leipzig. The experiment was carried out on a purpose-designed staircase with step height = 160 mm, tread length = 280 mm, and a resulting inclination angle of 30°. The staircase consisted of four steps, a stair landing at the upper end and handrails. It also consisted of a force plate (Kistler MiniDyn type 9119AA2, Switzerland) in the second step to record the ground reaction force (GRF). The tensile assistive force in the exoskeleton cable was recorded through a custom-built strain gauge implemented in the e-shank. A marker-based motion capture system (Qualisys AB, Sweden) consisting of twelve active infrared cameras distributed throughout the room was used for the kinematic recordings at 100 Hz. The software Qualisys Track Manager was used for recording and synchronization.

Two markers were attached at the shoulder and eight markers were attached medially and laterally at the knee and ankle joints of both the legs for the static trial to determine the joint axes and segment lengths based on the cast model (Cappozzo et al. 1995). No markers could be placed on the human thigh due to the presence of the exoskeleton. So, 26 markers were attached to the human body considering characteristic bony landmarks and 18 markers were attached to each exoskeleton leg. The distribution of the 18 exoskeleton markers is listed in Table 3.

**Table 3: Mass of the exoskeleton parts and marker distribution**

<b>Exoskeleton part</b>	<b>Mass (kg)</b>	<b>Markers per part</b>
e-thigh	3.56	4

thigh rail	0.82	3 (one at e-knee)
e-shank	1.08	3
shank upper rail	0.17	1
shank lower rail	0.24	2 (one at e-ankle)
foot rail	0.05	1
e-foot	0.17	4

The experiments were conducted with one healthy subject (male, 27 years, 77.4 kg, 1.83 m). Relevant body parameters such as segment lengths, body height and mass were measured first. Furthermore, the exoskeleton was adjusted to the participant's anthropometry as described in Table 4. Before the test was conducted, the participant was able to get familiar with the exoskeleton, donning the exoskeleton on both legs, and climbed the stairs several times without recording any data. The subject then carried out 13 ascents, at a self-selected speed, step-over-step and without the use of the handrails. One recording included one ascent, starting with the left leg on the first step (Figure 13). Due to the exclusion of incomplete data series, only eight ascents were analysable. After the trials, two static recordings were taken of the subject and the exoskeleton in the neutral standing posture. Subsequently, a check for completeness and errors was carried out. Due to partial masking of markers by the testbed, gaps in the trajectories were created, which could be filled by interpolation during data preparation.

**Table 4: Adjusted lengths of the exoskeleton to consider the anthropometry of the subject**

<b>Description of the adjustable length</b>	<b>Distance (cm)</b>
Distance between e-foot and foot rail	0.58
Distance between e-ankle and ground	7.5
Distance between e-ankle and e-knee	41.0
Distance between shank upper rail and e-shank	13.5
Distance between thigh rail and e-thigh	2.0



Figure 13: Trial of a stair ascent with the supporting exoskeleton on both legs. The experiment was conducted at the biomechanical lab of the University of Leipzig.

### 5.2.3 Musculoskeletal modelling

The musculoskeletal model was built and analysed in version 7.3.0 of AnyBody Modeling Systems (AMS) using the human model available in version 2.3.0 of the AnyBody Managed Model Repository (AMMR) (Lund et al. 2020). The muscle recruitment problem in the inverse dynamics analysis was solved using the polynomial criterion with power 3 (Rasmussen et al. 2001).

The exoskeleton system consisted of two separate exoskeletons for the right and left legs. Unless specifically mentioned, the methods described in this section were applied to both sides.

The CAD model of the exoskeleton was provided by the colleagues at HTWK Leipzig. The CAD model of the exoskeleton was updated in SolidWorks 2018 by creating reference frames at the thigh, shank, and foot interfaces for the contact model. For the e-thigh and e-shank interfaces, vertical lines were projected onto the surface of the interface at every  $15^\circ$  from the axis of either interface. Reference frames were created on these projected lines on the interface such that the vertical distance between the reference frames was about 1.8 cm. Each reference frame on the e-thigh represented a surface area of about  $5.65 \text{ cm}^2$ . Instead, each reference frame on the e-shank represented an area of about  $3.45 \text{ cm}^2$  due to a smaller diameter and, consequently, a greater density of reference frames compared to the thigh. However, on both the e-thigh and e-shank interfaces, the planar surfaces approximated curved surfaces that subtended an angle of  $15^\circ$  at the axis. The foot interface was divided into two distinct interfaces, the foot base and the foot strap. The GRF prediction method (Skals et al. 2017) was used to simulate the interface forces at the sole or the base of the foot. The CAD model of the foot strap was already divided into six surfaces spanning  $180^\circ$  about the foot. These surfaces were used to create a total of 18 reference frames, with each frame representing an area of about  $8.35 \text{ cm}^2$ . Just as in section 4.2.2, each reference frame had its normal aligned locally to the interface surface at the

origin of the reference frame. The second axis of the reference frame was aligned along the length of the interface.

Furthermore, additional reference frames were created in the CAD model of the exoskeleton for defining and adjusting the joints of the exoskeleton inside AMS. The exoskeleton consisted of revolute joints at the knee and the ankle that were driven from the mocap data. Thus, reference frames were created on the corresponding segments constituting these joints to define the joints inside AMS and drive the joints from the mocap data. Additionally, the exoskeleton also consisted of prismatic joints that allowed the adjustment of the exoskeleton rails to accommodate users of different anthropometry. These prismatic joints must be adjusted for different users but remain fixed during the movement of the exoskeleton. Reference frames were also created on segments at locations that could be conveniently measured during the trials to define the distances of the various prismatic joints so that the exoskeleton model could be adjusted quickly inside AMS.

Finally, the CAD model updated with the reference frames was translated into an AMS script file using version 1.2.0 of the AnyExp4SOLIDWORKS plugin for SolidWorks.

## **Human-Exoskeleton model**

The human-exoskeleton model was built using the “Plug-in-gait\_MultiTrial\_StandingRef” example available in the AMMR. This example is set up for studying multiple mocap trials for multiple subjects and is built using the Plug-in-Gait marker protocol. The example uses a reference trial in the standing posture for subject scaling and marker optimization. However, subject scaling was disabled and segment lengths estimated from the marker data in the static trial were inserted manually. The arms were also disabled in the model as handrails were not used during the trials.

The exoskeleton model was added to this human model. The prismatic joints of the exoskeleton essentially defined the size of the exoskeleton and were measured during the trials. So, these prismatic joints were fixed in the model and the whole exoskeleton system could be reduced to three segments (e-thigh, e-shank, and e-foot) connected by two revolute joints (e-knee and e-ankle), thereby resulting in eight DOF for the exoskeleton. As markers were located on the exoskeleton as well during the trials, the exoskeleton could be driven directly from the marker data. A procedure, similar to the one used for the kinematics of the human model, was used for the kinematics of the exoskeleton. In the first step, exoskeleton markers were tracked using an over-determinate solver (Andersen et al. 2009) and the position and orientation of the e-shank (6 DOF) and the angles of the e-knee and e-ankle joints (2 DOF) were saved for the entire movement. In the second step, these saved values were used as an input to drive the kinematics of the exoskeleton in the inverse dynamics analysis.

An alternative way to drive the exoskeleton was to use kinematic joints between the human and the exoskeleton by adding 8 constraints that could

suitably solve the kinematics of the exoskeleton from the mocap data of the human model. This approach was considered in the conventional interface model and is described in detail in the next section.

The GRF from the trials was applied to the right exoskeleton foot. The recorded assistance from the exoskeleton during the trials was synchronized with the movement and read into the model through an external file that stored the magnitude of the force at each time step. The assistive force was applied as tension at the endpoints of the cable and the via points for channelling the cable.

## **5.2.4 Interface models**

There are two aims of this chapter. Firstly, apply the contact model for this exoskeleton with multiple interfaces and dynamic assistance. Secondly, compare the contact model with the conventional model using kinematic joints. This section describes the different interface models.

### **Contact model**

Similar to the method described in chapter 4, a discretized approach was used to define the contact model for this exoskeleton. The curved interface of the exoskeleton was represented by multiple planar surfaces using the reference frames created in the CAD model, which ensured that the frames had the correct position and orientation. The reference frames on the exoskeleton were used to define the contact detection zone or the virtual force plates (VFPs) on the exoskeleton. Correspondingly, contact nodes were created on the human side, one for each VFP. On the thigh and shank interfaces, the normal direction of the VFPs was locally normal to the exoskeleton surface and one of the shear directions was aligned in the proximal-distal direction along the surface. At the foot interface, only the foot strap was modelled using the discretized approach to simulate the curved surface of the strap. VFPs and contact nodes were created on the e-foot and human foot correspondingly. The foot base was treated as a planar surface and the GRF prediction method (Skals et al. 2017) was used to simulate the interface forces at the base of the foot by creating a single contact detection zone on the e-foot and 25 contact nodes at the sole. At each contact node of all the interfaces, five contact elements were created to simulate the normal and shear contact forces as reported in the GRF prediction method. These contact elements were included in the muscle recruitment problem, along with the physiological muscles, to estimate the contact forces as a solution to the inverse dynamics problem.

In the contact model, the human and exoskeleton models were driven using their respective mocap data. This resulted in misalignments between the human and exoskeleton joint axes. The misalignments allowed the contact elements to contribute to the flexion/extension of the human joints such that the vastus lateralis and vastus medialis muscles were completely unloaded at large strengths of the contact elements.



Thus, a method was needed to compensate for the misalignments between the human and the exoskeleton joints. This was achieved by adding “dummy segments” in the model to ensure kinetic alignment of the human and exoskeleton joints despite the kinematic misalignment. They are called dummy segments because they are mass-less, inertia-less segments that do not directly contribute to the dynamics. However, the dummy segments were used to channel the internal forces of the exoskeleton through a new kinetic path that was aligned with the human leg. Three dummy segments corresponding to the human thigh, shank, and foot segments were added in the model to define a dummy leg with dummy knee and ankle joints. The dummy leg was kinematically constrained to the human leg such that the dummy and human joints were perfectly aligned. The inverse dynamics analysis was set up with the following three steps. The dummy knee and ankle joints were configured to generate the reaction forces (and moments) in the five constraints of the revolute joint. The reaction forces at the exoskeleton knee and ankle joints were disabled. Finally, reaction forces were added in all six coordinates between the corresponding exoskeleton and dummy segments defining the knee and ankle joints. In this way, a hybrid human-exoskeleton system was created where the exoskeleton joints were kinetically substituted by the dummy joints, which in turn were kinematically aligned with the human joints. All in all, the original human-exoskeleton interface using the contact model was not modified. The concept is summarized in Figure 14.

The introduction of dummy segments in the human-exoskeleton model kinetically aligned the human and exoskeleton joints. This prevented the contact elements from the unrealistic unloading of the physiological muscles as the contact elements could not contribute to the flexion/extension of the human joints. Finally, a high strength value of the contact elements was used such that their maximum activation was less than 0.1%.

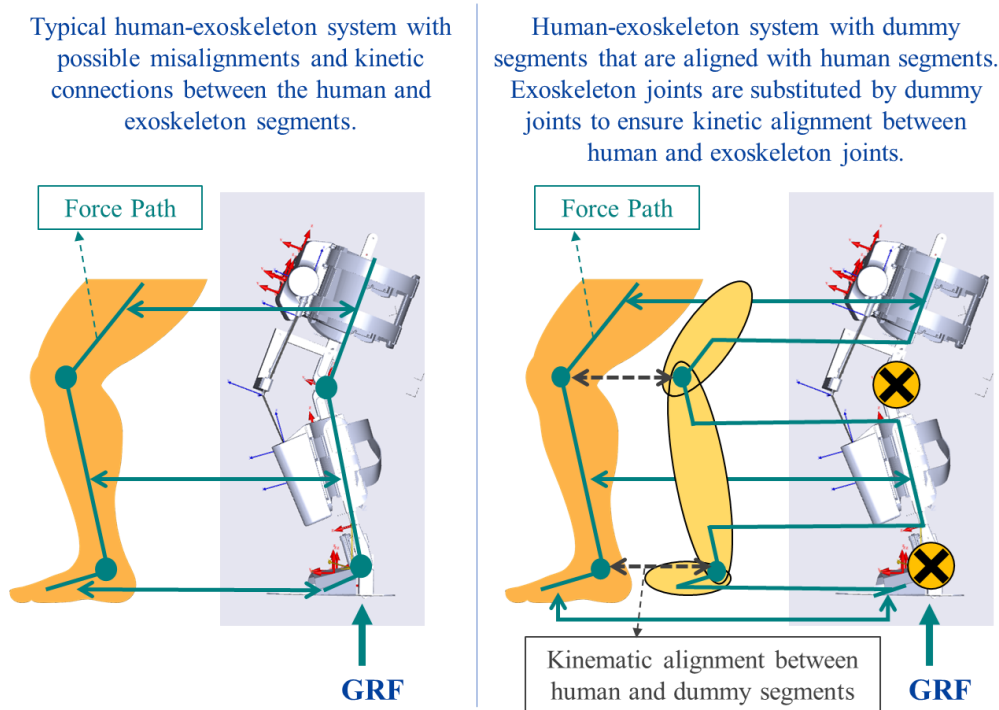


Figure 14: Adding dummy segments in the human-exoskeleton model. On the left is the typical human-exoskeleton model with the kinetic constraints between the human and the exoskeleton. On the right, dummy segments are added to align the exoskeleton joints with the human joints.

## Conventional model

In the conventional model, the human-exoskeleton interface forces were simulated using kinematic joints and the associated kinetic constraints between the human and exoskeleton. Staying true to the approach, the exoskeleton was driven using the kinematic joints instead of the mocap data from the markers on the exoskeleton. Constraints were added at each interface between the corresponding human and exoskeleton segments. Reference frames were defined at the centre of the axes of the e-thigh and e-shank. The reference frame on the e-foot was defined at the centre of the e-foot base. The reference frames are shown in Figure 15. Correspondingly, reference frames were defined on the human segments with the same convention for the axes.

At each interface, up to six constraints could be added (three translations and three rotations) between the corresponding human and exoskeleton segments. However, the exoskeleton has eight DOF requiring only eight constraints to fully constrain the exoskeleton. The choice of the eight constraints was a non-trivial problem. As the knee is the target joint of this exoskeleton, maximum constraints were provided around the knee, that is on the thigh and shank (Figure 15). Three constraints were added at the thigh interface (translation about X and Y; rotation about X). Four constraints were added at the shank interface (translation about X, Y, and Z; rotation about Y). One constraint was added at the foot interface (translation about Z).

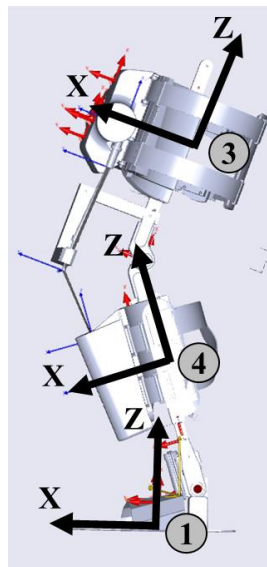


Figure 15: Reference frames on the exoskeleton used for defining the kinematic joints. The number in the grey circle indicates the number of constraints added at that interface.

## Reference models

The contact and conventional models described above were primarily intended to compare the difference in simulating the interface forces through contact elements and reaction forces. However, the two models also had different kinematics of the exoskeleton. Further, the contact model also required the use of dummy segments to ensure the kinetic alignment of the human and exoskeleton joints. Thus, two reference interface models were defined to investigate further these differences between the contact and conventional models. In the first model, dummy segments were introduced in the conventional model with the kinematic joints. In the second model, the kinematics of the exoskeleton in the contact model were driven using the same kinematic constraints from the conventional model while the interface forces were simulated using the contact model with dummy segments. These two reference models allowed the possibility to investigate purely the difference between the contact elements and reaction forces-based interface forces, negating the effects due to the difference in kinematics or the effect of the dummy segments. Finally, four interface models were defined and they are summarized in Table 5.

Table 5: Interface models studied

Interface model	Kinetics	Exoskeleton Kinematics	Dummy Segments
CMDS	Contact Model	Marker driven	Yes
KJ	Kinematic Joint	Kinematic Joint	No
KJDS	Kinematic Joint	Kinematic Joint	Yes
CMKJDS	Contact Model	Kinematic Joint	Yes

In addition to the interface models described above (Table 5), a baseline model was created in which there was no interface model between the human and

exoskeleton. The GRF and the exoskeleton assistance were directly applied to the human model, bypassing the exoskeleton completely. This baseline model was defined as the ideal assistance model or the “IA” model. This model simulates the perfect exoskeleton where the assistance was applied directly to the human model to see its intended effect on the human model. Reference frames were created on the human thigh and shank to reproduce the path of the exoskeleton cable. The assistive force was applied as tension directly at these reference frames on the human segments to simulate the assistance from the exoskeleton. This model ignored the mass and inertia effects of the exoskeleton, which should be relatively small compared to the effect of the assistance. The baseline model served as a reference to check if there were significant discrepancies in the biomechanical outputs from the different interface models.

### **5.2.5 Analyses**

A total of 8 trials of stair ascent with the exoskeleton were available. Only the stance phase of the right leg was analysed for each trial due to the availability of the recorded GRF. Each trial was trimmed, resampled and normalized to the duration of the stance phase. The point-based resampling technique (PBRT) was used to create 95% confidence bands about the baseline IA model using bootstrapping (Joch et al. 2019). Resampling techniques (such as bootstrapping) can assure that the true coverage probability of the confidence bands comes close to the desired nominal level, although it cannot overcome the limitation of a single subject in the study. Then, the mean curves of the interface models were tested to check if they remained within the confidence bands about the baseline model. The curves were tested at each time-step of the movement instead of a single representative value from the curve such as the mean or maximum. The PBRT approach was only used for biomechanical outputs. Instead, for the interface outputs, the results from only the four interface models are plotted. The baseline model did not have any human-exoskeleton interface, nor was there any empirical measure to use as a reference for the interface outputs.

## **5.3 Results**

In this section, the results of some key biomechanical outputs concerning the knee and ankle joints, and the interface forces from the four different interface models are presented.

### **5.3.1 Biomechanical outputs**

Figure 16 shows the results of the biomechanical outputs. IA refers to the ideal assistance model and the rest of the interface models have been summarized in Table 5. The figure shows the muscle activation of the vastus lateralis and gastrocnemius muscles. Then, it shows the knee flexion and ankle plantarflexion moments. Lastly, it shows the compression forces at the knee and ankle.

Looking at the outputs about the knee firstly, the activation of the vastus lateralis in all the models with the kinematics driven using the kinematic constraints between the human and exoskeleton was lower compared to the ideal case and the contact model (CMDS) using the marker data for independent exoskeleton kinematics. In the knee flexion moment, the differences between the KJ and CMDS were negligible and both lay within the confidence bands of the baseline model. Similarly, negligible differences between KJ and CMDS could be observed for the knee compression force. However, compared to the ideal assistance model, KJ showed lower compression force around the initial part of the peak. Notably, the curve of KJDS was overlapped by the curve of CMKJDS for all the three outputs about the knee.

The outputs concerning the ankle showed a greater inconsistency between the models compared to those about the knee joint. A higher gastrocnemius activation was observed with the KJDS model compared to the other three models. The IA model lay in between the KJDS and the remaining three models such that all the models remained mostly within the confidence interval. Instead, for the ankle plantarflexion moment, the conventional model (KJ) showed a reduced effort from the user. Whereas, for the ankle compression forces, the KJDS again indicated a higher load, as in the case of the gastrocnemius activation. Across the three ankle outputs, the conventional model, KJ, always underestimated the effort compared to the conventional model with the dummy segments, KJDS. Lastly, the KJDS and CMKJDS models overlapped only for ankle plantarflexion moment, unlike the trend seen in outputs about the knee joint.

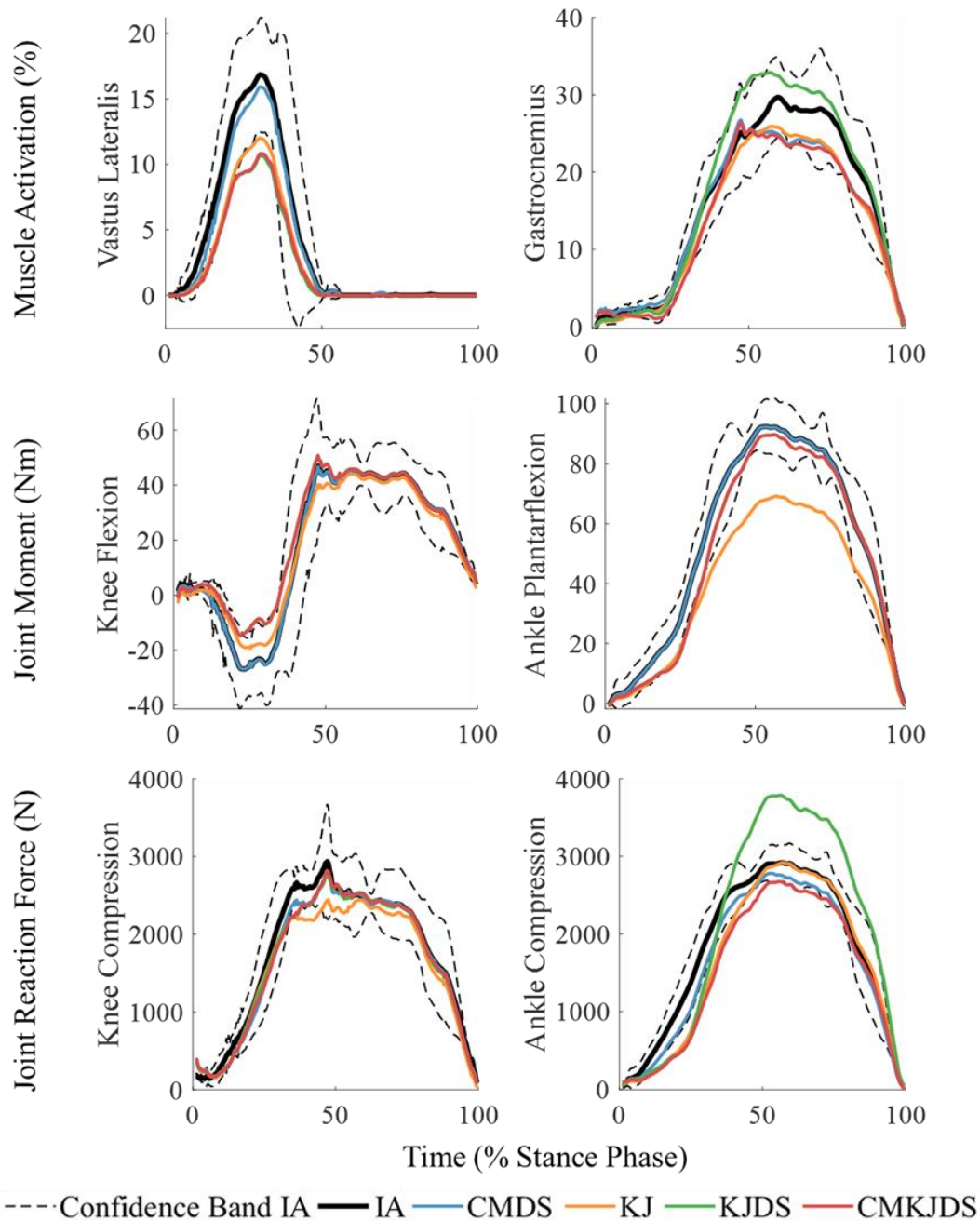


Figure 16: Biomechanical outputs from the Ideal Assistance (IA) reference case and the 4 interface models (please refer to Table 5 for the interface models). The confidence bands indicate a 95% confidence interval about the IA.

### 5.3.2 Interface outputs

Figure 17 shows the interface forces at the three human-exoskeleton interfaces from the four different interface models. The interface forces at the right thigh, shank and foot interfaces are plotted in the local reference frame of each interface (Figure 15). The plots represent the force from the exoskeleton to the human. The kinematic joint models (KJ and KJDS) used the reference frames for defining the constraints, and the resultant forces are expressed in those reference frames. In the case of contact models (CMDS and CMKJDS), the

resultant of the contact forces from all the contact elements of an interface was found at the same reference frames. The figure plots the mean and +/- 1 standard deviation from the eight trials for each model.

Firstly, Figure 17 shows that the kinematic joint models (KJ and KJDS) can only provide limited interface outputs due to the limited number of constraints that could be added in the kinematic joint models. No force outputs were available in the shear directions at the foot and the axial direction at the thigh. Even where the outputs were present, there was a significant difference between the outputs of the kinematic joint models (KJ and KJDS) and the contact models (CMDS and CMKJDS). Secondly, the peak vertical force at the foot interface of the contact models (CMDS and CMKJDS) was substantially closer to the subject weight of 760 N than that predicted by the kinematic joint models (KJ and KJDS). Thirdly, there was good agreement between CMDS and CMKJDS for all the interface forces except the vertical force at the thigh. Instead, the results between the two kinematic joint models (KJ and KJDS) showed differences in the forces in the X and Z axes.

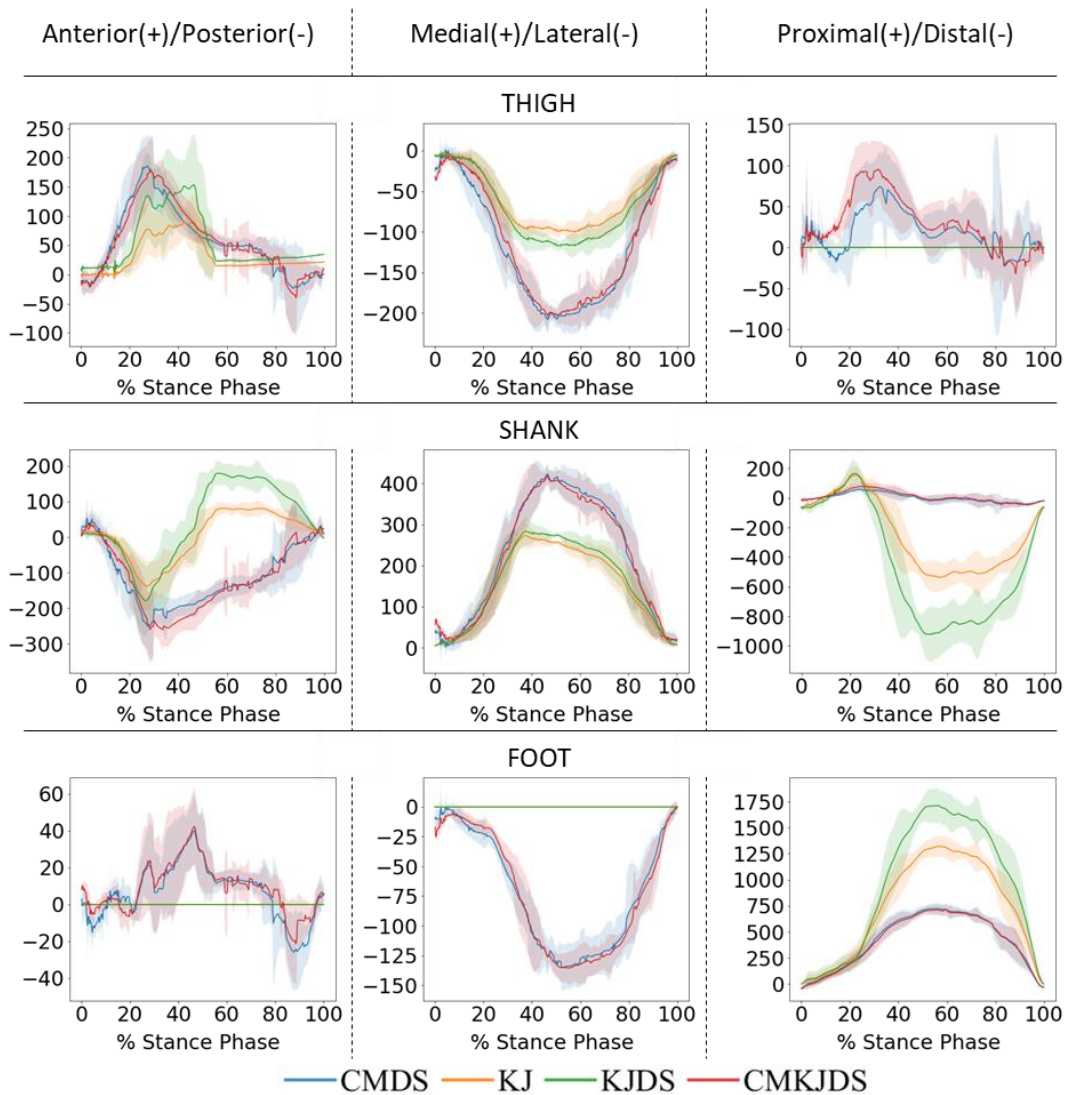


Figure 17: Interface forces from the four different models. Solid lines represent the mean of the eight trials and the shaded region represents +/- 1 std. deviation. Please refer to Figure 15 for the coordinate system and to Table 5 for the interface models.

## 5.4 Discussion

### 5.4.1 Contact model

The contact model for the exoskeleton used in this chapter, consisting of multiple interfaces that wrapped around the limbs, was developed using the same idea of simulating the curved surface through multiple planar surfaces, as described in chapter 4. In chapter 4, it was necessary to find the optimal strength of the contact elements that simulated the contact forces, otherwise, the contact elements unloaded the physiological muscles. In the current study as well, the contact elements unloaded the physiological muscles, however, there was no way to optimize the strength of the contact elements. There were different conditions that allowed the contact elements to unload the muscles in the two exoskeletons. The configuration of the current exoskeleton, with multiple interfaces that wrapped around the limb along with the misalignments between the human and exoskeleton joints, allowed the contact elements to unload the physiological muscles. Parametric studies of the strength of the contact muscles did not reveal any convergence of the interface outputs until some of the physiological muscles were completely unloaded, which was clearly unrealistic. The lack of convergence meant that potentially at any value of the strength of the contact elements, the recruitment of the physiological muscles could be influenced. Either the contact elements with high strength could be recruited to unload the physiological muscles or vice versa for contact elements with low strength.

Thus, dummy segments were introduced between the human and exoskeleton models to kinetically align the exoskeleton joints with the human joints. Once the misalignments were removed, the exoskeleton worked as an ideal exoskeleton. The contact elements were unable to exploit the misalignments and the model showed reasonable outputs even at high strengths of the contact elements to ensure the low activation of the contact elements. There was no need to optimize the strength of the contact elements.

However, human-exoskeleton misalignment is a real problem that affects the comfort of the user (Naf et al. 2018; Mallat et al. 2019). Joint misalignment has been shown to significantly affect the interface forces (Zanotto et al. 2015). The mocap data from the current study also demonstrated misalignments between the human and exoskeleton. One way to account for the misalignments in the model is to decompose the assistive torque from the exoskeleton into a functional component and an undesired interaction force (Gordon et al. 2018). The effect of the undesired interaction force on the biomechanical outputs could be studied by applying this undesired component additionally to the human model. However, the effect of this misaligned component on the interface force cannot be studied through the contact model with the dummy segments.



## 5.4.2 Comparison of different models: Biomechanical outputs

The second aim of this study was to compare the contact model with the conventional model of simulating the human-exoskeleton interface forces.

The biomechanical outputs of the different interface models were compared with the idealized case, ideal assistance (IA), where the exoskeleton assistance was applied directly on the human leg as a reference case (Figure 16). The IA case served to study the hypothetical case where the assistance could be applied without the device and its mass and inertia effects. It showed the desired effects of the exoskeleton. The biomechanical outputs from the contact model showed good agreement with the IA model. This confirmed that the biomechanical outputs from the contact model were reasonable and there was no unrealistic interaction between the contact elements and the physiological muscles.

The comparison between the contact model and the kinematic joint model was, however, not so straightforward. In a completely virtual assessment, the exoskeleton would be perfectly adapted to the anthropometry of the user with perfect alignment between the human and exoskeleton joints. However, the use of experimental data from actual trials would almost certainly induce misalignments as opposed to the ideal case of the virtual model. The contact model required the use of dummy segments to idealize the exoskeleton by removing the kinetic misalignments between the human and exoskeleton joints. Instead, the conventional model could allow some misalignments in the movement as the exoskeleton needed only eight constraints. Nonetheless, depending on the configuration of these eight constraints, the associated reaction forces could still be used to exploit the misalignments to unload the human muscles. This was a point of difference between the contact and conventional model. Thus, dummy segments were also added to the kinematic joint model to create an idealized kinematic joint model with dummy segments model (KJDS) and see if there was a substantial difference due to the dummy segments.

Secondly, the kinematics in the contact and conventional models were different. As markers were placed on both the subject and exoskeleton, sufficient mocap data were available to drive the subject and the exoskeleton individually from their respective markers. This was exactly the approach used in the contact model and it allowed relative motion in all the six DOF at each of the three interfaces. Instead, in the kinematic joint model, the kinematics of the human and exoskeleton model were linked through eight constraints, forcing their alignment, and changing the kinematics of the human-exoskeleton model. Thus, a new model (CMKJDS) was created with the contact model driven using the same kinematics from the kinematic joint model (KJ). Thus, the two reference models, KJDS and CMKJDS served to compare the outputs of the contact model and the conventional model considering only the difference in the kinetics.

The biomechanical outputs (Figure 16) about the knee, i.e., the activation of vastus lateralis, knee flexion moment, and knee compression force showed consistent results from the different models. Especially, the KJDS and CMKJDS models showed curves that overlapped each other for the most part. These models

were defined specifically to investigate the differences in the kinetics only and showed that the biomechanical outputs concerning the knee were not affected by the choice of the kinetic model. However, the presence of dummy segments or the change in kinematics affected the outputs slightly. CMDS was closest to the ideal assistance, while the other models showed some small differences that could be attributed to a change in kinematics (between CMDS and CMKJDS) or a change due to the presence of dummy segments (between KJ and KJDS). Nonetheless, the general consistency of the different interface models with regards to the biomechanical outputs about the knee joint is a positive result for the overall problem of modelling the physical human-exoskeleton interface. The knee joint is the target joint of this exoskeleton and consequently, the outputs concerning the knee joint would be of interest to evaluate the effects of the exoskeleton.

Contrary to the knee outputs, the outputs about the ankle joint showed a greater difference between the kinematic joint models (KJ and KJDS). Further, the KJDS and CMKJDS models showed consistent results only for the ankle plantarflexion moment. Instead, in the activation of the gastrocnemius and ankle compression force, CMKJDS was closer to the results of the KJ model. Additionally, the CMDS model did not match the activation of the gastrocnemius by the IA model. Even though the difference was not significant but, compared to the other outputs, where CMDS and IA showed consistent results, the difference in the gastrocnemius activation persisted for a greater duration.

The author could not identify a reason for the discrepancies in the results concerning the ankle joint. One reason could have been the choice of kinematic constraints. The kinematic constraints were chosen to provide ample support about the knee joint and seven of the eight constraints were distributed around the knee: three constraints at the thigh and four at the shank. Two other configurations were tested that had three constraints at the foot and one at the thigh, with the same four constraints at the shank. The biomechanical outputs about the ankle joint changed due to the different kinematics and different support provided by the different constraint configurations. However, they did not necessarily show consistent trends between the four models for the different outputs about the ankle.

### **5.4.3 Comparison of different models: Interface outputs**

In the unfortunate absence of experimental measurements of the interface outputs, not much can be said about the validity of the predicted interface outputs. The unpredictable consequences of Covid-19 pandemic limited the experimental data collection. Nonetheless, a few observations were already made in section 5.3.2. The kinematic joint models provided the reaction forces only in the added constraints. Thus, only limited information about the interface force was available, which should not be used to make reliable estimates of the interface forces in any case. The interface forces in the limited constraints must compensate for the absence of other constraints. A clear example of this could be seen in the vertical forces at the foot and shank. At the foot, the vertical force in the

kinematic joint models (KJ and KJDS) was much greater than the body weight of the subject, 760 N (Figure 17). This excessive force was then compensated at the shank. Instead, the contact models (CMDS and CMKJDS), that used the GRF prediction method at the foot base (Skals et al. 2017), showed much more reasonable forces at the foot interface and correspondingly an excessive vertical force at the shank (relatively speaking) was not observed. However, without any empirical data, it is difficult to say anything about the validity of the interface forces.

The contact model simulates contact forces that consist of the normal and shear forces. This is a potential advantage of the contact model over the kinematic joint model that simulates the interface forces as point forces without considering friction. However, further work is needed to estimate measures of pressure such as the average or peak pressure at the interface. The contact model simulates contact between rigid bodies. Instead, the interface pressure experienced by the user would depend on the initial strapping pressure, compliance of the soft tissues, and compliance of the interface, which were neither considered in the contact model nor the kinematic joint model. The initial strapping (or attachment) pressure has been shown to affect the comfort of the user (Schiele and van der Helm 2009; Langlois et al. 2020). The combined human-exoskeleton compliance at the interface can absorb and release the energy supplied by the exoskeleton during the different phases of the movement (Yandell et al. 2017). Human-exoskeleton misalignments can further affect the interface forces, potentially altering the energy absorbed and released by the compliance at the human-exoskeleton interface. The contact model, at best, can indicate the forces due to the assistance of the exoskeleton during the movement. It cannot account for the initial strapping pressure or the compliance at the interface.

Compliance at the human-exoskeleton interface can be accounted for in the model by modifying the assistive force/torque profile of the exoskeleton to compensate for the compliance (Gordon et al. 2018). Alternatively, the compliance can be simulated through the use of elastic models at the interface (Schiele 2008). More sophisticated modelling methods, such as force-dependent kinematics (Andersen et al. 2017), could be used in future studies to simulate the elastic compliance at the human-exoskeleton interface in musculoskeletal models. Nonetheless, whatever the approach, obtaining reliable estimates of model parameters for simulating human-exoskeleton compliance can be difficult without experiments. This renders the application of these models challenging during the virtual design phase.

#### **5.4.4 Limitations**

A limitation in this study was the kinematics of the human and exoskeleton feet. There was enough misalignment at the feet such that the human foot was partially outside of the exoskeleton foot in the model. There could be two reasons for this misalignment. Firstly, the recording of the mocap data for the feet was not optimal. Occluded markers were more frequent at the feet than elsewhere on the

leg. The presence of the stairs during the trials possibly led to the occlusion of the markers placed at the human and exoskeleton feet. Secondly, the model of the exoskeleton foot was a rather simplified rigid model of the actual compliant exoskeleton foot. The simplified model might have led to some errors in the relative location of the markers in the model of the exoskeleton foot. The consequence of the errors in the kinematics would have reflected in the biomechanical outputs, perhaps more so in the outputs concerning the ankle joint.

## 5.5 Conclusions

In this chapter, a method was developed to simulate the contact forces at the human-exoskeleton interfaces of an exoskeleton consisting of multiple curved interfaces. This chapter was the final part of the work performed in this PhD. It built on the work of the previous two chapters that simulated the contact forces for the Chairless Chair, simulating the interface first as a planar surface (chapter 3) and then as a curved surface (chapter 4). Instead, in the current chapter, the contact model was applied to a more general exoskeleton, consisting of multiple interfaces. The presence of multiple interfaces that wrapped completely around the limb added a complexity where the contact elements used to simulate the interface forces exploited the misalignments between the human and exoskeleton joints to unload the physiological muscles. The approach seen in chapter 4 to optimize the strength of the contact muscle did not work in this exoskeleton.

The human-exoskeleton misalignments were removed by introducing artificial mass-less and inertia-less segments, called dummy segments, between the human and exoskeleton. The dummy segments were used to kinetically align the exoskeleton joints with the human joints and prevented the contact elements to exploit the misalignments and unload the physiological muscles. Effectively, the dummy segments allowed a way to simulate the ideal exoskeleton even in the presence of real data. The biomechanical outputs from the contact model matched well with the biomechanical outputs from a reference case of the ideal assistance where the exoskeleton assistance was directly applied to the human model. A comparison of the contact model with the conventional model showed good agreement in the outputs about the knee joint but also some discrepancies in the outputs about the ankle joint.

The contact model can provide an estimate of interface forces. This could be a potential advantage of the contact model over the conventional model that relies on kinematic constraints and provides only limited outputs at the interface, depending on the configuration of the constraints. However, the interface forces could not be measured during the experiments. It is hoped that future studies could be organized to measure the interface forces and directly validate the predicted interface forces from the contact model.

The introduction of the dummy segments idealized the exoskeleton. Despite the use of real data showing misalignments between the human and exoskeleton, the effect of these misalignments on the human-exoskeleton interface could not be studied with this contact model utilizing the dummy segments. It would be of

interest to develop more sophisticated models capable of modelling soft-tissue deformation and compliance at the human-exoskeleton interface and investigating the effects of the misalignments between the human and exoskeleton joints. This could be the subject of future studies.



# Chapter 6

## Discussion

In the previous chapters, the results from the three individual studies have been discussed in isolation. In this chapter, the results from the three studies are discussed in the overall context of this thesis. The biomechanical and interface outputs from the three studies are discussed. Further, the two modelling methods are also discussed.

### 6.1 Biomechanical outputs

The biomechanical outputs are the most important outputs when using musculoskeletal models. The purpose of using musculoskeletal models is to assess the effects of the exoskeleton on the user. In this thesis, the outputs from the contact model were compared with the outputs of the conventional model and in both the exoskeletons, some discrepancies were observed. With the Chairless Chair (chapter 3), an unexpected trend was seen with the reaction force-based conventional model where the knee extension moment required by the user reduced as the postures became more challenging and required greater support of the body weight by the user's legs. It could be a limitation of the conventional model to simulate the seated surface of the Chairless Chair specifically. In the case of static simulations that were used for the analysis, reaction torques were added in the conventional model to simulate the supporting torques provided by the elongated surface of the seat. However, this allowed the model to exploit the supporting torque and reduce the knee extension moment, most notably in the lateral reaching posture.

The seat could be more suitable to be simulated by a contact model than a reaction force-based model. The interface supports the user only from a single side and acts as a surface on which the user can rest. In the simulation of the surface through the contact model, the model can only simulate the forces. The moment of the contact forces at each node can be calculated about a central point to determine the supporting torque of the seat. Consequently, the model can only

add more torque through a greater value of interface forces, or by providing the supporting forces as far away from the knee as possible. In the simulation of the seat as a planar surface, contact was simulated in a small part of the seat that was approximated as a planar surface. This created a boundary as to how far away from the knee the support could be provided. Indeed, in the simulation of the entire seat as a curved surface, it was seen that the most optimal location for providing the support was at the rear of the seat for high values of the strength of the contact elements. In this way, the model could provide the greatest counter moment about the knee, thereby reducing the effort required from the human model. Thus, an optimization of the strength of the contact elements was needed to ensure that the support was provided at the correct location on the seat, which would ensure a correct estimate of the effort required from the human model.

In chapter 5, another exoskeleton was studied. This exoskeleton from HTWK Leipzig offered the possibility to investigate the contact model on a more generic exoskeleton. The exoskeleton consisted of three interfaces that extended across the knee and ankle joints. It was seen that the biomechanical outputs about the knee joint from the contact and kinematic joint models were consistent. In fact, two extra models (CMKJDS and KJDS) were introduced in the study to see purely the differences between the two kinetic models. These two models showed good agreement with each other as far as the outputs concerned the knee: activation of the vastus lateralis, knee flexion moment and knee compression force. This similarity in the biomechanical outputs about the knee contrasted with the finding from the study of the Chairless Chair where the two models showed a difference in the knee extension moment trend (chapter 3). The contrasting results could be due to the different nature of the interfaces of the two exoskeletons. An interface that wraps completely around the limb could be better approximated by a kinematic joint than the interface of the Chairless Chair that supports only from a single side.

Going back to the exoskeleton from HTWK Leipzig (chapter 5), the two models (CMKJDS and KJDS), however, showed different results about the ankle joint. The reason for the discrepancies between the two models for the results about the ankle joint could not be identified, although the limitation in the mocap recording of the foot was suspected.

In the absence of any validation metric in chapter 5, a reference model was prepared that applied the exoskeleton assistance and the ground reaction force directly to the human model. With respect to the knee joint, all the models showed consistent results with the reference model. Instead, for the ankle joint, the contact models were closer to the reference model in all the outputs, while the kinematic joint models matched the reference model in some outputs only.

Overall, the biomechanical results from the contact model seemed reasonable. However, obtaining reasonable results from the contact model is not so straightforward. Muscle recruitment is calculated through an optimization problem that is geared to minimize the muscular effort required. Thus, the presence of contact elements in the muscle recruitment problem can influence the recruitment of the physiological muscles. The optimizer would exploit the contact



elements, if possible, to minimize the overall effort required. Thus, the results must be critically analysed to check if they are reasonable or not.

## 6.2 Interface outputs

In the first study with the simulation of the seat of the Chairless Chair as a planar surface (chapter 3), the interface forces from the contact model and the reaction force-based conventional model were compared. The reaction force-based model does not account for friction, and it was evident from the variation in the ratio of the normal to shear forces. Unlike the conventional model, the contact model accounted for friction at the interface, and this was seen from the consistent ratio of the normal to shear forces and the parametric studies of the coefficient of friction and angle of contact. As an empirical measure, the body weight distribution was used as a reference for the two models. Across the three test conditions, both the models showed similar trends and were able to capture the increasing difficulty of the test conditions. The conventional model consistently reported a lesser proportion of body weight supported by the exoskeleton than the contact model.

In the simulation of the seat of the Chairless Chair as a curved surface (chapter 4), only the contact model was simulated. The centre of pressure at the human-exoskeleton interface and the body weight distribution between the subject and the exoskeleton were used as the empirical measures. Although the area of contact was used as an input in the contact model, the model was able to closely estimate the interface forces and the centre of pressure. This was an advantage over the work in chapter 3, where the location of the support must be estimated by the modeller. As explained in chapter 4, the need to use the area of contact was specific to the Chairless Chair as the exoskeleton is designed to offer a variation in the sitting height, which changes the orientation of the seat and the contact condition.

In the final study with the exoskeleton from HTWK Leipzig (chapter 5), the comparison of the interface forces from the two models was limited as no empirical measures were available due to the restrictions for Covid-19. The key difference between the two models was the amount of information available for the interface outputs. Due to the design of the exoskeleton, only eight constraints were needed between the human and exoskeleton. Thus, the reaction forces were available only in the constraints added. Seven of these constraints were added at the thigh and shank to provide adequate support about the knee as it was the assisted joint. Only one constraint was added at the foot. The support from the limited constraints resulted in an excessive force at the foot interface. The vertical force at the foot interface is the only force where some conclusions can be made as it should roughly support the body weight of the subject. The contact model provided a closer estimate of the vertical force to the body weight than the kinematic joint model. Overall, the contact model could provide all-around support at the different interfaces. However, empirical observations at the interface are still needed to validate the interface forces predicted by the contact

model, especially as this study demonstrated that different interface outputs could still result in similar biomechanical outputs.

### **6.3 Comparison of modelling methods**

Modelling of human-exoskeleton interface forces using the reaction forces associated with kinematic constraints is a frequently used method in the literature (Ferrati et al. 2013; Agarwal et al. 2016; Guan et al. 2016; Harant et al. 2017; Zhou et al. 2017; Gordon et al. 2018; Jensen et al. 2018; Panero et al. 2020). The kinematic constraints serve to define the kinematics of the exoskeleton relative to the human. However, using the kinematic constraints requires critical thinking about the type of constraints that must be added, especially for exoskeletons that span more than one joint of the human. It can be challenging to identify the correct distribution of constraints across the multiple interfaces to simulate the interface forces when using real data, which leads to misalignments between the human and exoskeleton. The distribution of the constraints should be able to provide reaction forces in directions that ensure the correct transfer of the exoskeleton assistance to the user. Changing the distribution of the constraints across the interfaces not only changes the interface forces but can potentially alter the biomechanical outputs from the simulation.

The contact model, on the other hand, has its own challenges. The addition of contact elements can result in unrealistic solutions as the most optimal solution to the muscle recruitment problem. The contact model also requires a critical analysis of the results to understand if the results are reasonable or not. In this work, two different strategies have been presented to simulate the contact forces in two different types of exoskeletons. The strategy for the second exoskeleton with the use of dummy segments would not be necessary if a completely virtual analysis is made without using mocap data with a prototype exoskeleton. In this case, the exoskeleton kinematics can be driven using kinematic constraints that ensure kinematic alignment between the human and exoskeleton joints. The kinetics can then be simulated through the contact model.

In terms of modelling efforts, the kinematic constraints are easy to add in multibody tools. Only two reference frames and the type of constraint needs to be defined. Instead, the contact model requires significantly more effort. First, multiple reference frames need to be defined at the interface to replicate its geometry. This process can be accelerated if parametric surfaces, such as a cylinder, are used to define the interface. However, often intricately contoured interfaces are observed in exoskeletons. In such a case, the reference frames to define the contact points might need to be created manually. Second, implementing the contact model multiple times would require further time. However, programming shortcuts such as creating a custom class or function can accelerate the process of setting up the contact elements using the reference frames as input. Third, additional efforts would be required to aggregate the outputs from all the contact elements to calculate the resultant forces and moments at the interface.

Finally, in terms of computational resources as well, the kinematic joint model is more efficient than the contact model. The contact model adds several contact elements in the muscle recruitment optimization problem, which can significantly affect the computational time compared to simulating the interface forces through the reaction force-based model. The difference in the computational time would naturally depend on the number of contact elements added. In the mocap based simulations for the second exoskeleton in chapter 5, the parameter identification on a standing reference trial and the kinematics and inverse dynamics analysis of the eight stair ascent trials were run sequentially through batch processing. Indicatively, the simulations with the contact model took more than three times the time required for the simulations with the kinematic constraints model. Batch processing could be sped up by running parallel processes instead of sequential processing. However, another factor to consider in parallel processing is the greater memory needed to load and run the contact model with its additional reference frames and contact elements than the conventional model.

## 6.4 Limitations

A few general limitations in the development of this thesis must be addressed.

First, the limitations of the contact model must be mentioned. The contact model simulates contact between rigid bodies. The model cannot estimate soft-tissue artefacts, compliance of the interface or the initial strapping (attachment) pressure. Further, the contact model cannot simulate the effect of the human-exoskeleton misalignment on the interface forces. Thus, the estimated forces from the contact model are limited in their ability to estimate the actual forces that could be experienced by the user of an exoskeleton. These aspects have been discussed in greater detail in section 5.4 and could be the subject of future works.

Second, all the studies in this thesis were carried out with trials on a single subject. Both the studies with the Chairless Chair were developed with support from FCA and its research centre, CRF. The first study was an initial investigation into the applicability of the contact model. It was developed using data already collected by CRF for their internal investigations. The second study was a more detailed investigation into the simulation of the contact force at a generalized interface. However, recruiting multiple subjects for the Chairless Chair was rather challenging. Internal investigations of FCA and CRF had revealed that user confidence was a significant factor in the effective use of the Chairless Chair. A similar finding was subsequently also reported in another study with the Chairless Chair, where subjects without prior experience with the exoskeleton did not feel as safe as hoped during testing (Groos et al., 2020). User perception of an exoskeleton can change over extended use of an exoskeleton (Hensel and Keil 2019; Yandell et al. 2020). In the case of the Chairless Chair, it was absolutely essential that the subject had sufficient training time to feel confident with the exoskeleton and use it effectively, overcoming the fear of instability and falling. It was simply not possible to organize an experimental campaign with multiple

subjects. The limitation of drawing scientific conclusions from a single subject was recognized. More subjects and a greater anthropometric variation would have provided further insights into the model, such as the difference in the trend of the knee extension moment from the contact and conventional model, or the dependence of the optimal strength on the anthropometry of the subject. A more detailed experimental campaign with multiple subjects was planned for the second exoskeleton under development at HTWK Leipzig. Unfortunately, the plans were compromised by the unforeseen situation due to Covid-19. Approval for a more elaborate study with multiple subjects could not be obtained in those circumstances.

Finally, there is a limitation in the validity of the contact forces. In the studies with the Chairless Chair, the contact forces were indirectly validated using the body weight distribution, which indicated only the vertical component of the interface force. The field of quantifying the human-exoskeleton interaction forces is still nascent, and research is carried out using custom-built specialized instruments that are not commonly available. Moreover, the validity of contact forces would require the use of a real exoskeleton, which would mean kinematic misalignments and the consequent unwanted interface forces would come into play in the trials. The contact model can simulate the contact forces only for an ideal exoskeleton with perfect kinematic alignment. Depending on the misalignment, the parasitic interface forces in the trial may not be negligible.

# Chapter 7

## Conclusion

### 7.1 Summary of the thesis

Exoskeletons have received a lot of interest recently. They are being investigated as a potential aid in a diverse field of applications. In this thesis, a contact model was used for simulating the human-exoskeleton interface forces in musculoskeletal models. The motivation for using the contact model was the lack of realistic models to investigate the forces at the interface. The conventional approach of simulating the interface forces using reaction forces associated with kinematic joints may not be sufficient to investigate the interface forces and interface properties. Simulating contact forces at the interface could allow the investigation and optimization of the interface design.

This thesis aimed to apply the contact model to two different exoskeletons. This was achieved through three studies that progressively built more complex models based on the findings from each study. The first two studies were done with the Chairless Chair, which allowed the possibility to simplify the human-exoskeleton interface as a planar surface at first, and was followed by its simulation as a curved surface in the second study. Subsequently, the third and final study was done on the active lower-limb exoskeleton developed at HTWK Leipzig and simulated the contact forces at multiple curved interfaces.

In the first study (chapter 3), the exoskeleton seat of the Chairless Chair was simulated as a planar surface. An existing contact model that used contact elements for predicting the ground reaction force was implemented as it is to simulate contact forces at the human-exoskeleton interface. The aim of this study was to make an initial investigation into the application of this contact model to simulate the contact forces at the human-exoskeleton interface. The contact model simulated the ground as a planar surface and thus the exoskeleton interface was also simulated as a planar surface at first. The results from the contact model were compared to the results from the conventional model of simulating interface forces through the reaction forces associated with kinematic constraints. Further,

parameters of the contact model such as the coefficient of friction and the angle of contact were investigated in greater detail. Indeed, these parameters were relevant in the simulation of the contact forces. The angle of contact made a difference in the simulated support provided by the Chairless Chair.

Building on the findings from the first study, in the second study (chapter 4), the seat of the Chairless Chair was simulated as a curved surface. The contact forces were simulated at the curved interface of the exoskeleton to capture its intricate shape with a continuously changing orientation. The surface of the interface was represented as multiple planar surfaces and the planar contact model was implemented at each of these multiple planar surfaces, thereby representing the correct shape of the seat. It was seen that this method of discretization led to an unrealistic solution. The most optimal solution for the solver was to provide the support at the rear of the seat, furthest away from the knee, which led to a reduction of the biomechanical effort from the user. Thus, simulating the curved surface required an optimization of the strength of the contact elements to ensure that unrealistic solutions were not obtained. The second study defined a method to optimize the strength of the contact elements from the model outputs directly. The virtual centre of pressure and the interface force were used to optimize the strength of the contact elements.

However, the necessity to optimize the strength of the contact elements in the second study led to questions over the applicability of the contact model in other exoskeletons. The Chairless Chair was selected as the exoskeleton for this work due to the simplicity it offered in modelling the contact forces. Only a single interface was modelled, and the interface provided support from one side of the limb. Moreover, the simulations were static. In the final study (chapter 5), the contact model was implemented on another exoskeleton. The exoskeleton is an active exoskeleton for the lower limb consisting of three interfaces: the thigh, shank, and foot. Each interface wraps around the limb completely. Further, the analysis was done for a dynamic movement. This exoskeleton was chosen as an example of a more typical exoskeleton, rather than the Chairless Chair. It was observed that the presence of the contact elements allowed the inverse dynamics analysis to completely unload some of the physiological muscles in the second exoskeleton. The misalignments between the human and exoskeleton joints were identified as the root cause. The misalignments allowed the muscle recruitment algorithm to “exploit” the contact elements to create large interface forces where a component of the interface forces could contribute to the flexion/extension of the knee and unload the physiological muscles completely and unrealistically. The misalignments were corrected by introducing artificial dummy segments between the human and exoskeleton. The dummy segments aligned the exoskeleton joint with the human joints kinetically and, subsequently, the contact model showed reasonable results. The results of the contact model with dummy segments were compared with the conventional model consisting of kinematic joints and the associated reaction force. As the kinematic constraints resulted in slightly different kinematics and did not use the dummy segments, two more models were included in the comparison. These were the contact model using the kinematic

constraints for the kinematics, and the kinematic joint model with dummy segments. The results of all the different interface models were compared with a reference model where the exoskeleton assistance was applied directly to the human model. The biomechanical outputs from the contact model showed good agreement with those from the reference model.

## 7.2 Contributions of the thesis

The aims of this thesis were:

- Develop and disseminate methods for applying a contact model to simulate the forces at the human-exoskeleton interface of two different types of exoskeletons.
- Compare the biomechanical and interface outputs from the contact model with those from the conventional model of simulating interface forces using reaction forces associated with kinematic constraints for both the exoskeletons.

The key contributions of this thesis are the methods that allow the use of a contact model to simulate the human-exoskeleton interface forces. The application of the contact model is not always straightforward, and this thesis provides methods for two different types of exoskeletons and interfaces. In the first exoskeleton, consisting of a single interface supporting from a single side, a method was defined to optimize the strength of the contact elements using virtual outputs. This allowed the model to correctly estimate the support and the virtual centre of pressure. In the second exoskeleton, consisting of multiple interfaces that wrap around the limb, a method was provided that allowed the use of the contact model with misalignments between the human and exoskeleton joints. The latter method, with dummy segments, can be especially useful for the analysis of prototype exoskeletons where misalignments between the human and exoskeleton joints are commonly recorded.

Finally, the thesis provides a comprehensive comparison of the contact model with the conventional model using kinematic constraints. The author is not aware of other works that have compared different interface models. Not just the outputs from the two models but also the modelling methods and their implications are critically compared. The primary aim of musculoskeletal models is the biomechanical analysis of the human-exoskeleton system. The contact model showed reasonable biomechanical outputs for both the exoskeletons and overcame the limitations of the conventional method using kinematic constraints.

Finally, the contact model provides another layer of information that could be used in the design and analysis of exoskeletons. However, developing the contact model can be expensive in terms of time required and it should be left for the advanced phases of the design process where the focus is on defining a detailed model of the exoskeleton. The estimated contact force could be compared to thresholds for discomfort (Yandell et al. 2020). This virtual check could provide

additional confidence in the design. Further, the contact model could be utilized to optimize the design of the interface. Rigid bracing could be reshaped by studying the contact forces and identifying areas of the interface that are not critical for providing support. As an example, a complete cylindrical interface could be used as a starting shape for the interface of a lower limb exoskeleton. A lower-limb exoskeleton would predominantly see motions in the sagittal plane, such as gait. The interface could be split into anterior and posterior halves and the centre of pressures in the two halves could be tracked during a simulated gait. Due to the nature of the movement in gait, lower support would be needed from the medial or lateral sides of the exoskeleton compared to the anterior or posterior sides. Thus, the interface could be optimized by removing some part of the interface from the medial and lateral sides, potentially reducing the mass and cost of the exoskeleton. On the other hand, for regions that would be expected to bear the load, the interface shape could be optimized to better distribute the load, which could be a more effective way to distribute the load than the addition of extra padding (Levesque et al. 2017).



# Chapter 8

## Future Work

Exoskeleton research is still in a nascent stage and evolving rapidly. The lack of realistic models to investigate the interface forces motivated the development of this thesis. However, during the development of this thesis, the focus on the physical human-exoskeleton interface has increased, further validating the need for contact models to investigate the interface during the design phase. Recent literature to identify the discomfort thresholds for exoskeletons indicates the interest in studying the human-exoskeleton interaction, which is relevant for the overall comfort and user-acceptability of exoskeletons. It is hoped that the contact models could allow for virtual investigations of the contact forces at the interface, which could be relevant in the virtual design of the human-exoskeleton interface.

However, further work is needed. First of all, all the studies in this thesis had a single subject. While the first two studies were exploratory in nature, the experimental work for the third study was conducted in 2020 and was, unfortunately, affected by the restrictions to contain the spread of Covid-19. Studies with multiple subjects are needed to increase the confidence in some of the conclusions, especially, the comparison between the contact and conventional model. In the first study with the Chairless Chair, a difference in the trend of the knee extension moment, a key biomechanical output, was noted. In the second study, some discrepancies were noted in the biomechanical outputs about the ankle joint. The reason for these discrepancies in the second exoskeleton could not be identified. An experimental campaign with multiple subjects would have definitely provided a greater insight into both the exoskeletons. Further, work is also needed on the validity of the contact forces. The specialized instruments needed to quantify the human-exoskeleton interface forces are generally custom-built and not commonly available. This has also been a limiting factor in the development of this thesis.

However, the validity of interface forces would also require more advanced methods to simulate the interface. The contact model simulates contact between rigid bodies. However, the actual interface has some compliance due to the elastic

deformation on both the human and exoskeleton side (through elastic straps, padding, etc.). Measurement of the interface force would invariably be subjected to the energy absorption and return dynamics at the interface (Yandell et al. 2017). The contact model cannot account for the effect of this elastic deformation and more sophisticated models must be used for the validation of the contact forces. There are already examples of viscoelastic models of the human-exoskeleton interface in the literature (Schiele 2008). Further, advanced simulation methods, such as force-dependent kinematics (Andersen et al. 2017), could be used to predict the deformation and the forces at the interface during inverse dynamics analysis. However, identifying the model parameters for elastic models can be challenging and must be validated with experimental studies. The parameters would be specific to the exoskeleton in consideration and depend not only on the properties of the exoskeleton but also on the properties of the interface on the human side (for example, stiffness constant at upper and lower limbs would be different). This is evidenced by the vastly different values of optimal strapping pressure and interface stiffness reported in the literature. Schiele and van der Helm 2009 reported an optimal strapping pressure of 20 mmHg and a corresponding attachment stiffness of 300 N/m. In another study with another setup, an optimal strapping pressure in the range of 50 to 80 mmHg and an attachment stiffness of 1578 N/m at 50 mmHg were reported (Langlois et al. 2020). In fact, the latter study also showed that initial strapping pressure at the human exoskeleton interface can alter the stiffness at the interface. Considering that the initial strapping pressure can vary from trial to trial, if not controlled, it highlights how challenging identifying the model parameters can be. There is a trade-off between attachment stiffness and perceived comfort. A stiffer interface can allow for reduced losses at the interface but can be uncomfortable. It is clearly an important issue in the user-acceptability of exoskeletons. But, for now, it is an equally challenging issue to model and predict the correct trade-off virtually.

Another issue that affects the human-exoskeleton system is the misalignment between the human and exoskeleton joints. Joint misalignment can significantly affect the interface forces (Zanotto et al. 2015). The validity of contact forces would involve a real subject wearing a real exoskeleton and some joint misalignment would affect the interface forces. However, the contact model cannot estimate the effect of the joint misalignment on the interface force. The contact model requires the use of dummy segments to kinetically align the human-exoskeleton joints so that the contact elements do not contribute towards the normal motion of the joint and unload the muscles. The effect of joint misalignment has been studied previously by decomposing the assistive torque from the exoskeleton into a functional and undesirable component (Gordon et al. 2018). In the future, the contact model could be enhanced by implementing this functionality into the model. Dummy segments allow the possibility to use kinematic data with joint misalignments. The misalignment could be read during the kinematics analysis and could be used to modify the assistance from the exoskeleton accordingly.

# References

- Agarwal P, Narayanan MS, Lee L, Mendel F, Krovi VN (2010) Simulation-Based Design of Exoskeletons Using Musculoskeletal Analysis. Vol 3 30th Comput Inf Eng Conf Parts A B 1357–1364. <https://doi.org/10.1115/DETC2010-28572>
- Agarwal P, Neptune RR, Deshpande AD (2016) A Simulation Framework for Virtual Prototyping of Robotic Exoskeletons. *J Biomech Eng* 138:061004. <https://doi.org/10.1115/1.4033177>
- Alabdulkarim S, Nussbaum MA (2019) Influences of different exoskeleton designs and tool mass on physical demands and performance in a simulated overhead drilling task. *Appl Ergon* 74:55–66. <https://doi.org/10.1016/j.apergo.2018.08.004>
- Amandels S, Eyndt HO, Daenen L, Hermans V (2019) Introduction and Testing of a Passive Exoskeleton in an Industrial Working Environment. In: Bagnara S, Tartaglia R, Albolino S, Alexander T, Fujita Y (eds) *Proceedings of the 20th Congress of the International Ergonomics Association (IEA 2018)*. Springer International Publishing, Cham, pp 387–392
- Andersen MS, Damsgaard M, MacWilliams B, Rasmussen J (2010) A computationally efficient optimisation-based method for parameter identification of kinematically determinate and over-determinate biomechanical systems. *Comput Methods Biomech Biomed Engin* 13:171–183. <https://doi.org/10.1080/10255840903067080>
- Andersen MS, Damsgaard M, Rasmussen J (2009) Kinematic analysis of over-determinate biomechanical systems. *Comput Methods Biomech Biomed Engin* 12:371–384. <https://doi.org/10.1080/10255840802459412>
- Andersen MS, De Zee M, Damsgaard M, Nolte D, Rasmussen J (2017) Introduction to force-dependent kinematics: Theory and application to mandible modeling. *J Biomech Eng* 139 (9): 091001. <https://doi.org/10.1115/1.4037100>
- Ármanndóttir AL, Beckerle P, Moreno JC, van Asseldonk EHF, Manrique-Sancho MT, del-Ama AJ, Veneman JF, Briem K (2020) Assessing the Involvement of Users During Development of Lower Limb Wearable Robotic Exoskeletons: A Survey Study. *Hum Factors* 62:351–364. <https://doi.org/10.1177/0018720819883500>
- Bai S, Rasmussen J (2011) Modelling of Physical Human-Robot Interaction for Exoskeleton Designs. *Multibody Dyn 2011, ECCOMAS Themat Conf* 1–7
- Baltrusch SJ, van Dieën JH, van Bennekom CAM, Houdijk H (2018) The effect of a passive trunk exoskeleton on functional performance in healthy individuals. *Appl Ergon* 72:94–106.

- <https://doi.org/10.1016/j.apergo.2018.04.007>
- Bosch T, van Eck J, Knitel K, de Looze M (2016) The effects of a passive exoskeleton on muscle activity, discomfort and endurance time in forward bending work. *Appl Ergon* 54:212–217. <https://doi.org/10.1016/j.apergo.2015.12.003>
- Cappozzo A, Catani F, Della Croce U, Leardini A (1995) Position and orientation in space of bones during movement: anatomical frame definition and determination. *Clin Biomech* 10:171–178. [https://doi.org/10.1016/0268-0033\(95\)91394-T](https://doi.org/10.1016/0268-0033(95)91394-T)
- Carbone V, Fluit R, Pellikaan P, Krogt MM Van Der, Janssen D, Damsgaard M, Vigneron L, Feilkas T, Koopman HFJM, Verdonschot N (2015) TLEM 2.0 – A comprehensive musculoskeletal geometry dataset for subject-specific modeling of lower extremity. *J Biomech* 48:734–741. <https://doi.org/10.1016/j.jbiomech.2014.12.034>
- Castro MN, Rasmussen J, Bai S, Andersen MS (2019) Validation of subject-specific musculoskeletal models using the anatomical reachable 3-D workspace. *J Biomech* 90:92–102. <https://doi.org/10.1016/j.jbiomech.2019.04.037>
- Chander DS, Cavatorta MP (2019) Modelling friction at the mechanical interface between the human and the exoskeleton. *Int J Hum Factors Model Simul* 7:119–136. <https://doi.org/10.1504/IJHFMS.2019.105434>
- Chander DS, Cavatorta MP (2020) Modelling interaction forces at a curved physical human-exoskeleton interface. *Adv Transdiscipl Eng* 11:217–226. <https://doi.org/10.3233/ATDE200028>
- Chen B, Zi B, Wang Z, Qin L, Liao W-H (2019) Knee exoskeletons for gait rehabilitation and human performance augmentation: A state-of-the-art. *Mech Mach Theory* 134:499–511. <https://doi.org/10.1016/j.mechmachtheory.2019.01.016>
- Cho K, Kim Y, Yi D, Jung M, Lee K (2012) Analysis and Evaluation of a Combined Human-Exoskeleton Model Under Two Different Constraints Condition. *Int Summit Hum Simul (ISHS)*, St Pete Beach, FL, May 23–25
- Damsgaard M, Rasmussen J, Christensen ST, Surma E, de Zee M (2006) Analysis of musculoskeletal systems in the AnyBody Modeling System. *Simul Model Pract Theory* 14:1100–1111. <https://doi.org/10.1016/j.simpat.2006.09.001>
- de Kruif BJ, Schmidhauser E, Stadler KS, O’Sullivan LW (2017) Simulation Architecture for Modelling Interaction Between User and Elbow-articulated Exoskeleton. *J Bionic Eng* 14:706–715. [https://doi.org/10.1016/S1672-6529\(16\)60437-7](https://doi.org/10.1016/S1672-6529(16)60437-7)
- de Looze MP, Bosch T, Krause F, Stadler KS, O’Sullivan LW (2016) Exoskeletons for industrial application and their potential effects on physical work load. *Ergonomics* 59:671–681. <https://doi.org/10.1080/00140139.2015.1081988>
- De Rossi SMM, Vitiello N, Lenzi T, Ronsse R, Koopman B, Persichetti A,

- Vecchi F, Ijspeert AJ, Van der Kooij H, Carrozza MC (2010) Sensing Pressure Distribution on a Lower-Limb Exoskeleton Physical Human-Machine Interface. *Sensors* 11:207–227 . <https://doi.org/10.3390/s110100207>
- de Zee M, Hansen L, Wong C, Rasmussen J, Simonsen EB (2007) A generic detailed rigid-body lumbar spine model. *J Biomech* 40:1219–1227. <https://doi.org/https://doi.org/10.1016/j.jbiomech.2006.05.030>
- Ferrati F, Bortoletto R, Pagello E (2013) Virtual modelling of a real exoskeleton constrained to a human musculoskeletal model. *Lect Notes Comput Sci (including Subser Lect Notes Artif Intell Lect Notes Bioinformatics)* 8064 LNAI:96–107 . <https://doi.org/10.1007/978-3-642-39802-5-9>
- Fluit R, Andersen MS, Kolk S, Verdonshot N, Koopman HFJM (2014) Prediction of ground reaction forces and moments during various activities of daily living. *J Biomech* 47:2321–2329. <https://doi.org/10.1016/j.jbiomech.2014.04.030>
- Fournier BN, Lemaire ED, Smith AJJ, Doumit M (2018) Modeling and Simulation of a Lower Extremity Powered Exoskeleton. *IEEE Trans Neural Syst Rehabil Eng* 26:1596–1603. <https://doi.org/10.1109/TNSRE.2018.2854605>
- Fox S, Aranko O, Heilala J, Vahala P (2019) Exoskeletons: Comprehensive, comparative and critical analyses of their potential to improve manufacturing performance. *J Manuf Technol Manag* 31:1261–1280. <https://doi.org/10.1108/JMTM-01-2019-0023>
- Frankenfield DC, Rowe WA, Cooney RN, Smith JS, Becker D (2001) Limits of body mass index to detect obesity and predict body composition. *Nutrition* 17:26–30 . [https://doi.org/https://doi.org/10.1016/S0899-9007\(00\)00471-8](https://doi.org/https://doi.org/10.1016/S0899-9007(00)00471-8)
- Georgarakis A, St R, Wolf P, Riener R, Duarte JE (2018) A Method for Quantifying Interaction Forces in Wearable Robots \*. <https://doi.org/10.1109/BIOROB.2018.8487701>
- Gordon DFN, Henderson G, Vijayakumar S (2018) Effectively Quantifying the Performance of Lower-Limb Exoskeletons Over a Range of Walking Conditions. *Front Robot AI* 5:1–16. <https://doi.org/10.3389/frobt.2018.00061>
- Groos S, Fuchs M, Kluth K (2020) Determination of the Subjective Strain Experiences During Assembly Activities Using the Exoskeleton “Chairless Chair .” Springer International Publishing
- Guan X, Ji L, Wang R, Huang W (2016) Optimization of an unpowered energy-stored exoskeleton for patients with spinal cord injury. *Proc Annu Int Conf IEEE Eng Med Biol Soc EMBS* 2016-Octob:5030–5033. <https://doi.org/10.1109/EMBC.2016.7591857>
- Halonen KS, Dzialo CM, Mannisi M, Venäläinen MS, De Zee M, Andersen MS (2017) Workflow assessing the effect of gait alterations on stresses in the medial tibial cartilage - Combined musculoskeletal modelling and finite element analysis. *Sci Rep* 7:1–14. <https://doi.org/10.1038/s41598-017-17228-x>

- Hansen C, Gosselin F, Mansour K Ben, Devos P, Marin F (2018) Design-validation of a hand exoskeleton using musculoskeletal modeling. *Appl Ergon* 68:283–288. <https://doi.org/https://doi.org/10.1016/j.apergo.2017.11.015>
- Harant M, Sreenivasa M, Millard M, Sarabon N, Mombaur K (2017) Parameter optimization for passive spinal exoskeletons based on experimental data and optimal control. *IEEE-RAS Int Conf Humanoid Robot* 535–540. <https://doi.org/10.1109/HUMANOIDS.2017.8246924>
- Hensel R, Keil M (2019) Subjective Evaluation of a Passive Industrial Exoskeleton for Lower-back Support: A Field Study in the Automotive Sector. *IISE Trans Occup Ergon Hum Factors* 0:1–9. <https://doi.org/10.1080/24725838.2019.1573770>
- Horsman MDK, Koopman HFJM, Helm FCT Van Der, Prose LP (2007) Morphological muscle and joint parameters for musculoskeletal modelling of the lower extremity. *Ergonomics* 50:223–247. <https://doi.org/10.1016/j.clinbiomech.2006.10.003>
- Huysamen K, Bosch T, de Looze M, Stadler KS, Graf E, O’Sullivan LW (2018a) Evaluation of a passive exoskeleton for static upper limb activities. *Appl Ergon* 70:148–155. <https://doi.org/10.1016/J.APERGO.2018.02.009>
- Huysamen K, de Looze M, Bosch T, Ortiz J, Toxiri S, O’Sullivan LW (2018b) Assessment of an active industrial exoskeleton to aid dynamic lifting and lowering manual handling tasks. *Appl Ergon* 68:125–131. <https://doi.org/10.1016/j.apergo.2017.11.004>
- Jensen EF, Raunsbæk J, Lund JN, Rahman T, Rasmussen J, Castro MN (2018) Development and simulation of a passive upper extremity orthosis for amyoplasia. *J Rehabil Assist Technol Eng* 5:1–10. <https://doi.org/10.1177/2055668318761525>
- Joch M, Döhring FR, Maurer LK, Müller H (2019) Inference statistical analysis of continuous data based on confidence bands—Traditional and new approaches. *Behav Res Methods* 51:1244–1257. <https://doi.org/10.3758/s13428-018-1060-5>
- Jung M, Fau G, Letier P, Mittag U, Zange J, Rittweger J, Runge A (2017) Musculoskeletal Simulation of SOLEUS Ankle Exoskeleton for Countermeasure Exercise in Space. In: González-Vargas J, Ibáñez J, Contreras-Vidal JL, van der Kooij H, Pons JL (eds) *Wearable Robotics: Challenges and Trends*. Springer International Publishing, Cham, pp 391–396
- Jung Y, Jung M, Lee K, Koo S (2014) Ground reaction force estimation using an insole-type pressure mat and joint kinematics during walking. *J Biomech* 47:2693–2699. <https://doi.org/10.1016/j.jbiomech.2014.05.007>
- Karatsidis A, Bellusci G, Schepers HM, de Zee M, Andersen MS, Veltink PH (2017) Estimation of ground reaction forces and moments during gait using only inertial motion capture. *Sensors (Switzerland)* 17:1–22.

- <https://doi.org/10.3390/s17010075>
- Karatsidis A, Jung M, Schepers HM, Bellusci G, de Zee M, Veltink PH, Andersen MS (2019) Musculoskeletal model-based inverse dynamic analysis under ambulatory conditions using inertial motion capture. *Med Eng Phys* 65:68–77 . <https://doi.org/10.1016/j.medengphy.2018.12.021>
- Kermavnar T, O’Sullivan KJ, Casey V, de Eyto A, O’Sullivan LW (2020a) Circumferential tissue compression at the lower limb during walking, and its effect on discomfort, pain and tissue oxygenation: Application to soft exoskeleton design. *Appl Ergon* 86:103093. <https://doi.org/10.1016/j.apergo.2020.103093>
- Kermavnar T, O’Sullivan KJ, de Eyto A, O’Sullivan LW (2020b) The effect of simulated circumferential soft exoskeleton compression at the knee on discomfort and pain. *Ergonomics* 63:618–628. <https://doi.org/10.1080/00140139.2020.1743373>
- Khamar M, Edrisi M, Zahiri M (2019) Human-exoskeleton control simulation, kinetic and kinematic modeling and parameters extraction. *MethodsX* 6:1838–1846 . <https://doi.org/10.1016/j.mex.2019.08.014>
- Kim S, Nussbaum MA, Mokhlespour Esfahani MI, Alemi MM, Alabdulkarim S, Rashedi E (2018) Assessing the influence of a passive, upper extremity exoskeletal vest for tasks requiring arm elevation: Part I – “Expected” effects on discomfort, shoulder muscle activity, and work task performance. *Appl Ergon* 70:315–322 . <https://doi.org/10.1016/j.apergo.2018.02.025>
- Koopman AS, Kingma I, Faber GS, de Looze MP, van Dieën JH (2019) Effects of a passive exoskeleton on the mechanical loading of the low back in static holding tasks. *J Biomech* 83:97–103. <https://doi.org/10.1016/j.jbiomech.2018.11.033>
- Langlois K, Rodriguez-Cianca D, Serrien B, De Winter J, Verstraten T, Rodriguez-Guerrero C, Vanderborght B, Lefeber D (2020) Investigating the Effects of Strapping Pressure on Human-Robot Interface Dynamics Using a Soft Robotic Cuff. *IEEE Trans Med Robot Bionics* 1. <https://doi.org/10.1109/TMRB.2020.3042255>
- Larsen FG, Svenningsen FP, Andersen MS, de Zee M, Skals S (2020) Estimation of Spinal Loading During Manual Materials Handling Using Inertial Motion Capture. *Ann Biomed Eng* 48:805–821. <https://doi.org/10.1007/s10439-019-02409-8>
- Levesque L, Pardoel S, Lovrenovic Z, Doumit M (2017) Experimental comfort assessment of an active exoskeleton interface. In: 2017 IEEE International Symposium on Robotics and Intelligent Sensors (IRIS). pp 38–43
- Luger T, Seibt R, Cobb TJ, Rieger MA, Steinhilber B (2019) Influence of a passive lower-limb exoskeleton during simulated industrial work tasks on physical load, upper body posture, postural control and discomfort. *Appl Ergon* 80:152–160. <https://doi.org/10.1016/j.apergo.2019.05.018>
- Lund ME, Damsgaard M, Tørholm S, Galibarov PE, Jung M (2017a) The

- AnyBody Managed Model Repository (AMMR) (Version 1.6.6). <https://doi.org/10.5281/ZENODO.1250765>
- Lund ME, Tørholm S, Galibarov PE, Jung M, Rasmussen KP, Gopalakrishnan A, Damsgaard M (2017b) The AnyBody Managed Model Repository (AMMR)
- Lund ME, Tørholm S, Jensen BK, Galibarov PE, Dzialo CM, Iversen K, Sarivan M, Marra MA, Simonsen ST (2020) The AnyBody Managed Model Repository (AMMR). <https://doi.org/10.5281/ZENODO.3932764>
- Lund ME, Tørholm S, Jung M (2018) The AnyBody Managed Model Repository (AMMR) (Version 2.1.1). <https://doi.org/10.5281/ZENODO.1287730>
- Mallat R, Khalil M, Venture G, Bonnet V, Mohammed S (2019) Human-Exoskeleton Joint Misalignment: A Systematic Review. *Int Conf Adv Biomed Eng ICABME* 2019-October:1–4. <https://doi.org/10.1109/ICABME47164.2019.8940321>
- Manna SK, Dubey VN (2018) Comparative study of actuation systems for portable upper limb exoskeletons. *Med Eng Phys* 60:1–13. <https://doi.org/10.1016/j.medengphys.2018.07.017>
- Marra MA, Vanheule V, Fluit R, Koopman BHFJM, Rasmussen J, Verdonshot N, Andersen MS (2015) A Subject-Specific Musculoskeletal Modeling Framework to Predict in Vivo Mechanics of Total Knee Arthroplasty. *J Biomech Eng* 137:1–12. <https://doi.org/10.1115/1.4029258>
- Mouzo F, Michaud F, Lugris U, Cuadrado J (2020) Leg-orthosis contact force estimation from gait analysis. *Mech Mach Theory* 148:103800. <https://doi.org/10.1016/j.mechmachtheory.2020.103800>
- Muller A, Pontonnier C, Puchaud P, Dumont G (2019) CusToM: a Matlab toolbox for musculoskeletal simulation. *J Open Source Softw* 4:927. <https://doi.org/10.21105/joss.00927>
- Naf MB, Junius K, Rossini M, Rodriguez-Guerrero C, Vanderborght B, Lefeber D (2018) Misalignment Compensation for Full Human-Exoskeleton Kinematic Compatibility: State of the Art and Evaluation. *Appl Mech Rev* 70:1–19. <https://doi.org/10.1115/1.4042523>
- Nikravesh PE (1988) *Computer-Aided analysis of mechanical systems*. Prentice-Hall Int., Englewood Cliffs, NJ.
- Olivier J, Ortlieb A, Bertusi P, Vouga T, Bouri M, Bleuler H (2015) Impact of ankle locking on gait implications for the design of hip and knee exoskeletons. *IEEE Int Conf Rehabil Robot* 2015-Sept:618–622. <https://doi.org/10.1109/ICORR.2015.7281269>
- Pamungkas DS, Caesarendra W, Susanto S, Soebakti H, Analia R (2019) Overview: Types of lower limb exoskeletons. *Electron* 8:1–12. <https://doi.org/10.3390/electronics8111283>
- Panero E, Muscolo GG, Gastaldi L, Pastorelli S (2020) *Multibody Analysis of a 3D Human Model with Trunk Exoskeleton for Industrial Applications*. Springer International Publishing
- Picchiotti MT, Weston EB, Knapik GG, Dufour JS, Marras WS (2019) Impact of



- two postural assist exoskeletons on biomechanical loading of the lumbar spine. *Appl Ergon* 75:1–7. <https://doi.org/10.1016/j.apergo.2018.09.006>
- Power V, de Eyto A, Hartigan B, Ortiz J, O’Sullivan LW (2019) Application of a user-centered design approach to the development of XoSoft – A lower body soft exoskeleton. *Biosyst Biorobotics* 22:44–48. [https://doi.org/10.1007/978-3-030-01887-0\\_9](https://doi.org/10.1007/978-3-030-01887-0_9)
- Rasmussen J (2019) Chapter 8 - The AnyBody Modeling System. In: Scataglini S, Paul GBT-DHM and P (eds). Academic Press, pp 85–96
- Rasmussen J, Andersen MS, Munajjed AAA-, Rausch J, Upmann A (2014) H-point simulation in musculoskeletal models of seating. In: Proceedings of the 3rd International Digital Human Modeling Symposium. National Institute of Advanced Industrial Science and Technology (AIST)
- Rasmussen J, Damsgaard M, Voigt M (2001) Muscle recruitment by the min/max criterion - A comparative numerical study. *J Biomech* 34:409–415. [https://doi.org/10.1016/S0021-9290\(00\)00191-3](https://doi.org/10.1016/S0021-9290(00)00191-3)
- Rasmussen J, De Zee M, Damsgaard M, Christensen ST, Marek C, Siebertz K (2005) A general method for scaling musculo-skeletal models. 2005 Int Symp Comput Simul Biomech 3
- Rathore A, Wilcox M, Morgado Ramirez DZ, Loureiro R, Carlson T (2016) Quantifying the human-robot interaction forces between a lower limb exoskeleton and healthy users. In: 2016 38th Annual International Conference of the IEEE Engineering in Medicine and Biology Society (EMBC). IEEE, pp 586–589
- Schiele A (2008) An explicit model to predict and interpret constraint force creation in phri with exoskeletons. *Proc - IEEE Int Conf Robot Autom* 1324–1330. <https://doi.org/10.1109/ROBOT.2008.4543387>
- Schiele A, van der Helm FCT (2009) Influence of attachment pressure and kinematic configuration on pHRI with wearable robots. *Appl Bionics Biomech* 6:157–173. <https://doi.org/10.1080/11762320902879961>
- Shi D, Zhang W, Zhang W, Ding X (2019) A Review on Lower Limb Rehabilitation Exoskeleton Robots. *Chinese J Mech Eng*. <https://doi.org/10.1186/s10033-019-0389-8>
- Shourijeh MS, Jung M, Damsgaard M (2017) Metabolic Energy Consumption in a Box-Lifting Task: A Parametric Study on the Assistive Torque. In: González-Vargas J, Ibáñez J, Contreras-Vidal JL, van der Kooij H, Pons JL (eds) *Wearable Robotics: Challenges and Trends*. Springer International Publishing, Cham, pp 143–148
- Skals S, Jung MK, Damsgaard M, Andersen MS (2017) Prediction of ground reaction forces and moments during sports-related movements. *Multibody Syst Dyn* 39:175–195. <https://doi.org/10.1007/s11044-016-9537-4>
- Spada S, Ghibaudo L, Carnazzo C, Di Pardo M, Chander DS, Gastaldi L, Cavatorta MP (2019a) Physical and Virtual Assessment of a Passive Exoskeleton. In: Bagnara S, Tartaglia R, Albolino S, Alexander T, Fujita Y

- (eds) Proceedings of the 20th Congress of the International Ergonomics Association (IEA 2018). Springer International Publishing, Cham, pp 247–257
- Spada S, Ghibaudo L, Carnazzo C, Gastaldi L, Cavatorta MP (2019b) Passive Upper Limb Exoskeletons: An Experimental Campaign with Workers. In: Bagnara S, Tartaglia R, Albolino S, Alexander T, Fujita Y (eds) Proceedings of the 20th Congress of the International Ergonomics Association (IEA 2018). Springer International Publishing, Cham, pp 230–239
- Spada S, Ghibaudo L, Gilotta S, Gastaldi L, Cavatorta MP (2017) Investigation into the applicability of a passive upper-limb exoskeleton in automotive industry. *Procedia Manuf* 11:1255–1262. <https://doi.org/10.1016/j.promfg.2017.07.252>
- Spada S, Ghibaudo L, Gilotta S, Gastaldi L, Cavatorta MP (2018) Analysis of Exoskeleton Introduction in Industrial Reality: Main Issues and EAWS Risk Assessment. Springer, Cham, pp 236–244
- Sposito M, Toxiri S, Caldwell DG, Ortiz J, De Momi E (2019) Towards design guidelines for physical interfaces on industrial exoskeletons: Overview on evaluation metrics. Springer International Publishing
- Stegall P, Winfree K, Zanutto D, Agrawal SK (2013) Rehabilitation exoskeleton design: Exploring the effect of the anterior lunge degree of freedom. *IEEE Trans Robot* 29:838–846. <https://doi.org/10.1109/TRO.2013.2256309>
- Tamez-duque J, Cobian-ugalde R, Kilicarslan A, Venkatakrishnan A, Soto R, Contreras-vidal JL (2015) Real-Time Strap Pressure Sensor System for Powered Exoskeletons. 4550–4563. <https://doi.org/10.3390/s150204550>
- Tröster M, Schneider U, Bauernhansl T, Rasmussen J (2018) Simulation Framework for Active Upper Limb Exoskeleton Design Optimization Based on Musculoskeletal Modeling. *Dritte Transdisziplinäre Konf* 345–353
- Tröster M, Wagner D, Müller-Graf F, Maufroy C, Schneider U, Bauernhansl T (2020) Biomechanical model-based development of an active occupational upper-limb exoskeleton to support healthcare workers in the surgery waiting room. *Int J Environ Res Public Health* 17:1–16. <https://doi.org/10.3390/ijerph17145140>
- Van der Helm FCT, Veeger HEJ, Pronk GM, Van der Woude LH V, Rozendal RH (1992) Geometry parameters for musculoskeletal modelling of the shoulder system. *J Biomech* 25:129–144. [https://doi.org/10.1016/0021-9290\(92\)90270-B](https://doi.org/10.1016/0021-9290(92)90270-B)
- Veeger HEJ, Van Der Helm FCT, Van Der Woude LH V, Pronk GM, Rozendal RH (1991) Inertia and muscle contraction parameters for musculoskeletal modelling of the shoulder mechanism. *J Biomech* 24:615–629. [https://doi.org/https://doi.org/10.1016/0021-9290\(91\)90294-W](https://doi.org/https://doi.org/10.1016/0021-9290(91)90294-W)
- Veeger HEJ, Yu B, An K-N, Rozendal RH (1997) Parameters for modeling the upper extremity. *J Biomech* 30:647–652. [https://doi.org/https://doi.org/10.1016/S0021-9290\(97\)00011-0](https://doi.org/https://doi.org/10.1016/S0021-9290(97)00011-0)

- Weston EB, Alizadeh M, Knapik GG, Wang X, Marras WS (2018) Biomechanical evaluation of exoskeleton use on loading of the lumbar spine. *Appl Ergon* 68:101–108. <https://doi.org/10.1016/j.apergo.2017.11.006>
- Yandell MB, Quinlivan BT, Popov D, Walsh C, Zelik KE (2017) Physical interface dynamics alter how robotic exosuits augment human movement: implications for optimizing wearable assistive devices. *J Neuroeng Rehabil* 14:40. <https://doi.org/10.1186/s12984-017-0247-9>
- Yandell MB, Ziemnicki DM, McDonald KA, Zelik KE (2020) Characterizing the comfort limits of forces applied to the shoulders, thigh and shank to inform exosuit design. *PLoS One* 15:1–12. <https://doi.org/10.1371/journal.pone.0228536>
- Zajac FE (1989) Muscle and tendon: Properties, models, scaling, and application to biomechanics and motor control. *Crit Rev Biomed Eng* 17:359–411
- Zanotto D, Akiyama Y, Stegall P, Agrawal SK (2015) Knee Joint Misalignment in Exoskeletons for the Lower Extremities: Effects on User's Gait. *IEEE Trans Robot* 31:978–987. <https://doi.org/10.1109/TRO.2015.2450414>
- Zhou L, Bai S, Andersen MS, Rasmussen J (2015) Modeling and design of a spring-loaded, cable-driven, wearable exoskeleton for the upper extremity. *Model Identif Control* 36:167–177. <https://doi.org/10.4173/mic.2015.3.4>
- Zhou L, Bai S, Andersen MS, Rasmussen J (2012) Design and Optimization of a Spring-loaded Cable-driven Robotic Exoskeleton. *25th Nord Semin Comput Mech* 205–208
- Zhou L, Li Y, Bai S (2017) A human-centered design optimization approach for robotic exoskeletons through biomechanical simulation. *Rob Auton Syst* 91:337–347. <https://doi.org/10.1016/j.robot.2016.12.012>